



HAL
open science

Conducting Polymer Devices for in vitro Electrophysiology

Dimitrios Koutsouras

► **To cite this version:**

Dimitrios Koutsouras. Conducting Polymer Devices for in vitro Electrophysiology. Other. Université de Lyon, 2016. English. NNT : 2016LYSEM017 . tel-01665199

HAL Id: tel-01665199

<https://theses.hal.science/tel-01665199>

Submitted on 15 Dec 2017

HAL is a multi-disciplinary open access archive for the deposit and dissemination of scientific research documents, whether they are published or not. The documents may come from teaching and research institutions in France or abroad, or from public or private research centers.

L'archive ouverte pluridisciplinaire **HAL**, est destinée au dépôt et à la diffusion de documents scientifiques de niveau recherche, publiés ou non, émanant des établissements d'enseignement et de recherche français ou étrangers, des laboratoires publics ou privés.



N°d'ordre NNT : 2016LYSEM017

THESE de DOCTORAT DE L'UNIVERSITE DE LYON
opérée au sein de
l'Ecole des Mines de Saint-Etienne

Ecole Doctorale N° 488
Sciences, Ingénierie, Santé

Spécialité de doctorat : Bioélectronique
Discipline : Microélectronique

Soutenue publiquement à Gardanne le 30/09/2016, par :

Dimitrios A. Koutsouras

Titre de la thèse

Conducting Polymer Devices for *in vitro* Electrophysiology

Devant le jury composé de :

BENFENATI, Valentina	Professoressa a contratto UNIBO	Présidente
IANNOTTA, Salvatore	Professeur /Directeur de IMEM	Rapporteur
LANG, Jochen	Professeur CBMN	Rapporteur
OWENS, Róisín	Maître Assistante EMSE	Examinatrice
SISKOS, Stylianos	Professeur AUTH	Examineur
MALLIARAS, George	Professeur EMSE	Directeur de thèse

Spécialités doctorales	Responsables :	Spécialités doctorales	Responsables
SCIENCES ET GENIE DES MATERIAUX MECANIQUE ET INGENIERIE GENIE DES PROCEDES SCIENCES DE LA TERRE SCIENCES ET GENIE DE L'ENVIRONNEMENT	K. Wolski Directeur de recherche S. Drapier, professeur F. Gruy, Maître de recherche B. Guy, Directeur de recherche D. Graillet, Directeur de recherche	MATHEMATIQUES APPLIQUEES INFORMATIQUE IMAGE, VISION, SIGNAL GENIE INDUSTRIEL MICROELECTRONIQUE	O. Roustant, Maître-assistant O. Boissier, Professeur JC. Pinoli, Professeur A. Dolgui, Professeur S. Dauzere Peres, Professeur

EMSE : Enseignants-chercheurs et chercheurs autorisés à diriger des thèses de doctorat (titulaires d'un doctorat d'État ou d'une HDR)

ABSI	Nabil	CR	Génie industriel	CMP
AVRIL	Stéphane	PR2	Mécanique et ingénierie	CIS
BALBO	Flavien	PR2	Informatique	FAYOL
BASSEREAU	Jean-François	PR	Sciences et génie des matériaux	SMS
BATTAIA-GUSCHINSKAYA	Olga	CR	Génie industriel	FAYOL
BATTON-HUBERT	Mireille	PR2	Sciences et génie de l'environnement	FAYOL
BERGER DOUCE	Sandrine	PR2	Sciences de gestion	FAYOL
BIGOT	Jean Pierre	MR(DR2)	Génie des Procédés	SPIN
BILAL	Essaid	DR	Sciences de la Terre	SPIN
BLAYAC	Sylvain	MA(MDC)	Microélectronique	CMP
BOISSIER	Olivier	PR1	Informatique	FAYOL
BONNEFOY	Olivier	MA(MDC)	Génie des Procédés	SPIN
BORBELY	Andras	MR(DR2)	Sciences et génie des matériaux	SMS
BOUCHER	Xavier	PR2	Génie Industriel	FAYOL
BRODHAG	Christian	DR	Sciences et génie de l'environnement	FAYOL
BRUCHON	Julien	MA(MDC)	Mécanique et ingénierie	SMS
BURLAT	Patrick	PR1	Génie Industriel	FAYOL
COURNIL	Michel	PR0	Génie des Procédés	DIR
DAUZERE-PERES	Stéphane	PR1	Génie Industriel	CMP
DEBAYLE	Johan	CR	Image Vision Signal	CIS
DELAFOSSSE	David	PR0	Sciences et génie des matériaux	SMS
DELORME	Xavier	MA(MDC)	Génie industriel	FAYOL
DESRAYAUD	Christophe	PR1	Mécanique et ingénierie	SMS
DOLGUI	Alexandre	PR0	Génie Industriel	FAYOL
DRAPIER	Sylvain	PR1	Mécanique et ingénierie	SMS
FAVERGEON	Loïc	CR	Génie des Procédés	SPIN
FEILLET	Dominique	PR1	Génie Industriel	CMP
FRACZKIEWICZ	Anna	DR	Sciences et génie des matériaux	SMS
GARCIA	Daniel	MR(DR2)	Génie des Procédés	SPIN
GAVET	Yann	MA(MDC)	Image Vision Signal	CIS
GERINGER	Jean	MA(MDC)	Sciences et génie des matériaux	CIS
GOEURIOT	Dominique	DR	Sciences et génie des matériaux	SMS
GONDRAN	Natacha	MA(MDC)	Sciences et génie de l'environnement	FAYOL
GRAILLOT	Didier	DR	Sciences et génie de l'environnement	SPIN
GROSSEAU	Philippe	DR	Génie des Procédés	SPIN
GRUY	Frédéric	PR1	Génie des Procédés	SPIN
GUY	Bernard	DR	Sciences de la Terre	SPIN
HAN	Woo-Suck	MR	Mécanique et ingénierie	SMS
HERRI	Jean Michel	PR1	Génie des Procédés	SPIN
KERMOUCHE	Guillaume	PR2	Mécanique et Ingénierie	SMS
KLOCKER	Helmut	DR	Sciences et génie des matériaux	SMS
LAFORREST	Valérie	MR(DR2)	Sciences et génie de l'environnement	FAYOL
LERICHE	Rodolphe	CR	Mécanique et ingénierie	FAYOL
LI	Jean-Michel		Microélectronique	CMP
MALLIARAS	Georges	PR1	Microélectronique	CMP
MAURINE	Philippe	Ingénieur de recherche	Microélectronique	CMP
MOLIMARD	Jérôme	PR2	Mécanique et ingénierie	CIS
MONTHILLET	Frank	DR	Sciences et génie des matériaux	SMS
MOUTTE	Jacques	CR	Génie des Procédés	SPIN
NEUBERT	Gilles	PR	Génie industriel	FAYOL
NIKOLOVSKI	Jean-Pierre	Ingénieur de recherche		CMP
NORTIER	Patrice	PR1		SPIN
OWENS	Rosin	MA(MDC)	Microélectronique	CMP
PICARD	Gauthier	MA(MDC)	Informatique	FAYOL
PIJOLAT	Christophe	PR0	Génie des Procédés	SPIN
PIJOLAT	Michèle	PR1	Génie des Procédés	SPIN
PINOLI	Jean Charles	PR0	Image Vision Signal	CIS
POURCHEZ	Jérémy	MR	Génie des Procédés	CIS
ROBISSON	Bruno	Ingénieur de recherche	Microélectronique	CMP
ROUSSY	Agnès	MA(MDC)	Génie industriel	CMP
ROUSTANT	Olivier	MA(MDC)	Mathématiques appliquées	FAYOL
ROUX	Christian	PR	Image Vision Signal	CIS
STOLARZ	Jacques	CR	Sciences et génie des matériaux	SMS
TRIA	Assia	Ingénieur de recherche	Microélectronique	CMP
VALDIVIESO	François	PR2	Sciences et génie des matériaux	SMS
VIRICELLE	Jean Paul	DR	Génie des Procédés	SPIN
WOLSKI	Krzysztof	DR	Sciences et génie des matériaux	SMS
XIE	Xiaolan	PR1	Génie industriel	CIS
YUGMA	Gallian	CR	Génie industriel	CMP

ENISE : Enseignants-chercheurs et chercheurs autorisés à diriger des thèses de doctorat (titulaires d'un doctorat d'État ou d'une HDR)

BERGHEAU	Jean-Michel	PU	Mécanique et Ingénierie	ENISE
BERTRAND	Philippe	MCF	Génie des procédés	ENISE
DUBUJET	Philippe	PU	Mécanique et Ingénierie	ENISE
FEULVARCH	Eric	MCF	Mécanique et Ingénierie	ENISE
FORTUNIER	Roland	PR	Sciences et Génie des matériaux	ENISE
GUSSAROV	Andrey	Enseignant contractuel	Génie des procédés	ENISE
HAMDI	Hédi	MCF	Mécanique et Ingénierie	ENISE
LYONNET	Patrick	PU	Mécanique et Ingénierie	ENISE
RECH	Joël	PU	Mécanique et Ingénierie	ENISE
SMUROV	Igor	PU	Mécanique et Ingénierie	ENISE
TOSCANO	Rosario	PU	Mécanique et Ingénierie	ENISE
ZAHOUANI	Hassan	PU	Mécanique et Ingénierie	ENISE

“To my family”

Table of Contents

Acknowledgments	1
Chapter 1: Introduction	4
1.1 Bioelectronics – Organic Devices	4
1.2 Organic Electronics Fabrication Processes.....	6
1.2.1 Photolithography	8
1.2.2 Basic principles.....	9
1.2.3 Fabrication steps	11
Substrate cleaning.....	11
Deposition of the photoresist.....	12
Post-apply bake.....	14
Use of the mask/alignment/exposure.....	15
Development.....	17
Descumming and postbaking.....	17
Pattern transfer.....	18
Stripping	19
1.2.4 Photolithography in polymer device fabrication	20
Sacrificial layer methods	20
Orthogonal photoresist method	24
1.3 Concepts of Neuroscience	27
1.3.1 Neurons.....	27
1.3.2 Glia	30
1.3.3 Action Potential	31
1.4 Concepts of Electrophysiology	33
<i>In vitro</i> electrophysiology.....	34
References	38
Chapter 2: Biopotential Electrodes	40
2.1 Introduction	40
2.2 Theoretical model of the neural recording	43
2.3 Conducting Polymer Coated Electrodes	46
2.4 Impedance Spectroscopy of PEDOT: PSS Coated Electrodes as a Function of Area	49

2.5 Electrodeposition	61
2.6 Conclusions	65
References	67
Chapter 3: <i>In vitro</i> PEDOT:PSS Microelectrode Arrays for hippocampal cell culture electrophysiological recordings	68
3.1 Abstract	68
3.2 Experiment-Results	69
3.3 Conclusions	77
3.4 Experimental Section	77
3.4.1 Microelectrode Arrays fabrication:	77
3.4.2 Preparation of the rat hippocampal cell cultures:	78
3.4.3 Electrical and electrophysiological recordings:	78
References	80
Supplementary Information	81
Chapter 4: A PEDOT:PSS <i>in vitro</i> Platform for Pancreatic Islet Cell Electrophysiology	84
4.1 Abstract	84
4.2 Experiment – Results	85
4.3 Conclusions	93
4.4 Experimental Section	94
4.4.1 Device Fabrication.....	94
4.4.2 Islets isolation and cell culture	95
4.4.3 Device characterization and electrophysiological recordings	95
References	96
Supplementary Information.....	97
Chapter 5: Organic Electrochemical Transistors	99
5.1 Introduction	99
5.2 Organic Electrochemical Transistors measuring system	103
5.3 Conclusions	111
References	112
Chapter 6 Organic Electrochemical Transistor for Astrocytes activity recordings.....	113
6.1 Introduction	113
6.2 Experiment- Results.....	114
6.2.1 Astrocytes biocompatibility on PEDOT: PSS	114

6.2.2 Device characterization in external standard solution	114
6.2.3 Recordings of astrocytes' activity using OECT	116
6.2.4 OECT astrocytes recordings using pharmacological inhibitor and ATP ..	117
6.2.5 OECT Astrocytes recordings during calcium microfluorimetry	118
6.3 Conclusions	119
6.4 Experimental Section	120
6.4.1 Cell viability assay:	120
6.4.2 Device Fabrication:.....	120
6.4.3 Biological measurement:	121
6.4.4 Calcium microfluorometry:	121
References	122
Supplementary Information.....	123
Chapter 7: Conclusion – Outlook.....	124
Appendix A: Noise characterization and modeling	127
Appendix B: Spreading resistance R_s	133
Appendix C: List of Abbreviations	137
Appendix D: List of Publications.....	138

Acknowledgments

It is often argued that the 3 years of the PhD studies is a special period in every student's life. I think this cannot be truer in my case. I am not sure if those have been the best three years in my life but I am absolutely sure that are the years that marked me the most and will follow me forever. Those are the years that has changed me as a person (hopefully made me grow more mature) and that is why I will always recall my time in France full of emotions and memories.

To begin with, I would like to thank my advisor Professor George G. Malliaras for offering me the opportunity to come, study and work in the Department of Bioelectronics in Gardanne under his supervision. First, I would like to thank him for his trust, his guidance, his support and his encouragement these 3 years. I would also like to thank him for introducing me to the way research in a high scientific level is done and for being a continuous source of inspiration during my project. Foremost, I would like to thank him because he is the reason of me being in this scientific field making a turn in my carrier. If it was not for him there is no way I could have followed my dreams and this is why I shall be forever in his debt.

I am especially thankful to Professor David C. Martin for his guidance and his support. Luckily for me, my time in BEL co-existed with his Sabbatical time in our lab. The result was a project on the effect of electrodes area in their impedance Spectra and countless hours of fruitful scientific, and not, conversations. I am also grateful to Professor Eric di Pasquale who was the man to provide me with beautiful hippocampal cell cultures exactly the moment I needed them the most in order to finish my project. He was the one who introduced me to the world of electrophysiology and we spend many hours together talking about science and philosophy. Of course, our relationship has evolved to something more than a professional one and I would like to consider him as one of my friends.

I would also like to thank Assistant Professor Roisin Owens who, with her knowledge in biology, her will to offer help at any time and her guidance, made my work life much easier. I am also thankful to Professor Stylianos Siskos with whom we

run a project that I am sure it will pay off very soon. I strongly believe that read out system that was designed will allow the OECTs to fulfil their true potential.

My special thanks go to Professor Jochen Lang who gave me the opportunity to experiment the use of organics to cells other than neurons and to broaden my electrophysiological horizons to pancreas cells and to Valentina Benfenati who hosted me for a month in her lab in Bologna and gave me the opportunity to work with astrocytes. The four above along with Professor Salvatore Iannotta are the members of my jury and I would like to thank them for reading and correcting my thesis.

I would also like to thank all the PhD students, Post docs and P.I.s involved in OLIMPIA project. Every OLIMPIA meeting was a great opportunity for scientific discussions and lots of fun!

During my PhD studies I was lucky enough to supervise three master students. Maria Villiou, Petros Sideris and Clemens Stolz. I cannot thank them enough for their help and for the fact that I also learned from them maybe even more than I taught them!

Many thanks go to Eileen Pedraza, Romain Perrier, Ariana Villarreal and to Assistant Professor Matthieu Raoux from CBMN UMR-CNRS in Bordeaux and to Simone Bonetti, Ana Borrachero from CNR-ISMN in Bologna for their help during the projects we run together.

The number of people from BEL that I would like to thank are way more than those that I can fit in a couple of pages. So I would like to thank, from the bottom of my heart, all the people that I met, worked with and had fun with during these 3 years of my presence in the department of bioelectronics. Thank you all for the memories! I really appreciate what you did for me!

Special thanks go to Jolien Pas and Adel Hama for their help in the neuron recording project and to Anton Ivanon from Institut de Neurosciences des Systèmes of Aix-Marseille University for introducing me to electrophysiology. Special thanks also go to the technicians of the clean room, to the employees at CMP for their help and particularly to Sabine Salmeron for giving me “shelter” in the library and teaching me French. I also thank my former supervisor Professor Stergios Logothetidis as I owe

him my presence in France and my friends and relatives back in Greece for never forgetting me.

It is very difficult to describe how much grateful I feel to postdoc Paschalis Gkoupidenis. It is not only the fact that he taught me how to do scientific research. He also changed my mentality and gave me guidance when I needed it the most. Paschalis is not only one of the best colleagues I have ever had, he is also a true friend and I am extremely lucky to have met him.

Last but not least, I would like to thank my family. I do not think there is any word that can express my gratefulness towards them. My father Thanasis , my mother Spyridoula and my brother Nikos have been always there for me and I do not think I would have made it without them. Of course, I am also grateful to Athina for her love and her support. Above all, I want to apologize to all of them for the pressure I was putting on their shoulders when my problems were, so unfairly, affecting their lives and to thank them for putting up with me. Thank you from the bottom of my heart!

Dimitrios A. Koutsouras

September 2016

Chapter 1: Introduction

1.1 Bioelectronics – Organic Devices

Bioelectronics is the field of science that tries to merge two very different worlds .The world of Biology and the one of Electronics. The motivation behind such an effort is, obviously, the continuous need to find better ways of interaction between electronic devices and living tissue both in fundamental research level but also in diagnostics and therapeutics.

The problems start the moment we realize the fundamental differences between the two systems. Conventional electronics are made, mostly, out of silicon which is a tough and rigid material held together by a network of covalent bonds. Furthermore, they are solid and conduct charge with electrons and holes. Biological matter, on the other hand, is “soft”, wet and conduct charge by ion transport. These differences in the materials’ structure and properties are the reason behind a problematic matching that needs to be taken into account for any transducer functioning between biotic tissue and abiotic medical devices ^[1, 2].

Organic electronics came into light as the new way to bridge this mismatch and to offer alternative interfacing approaches. The term “Organic Bioelectronics”,in particularly, was firstly introduced by Magnus Berggren and Agneta Richter-Dahlfors in 2007 in a seminal review^[3] describing this new research approach.

Long before that , Organic electronics had attracted the increasing interest of the scientific community mostly due to their synthetic tunability, their electronic properties and their low temperature processing^[1]. By definition, organic electronics refers to the use of carbon based semiconductors either as conjugated small molecules or as conjugated polymers. Especially for the case of conjugated polymers by the end of 1970s Heeger et al, demonstrated that acetylene can become highly conducting when doped with iodine^[4] (Nobel Prize in Chemistry 2000). The 1980’s was the decade of blossom of organics in electrophotography and by the end of the decade the first organic light emitting diode (OLED) was produced^[5]. Naturally, during 1990’s OLEDs, organic thin film transistors (OTFTs) and organic photovoltaics (OPVs) where intensively studied resulting in their extensive commercialization.

The real question is, though, whether organic electronics can provide any significant advantage in comparison to the existing silicon technology in the field of bioelectronics or not.

There are a couple of reasons that support organics potential to revolutionize the field and they can be summarized as follow. First, it is the mechanical properties of conducting polymers that distinguish them from their inorganic counterparts. Organic electronic materials are “soft” to their nature, a fact that gives them better mechanical compatibility to tissue and to flexible substrates that very commonly are used as implantable devices. Second, they support mixed ionic/electronic conductivity. This is a tremendous advantage since living tissue communicates through ion movement while solid electronics communicate through electrons and holes. Conjugated polymers can bridge this gap by speaking both languages. Third, the weak van der Waals bonding of organics results in dangling and oxide free interfaces with aqueous electrolytes. This is translated into a direct contact between the sensing/recording device and the biomoiety offering better, more direct and cleaner interaction. Last, but not least, polymers provide freedom in chemical modification. This means the whole arsenal of organic chemistry is available for modifications in the polymer chain which result in an increased biological functionality^[1, 2].

Consequently, the term organic bioelectronics obtains a completely new meaning. It reflects a new effort of coupling electronic devices and biological objects; a coupling that is not only extremely advantageous but also work in a bilateral way. In one direction, a biological process creates a signal to an organic device; for example an enzymatic reaction (glucose oxidation) causes the current in an Organic Electrochemical Transistor to change (glucose sensing). In the other direction, an organic electronic device causes a biological phenomenon to occur; voltage applied through a polymer covered stimulates a neuron to fire action potentials (Figure 1.1).

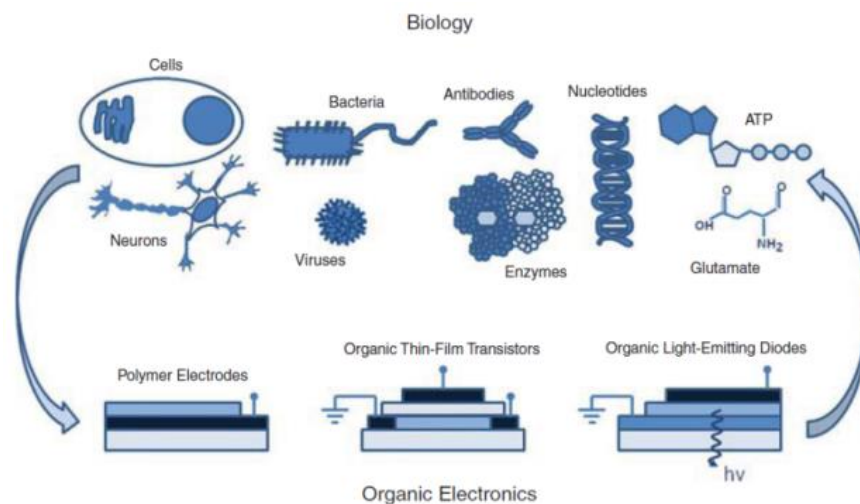


Figure 1.1: The two way coupling between organic electronic devices and biology^[1].

For the reasons above, organic electronics seems to be the ideal candidate for allowing bioelectronics to fulfil its true potential. That does not mean that organic electronics are here to replace existing silicon technology but rather that they can act complementary to it by offering a novel toolbox for interfacing with biology.

Next we are going to focus a bit on the organic electronics device fabrication process as it poses a number of challenges which inevitably come hand to hand with the conducting polymer special nature.

1.2 Organic Electronics Fabrication Processes

As extensively presented in the previous part, during the past decades the field of Organic Electronics has attracted the increasing attention of the scientific community as an attempt to complement traditional silicon electronics and to broaden their horizons^[6]. There are a number of good reasons justifying this trend as organic materials present a unique set of properties. In particular, they allow fabrication of thin, flexible, lightweight, environmental friendly and low cost devices^[7]. Moreover, they offer ease of processability, low temperature solution-based deposition, and the degree of freedom that comes with their chemically tunable properties^[8].

Nevertheless, before this new emerging technology becomes mature enough to influence the electronic industry, the major issue of organic film patterning must be addressed. There is an inextricable link between electronic device performance and

electronic material patterning and that is the reason why many different methods have been developed throughout the past years to optimize the fabrication process. Especially when it comes to organics, patterning is a challenging task as the technique of choice should be compatible with their special nature.

Unfortunately, despite its comparative advantages, conventional photolithography lacks compatibility with the vast majority of organic electronic materials. This is due to the fact that solvents used during deposition, development, and removal of photoresists have, in most cases, adverse effect on organic films. As a result, the already existing and well-developed industry of conventional silicon-based electronics can only provide limited tools for organics electronics^[9]. Thus, the goal of overcoming those incompatibilities is of great importance as it will allow the use of the accumulated knowledge of an already well established and commercially successful fabrication approach.

In contrast, other nondestructive patterning techniques employed throughout the past years did not manage to live up to their potential. Vapor deposition through shadow masks, soft and hard imprint lithography, thermal transfer process and laser assisted printing were originally introduced as alternative approaches promising a convenient and easy way of device fabrication. Nevertheless, all these techniques suffer from numerous drawbacks. In particular, shadow mask deposition is the technique of choice for small-molecule patterning but lacks the ability of high resolution fabrication. Imprint technology on the other hand can offer resolution down to 10nm but it can be used only with a limited number of materials and device architectures^[10]. In addition all of the above techniques have issues with low resolution, poor scalability to larger areas, lack of registration and the fact that they tend to follow complex and costly processing protocols^[11]. These disadvantages render them unable to compete with today's state of the art fabrication processes.

In this part of the thesis we introduce novel approaches for conducting polymer device fabrication. In particular, what we are interested in is high throughput, cost effective and simple fabrication techniques, applicable to polymers and able to reproducibly create organic devices with high yield and efficiency. That is why we focus on polymer-friendly photolithography.

1.2.1 Photolithography

The term photolithography is a compound word made up from the Greek words Photo (Φως=light), litho (λίθος=stone) and graphy (γραφή=writing). As implied by its name, Photolithography is the process of transferring (writing) a pattern onto a substrate with the help of light.

Going back in time, there are two main landmarks in the development of photolithography. The first is the experiments of the Swiss pastor Jean Senebier (1742-1808) of Geneva with resins, in 1782. Senebier noticed that certain resins become insoluble in a solvent (turpentine) after sunlight exposure. The second pivotal moment comes with the work of Nicéphore Niépce on photography in 1826. Niépce, inspired by Senebier, was the first one to produce an image using the properties of light in Chalon (France). He used bitumen of Judea (a form of asphalt) dissolved in lavender oil, to coat a pewter plate and then he covered it with an etched print on oiled paper. The latter would serve as a mask for the three hours exposure to sunlight which was to follow. During this time, the exposed parts of the resist became insoluble while the protected ones could easily be removed by a mixture of turpentine and lavender oil corresponding to a photoresist behavior classified later as negative. Nevertheless, the first photolithography pattern transfer took place five years later, in 1827, by the Parisian engraver Augustin Francois Lemaître. Lemaître used a strong acid to etch a Niépce plate and to create a copy of a gravure of Cardinal d'Amboise, employing for the first time both photolithography and the chemical etching technique in a pattern transfer^[12, 13].

Photolithography gradually became popular between the members of the scientific community as many of them started to realize the potential of the new technique. A little more than 100 years later, William Shockley and his co-workers at Bell Laboratories wanted to use photolithography for the fabrication of the first integrated circuit. However the need for a photoresist that could withstand the hydrofluoric etching of silicon dioxide (an important feature for their microfabrication process) made them turn to Kenneth Mees, Director of the Eastman Kodak Laboratories at Rochester New York. Mees contacted Louis Minsk, who in 1935 developed the first synthetic photopolymer known as poly(vinyl cinnamate), the basis of the first negative photoresist. His idea relied on the photoresist becoming less soluble upon exposure to light. Misk used that feature in order to define which part of

the photoresist would dissolve and which would remain on the substrate. In his approach the dissolved parts would be the ones to create the desired pattern. Five years later, in 1940, Oskar Süß developed a positive photoresist (diazonaphthoquinone)^[13] which worked in the opposite way with the pattern formed by the part of the photoresist that remains after exposure to light.

Today, many more chemical substances have been synthesized, characterized and used in photolithography both as negative and positive photoresists. At the same time, optimization and variation of radiation sources in lithography and (X-ray lithography, charged particles lithography etc.) allow the patterning with nanometric resolution. The comparison with the 0,5-1mm accuracy achieved by Lemaître during the first photolithographic attempt shows the extent of progress^[12].

1.2.2 Basic principles

The basic principle behind photolithography is the use of light in order to alter the solubility of a thin film that is exposed to it. A mask is a stencil, usually made out of chromium, that protects selected parts of the photosensitive material while the uncovered ones undergo changes in their properties (solubility) during the exposure. After immersion into a developer, the parts that became more soluble are dissolved leaving the desired pattern on the film behind. It is obvious that the photosensitive material plays a key role in the success of the process. This material is typically an organic polymer, called photoresist, which can go through a series of photochemical reactions when exposed to light.

It should also be noted that the term Photolithography usually refers to the use of ultra violet light (UV- wavelengths 436nm and 365nm) during patterning. Nevertheless, deep ultraviolet (DUV- wavelengths 248nm and 193nm) and extreme ultraviolet (EUV- wavelengths 5-100nm) photolithography techniques are both feasible and appealing, as in theory when the wavelengths of the light sources diminish the feature resolution increases. Nevertheless, it is difficult to find light sources with enough output power, the proper photoresists and the optical elements^[14] for those short wavelengths. Moving a step further, X-Ray lithography, charged particle lithography or atomic force microscopy (AFM) lithography promise even better resolution, posing at the same time extra technological challenges. In this

chapter every time we use the term Photolithography it will be implied that we refer to UV Photolithography.

Returning to photoresists, they can roughly be divided into two categories. Positive photoresists (positive tone) and negative ones (negative tone). A positive photoresist is a photoresist which, when exposed to light, changes chemically and/or structurally becoming more soluble to an organic developer while, ideally, it was insoluble before. The mechanism behind this transformation can be either a polymer chain scission (e.g. poly(methylmethacrylate)- PMMA photoresist) or a photo induced change in the polarity of the molecule (e.g. two components DNQ-phenolic novolac resin)^[12, 15]. A negative photoresist works in the exact opposite way. The photoresist is soluble to the developer and exposure to UV light either promotes polymeric cross-linking or starts the polymerization of the monomers. That renders the exposed photoresist insoluble to the developer, hence unexposed parts of the film are removed during the development step that follows. Common negative tone photoresists are the two-component bis(aryl)azide rubber resists (Kodak KTFR- azide-sensitivity poly(isoprene) rubber)^[12, 15].

For both these types of photoresists the exposure, the development and the final pattern formation on the substrate is depicted in Figure 1.2.

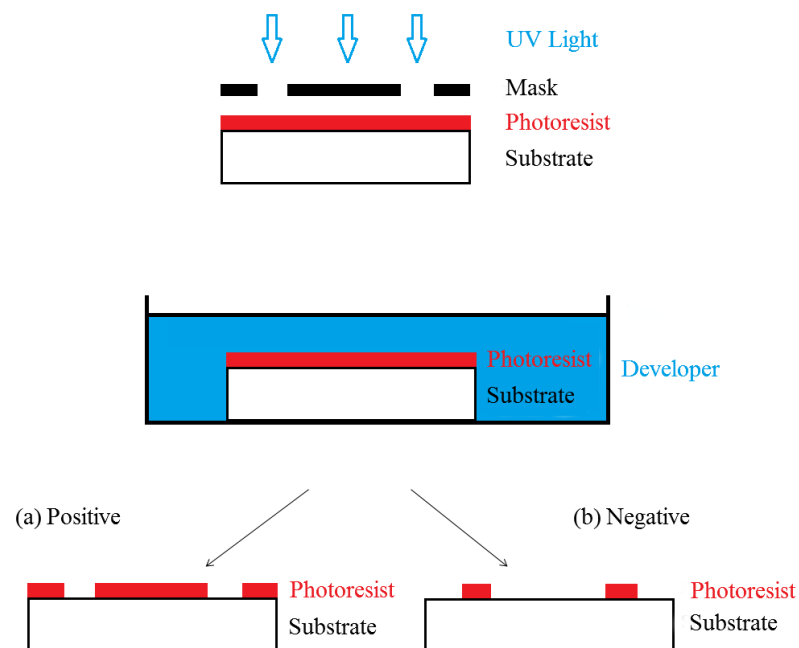


Figure 1.2: Pattern transfer for a positive (a) and a negative (b) photoresist

In general, positive photoresists are more expensive than the negative ones but can offer higher resolution. This feature, along with the fact that positive photoresists can be developed in less toxic water based developers, made them more popular than the negative in industry. Nevertheless, many steps forward have been made lately in the synthesis and development of new negative resists. As a result, the newer negative tone resists are water developable and can also offer high resolution^[12]. In addition, negative photoresists traditionally adhere better on substrates and they are more resistant to wet or dry etching than positive ones^[12]. In conclusion, the choice of the proper photoresist depends on many different parameters (cost, resolution, pattern geometry etc.) all of which need to be taken into account before a decision is made.

Nowadays, photolithography is the most popular technique of patterning in the Integrated Circuits Industry. It offers a reliable and reproducible way of building up electronic devices with great accuracy and high resolution. Its main disadvantage is the limitations in the topography as it can only be implemented on planar substrates. The process performance can be evaluated through three figures of merit:

- **Resolution**: It is a measure of the minimum size of a feature that can be patterned. It needs to be as high as possible in order for the feature size to be small
- **Registration**: It is a measure of how accurately patterns on different layers can be aligned with respect to each other.
- **Throughput**: It is the number of substrates that can be exposed per hour. The higher the throughput the more efficient the process.

1.2.3 Fabrication steps

The typical fabrication steps that take place during microfabrication are briefly reviewed below.

Substrate cleaning

The first, but definitely one of the most important steps in device fabrication is substrate cleaning. There are several different types of substrates that can be used for electronic circuit development. Silicon wafers are very common, especially in silicon-based semiconductor industry, but other kinds of substrates may also be employed.

Glass slides, conformable substrates (like Parylene-C) or even less conventional substrates as textiles and silk are among them. Despite the fact that some of those substrates may have special requirements or even incompatibilities with the standard cleaning protocols, the cleaning step cannot be easily omitted. Keeping the substrate free of contaminants is a matter of great importance as the degree of its cleanness affects the quality of the deposited film. Moreover, particles on the substrate could potentially lead to damage of the photomask during contact photolithography exposure (Figure 1.3) or even cause, in some cases, undesirable masking effects due to light diffraction. Among the contaminants that should be removed before coating the substrate with photoresist are atmospheric dust from operators and equipment, organic particles, moisture, H₂O residue films, solvent stains, smoke particles, residual resist, particulates and chunks of granular matter^[12, 16].

The cleanliness of the fabrication environment is of critical importance hence all fabrication steps take place in a clean room environment (typically class 100) which allows the presence of up to 100 particles (sized 0.5µm or larger) per cubic foot of atmosphere. An environment like this minimizes the amount of unwanted particles in the milieu and a result minimizes the number of unwanted contaminants on the device as well. Taking this environment as granted, typical cleaning procedures may include both wet and dry methods. Sonication in water soap baths or solvent baths are normally employed for the removal of particles (both inorganic and organic). In some cases piranha solution (a 3:1 mixture of sulfuric acid and hydrogen peroxide) can also be used for organic particles detachment. Additional approaches include thermal treatment at high temperature (dehydration bake), plasma cleaning, vapor cleaning and supercritical cleaning with CO₂ during which supercritical fluid of carbon dioxide is used for removal of inorganic and organic contaminants from cracks and clefts due to its ability to penetrate into crevices.^[12, 16, 17]

Deposition of the photoresist

Once substrate cleanliness is ensured, deposition of the photoresist on the substrate follows. Among the ways of depositing polymers on a substrate spin coating is the one which can guarantee uniformity, reproducibility and precision during deposition. It is a well-known, traditional technique which is rather easy to use and

offers control of the film thickness. The main drawback is the fact that the majority of the processed material is wasted.

Consequently, spin coating deposition has been the method of choice for photoresist thin film formation during fabrication for several decades now. During this approach, a small droplet of the photoresist is placed in the middle of the substrate which is secured on a chuck via vacuum. Centripetal acceleration spreads the photoresist on the substrate. Although almost 98% of the initial material is wasted, eventually a thin film of photoresist is deposited on the substrate. (Figure 1.3)

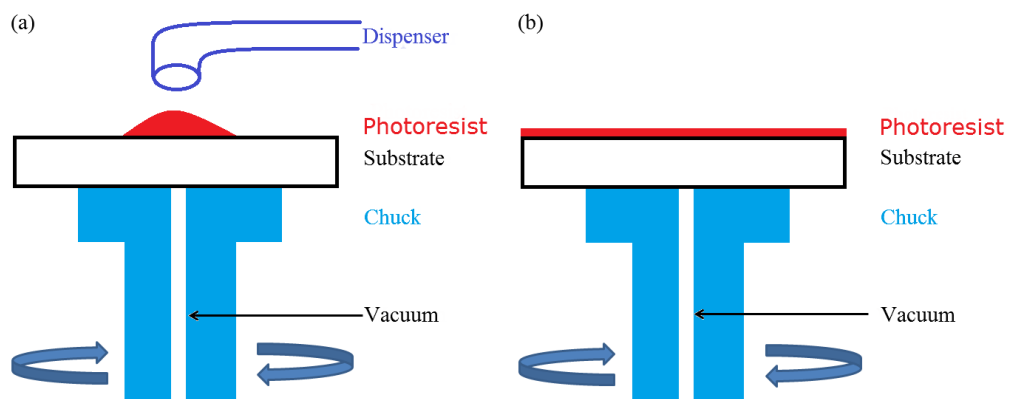


Figure 1.3: (a) Photoresist is placed on the substrate. (b) Film formation due to centripetal acceleration.

Thickness h of the photoresist is controlled through specific parameters of the process. Angular spinning speed ω and time t as well as the liquid density ρ , material viscosity η and evaporation rate e_e are the most important factors affecting film's formation. During this process complex non-equilibrium phenomena take place and it is believed that two parts contribute to the rate by which the thickness of the film changes over time. A part that refers to the effect of the angular spinning speed and a part connected to the evaporation rate of the photoresist e_e . Generally the spinning cycle can be separated into two stages: a very fast coating stage (when the photoresist is spread on the substrate) and a longer drying stage (during which the solvent evaporates). In any case, the rheology behind the film formation is rather complex especially if the evaporation of the photoresist is taken into account. Therefore, the film thickness is usually given by the empirical expression (1)^[12, 16, 17] :

$$h = \frac{K C^\beta \eta^\gamma}{\omega^\alpha} \quad (1)$$

where K is an overall calibration constant, C is the polymer concentration in g/100mL and η is the solution's viscosity. The exponential parameters α , β and γ are determined experimentally. Once these parameters are set, a calibration curve is obtained which can provide the film thickness for a given polymer and solvent. Usually, film thickness is inversely proportional to the square root of the angular spinning speed ω and proportional to the solutions viscosity η to the 0.4-0.6 power^[17].

$$h \propto \frac{\eta^{0.4-0.6}}{\sqrt{\omega}} \quad (2)$$

There are two common ways to realize photoresist's dispersion on the substrate: the static dispense and the dynamic dispense. During the static dispense a small droplet of photoresist is deposited on the substrate while it is immobile. The amount of material deposited is in direct correlation with the viscosity of the photoresist (more viscous photoresists need more material to be placed) and the size of the substrate (bigger substrates need more material for the total coverage of the substrate to be ensured). On the other hand, dynamic dispersion dictates an initial step of spinning at a low speed (typically 500 rpm) while the dispense takes place. After that the substrate is accelerated to its final speed. Theoretically, this approach facilitates the wetting of the substrate the spreading of the material and consequently the film formation especially in the case of photoresists with poor wetability. ^[12, 17, 18]

For both approaches the angular spinning speed and the time of the spinning are the two parameters that affect the final thickness of the film. In general high speed and longer spinning times end up in thinner film formation.

Post-apply bake

What follows is a thermal treatment step called post-apply bake (PAB) (or soft bake). It usually lasts for a minute or two on a hot plate at 110°C. The purpose of this step is to evaporate the remaining solvent from the photoresist and to densify it just before exposure. That renders the coated film more stable and reduces the probability of the covered substrate to stick on the mask during exposure.

Use of the mask/alignment/exposure

Exposure stands at the very heart of the fabrication process. The basic principle behind photolithography, after all, is altering a photoresist's solubility by delivering energy to it via radiation. The stencil that is used to transfer the desired pattern on the photosensitive film is called the "mask". Generally a mask is made of glass (transparent to UV radiation) with a metal pattern on it (usually it is used a 800 Å Chromium film). The glass windows allow the radiation to pass through it with very little absorption while the metal pattern protects the underlying photoresist from any interaction with light. Masks are constructed with electron beam lithography which can result in higher resolution than photolithography^[12]. Special care is also taken in the proper alignment of different device layers to each other during the exposure. As previously stated this is one of photolithography's figure of merit (Registration) and is handled with the use of special marks (alignment marks) strategically placed on the different layers^[14]. After all, registration is one of the main of the advantage of photolithography compared to the rest of the techniques along with its high throughput due to its parallel nature.

There are three different ways to perform the exposure: Contact, Proximity and Projection mode as shown in Figure 1.4.

Contact mode

Contact mode lithography was the first mode to be used in the early 1960s. In this approach the substrate is in physical contact with the mask during the exposure. The alignment of the substrate is made, yet, with the creation of a temporal gap between the two. The resolution of contact printing is rather high as it can go down to the wavelength of the radiation. Nevertheless, the high risk of mask damage due to the contact with the substrate motivated a search for alternative modes of photolithography.

Proximity mode

Here mask and substrate are not in contact anymore as there is a small gap (10-50 μm) between the two. That protects the mask from damage but at the same time lowers resolution due to diffraction effects.

Contact and proximity mode printing are known together as shadow printing. The resolution r for them is given by the formula ^[14, 16, 17]:

$$r = \frac{3}{2} \sqrt{\lambda \left(s + \frac{d}{2} \right)} \quad (3)$$

where λ is the radiation wavelength, s is the distance between the mask and the substrate and d is the photoresist thickness

Projection mode

This is the mode of choice used in semiconductor industry from the mid-1970s to today. In projection printing, there is no direct contact between the mask and the substrate as the mask is projected onto the substrate through a lens system. This approach protects the mask from damage since there is no physical contact involved. In addition, the demagnification of the mask pattern achieved with the optics results in high resolution and makes the mask fabrication a little easier^[12].

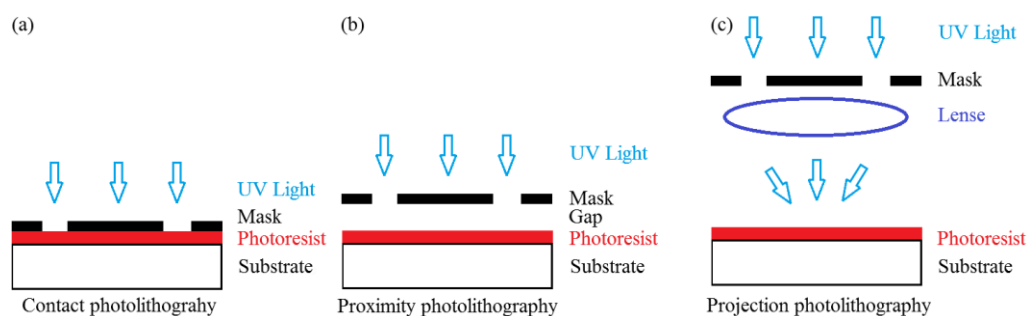


Figure 1.4: Schematic representation of the three exposing modes. (a) Contact photolithography. (b) Proximity Photolithography. (c) Projection mode.

The resolution r for projection printing is given by ^[14, 16, 17] :

$$r = k \frac{\lambda}{NA} \quad (4)$$

where k is a coefficient that depends on process-related factors and NA is the numerical aperture.

Development

After exposure, a development step will allow the latent resist pattern formed to be revealed. A selective dissolution creates a relief that will serve as a mold for the next fabrication steps. Development is of extreme importance as it controls the quality of the transferred motif.

There are two main approaches to perform this step: wet development and dry development.

Wet development

In wet development aqueous and organic solvents are used to dissolve selectively the exposed photoresist. Positive photoresists are developed in aqueous alkaline solutions while negative photoresists are developed in organic solutions. Aqueous development is preferable for environmental reasons and that is why newer negative resist may also be developed in aqueous solutions^[12]. The aqueous solutions are usually tetramethyl ammonium hydroxide (TMAH)-based. The solvent is applied either by immersion or by spraying (with or without substrate spinning)^[12, 17].

Dry development

Dry development is an alternative approach dictated mostly by the need for developing cleaner fabrications techniques. It is based on oxygen-reactive etching for the appearance of the desired pattern. Exposure alters the photoresist's etching resistance rather than its solubility to a solvent^[12, 17]. After development, the substrate is rinsed and dried with dry air or nitrogen. Visual inspection guarantees the quality of the pattern and the lack of defects.

Descumming and postbaking

Descumming is a mild oxygen plasma treatment to remove any residual resist after development. It removes tiny amounts of unwanted material without harming the

desired features. Patterned resist is also affected but as long as only a few hundred Angstroms are removed this is not causing any fabrication concerns^[16].

Just before the printed, in the photoresist, pattern is transferred onto the substrate, a post baking step (also known as hard baking) takes place. Hard baking promotes interfacial adhesion of the film and removes the residual solvent. It usually occurs at the temperature of 120°C (slightly higher than the one used for soft baking) which additionally cross-links the photoresist making it harder and more resistant to the etching steps that follow. Special care should be taken in order for the temperature not to cause flow or melting of the photoresist as this will cause degradation of the profile of the resist.

Pattern transfer

The previous steps create the desired pattern on the photoresist. The next goal is to transfer this pattern (or its negative) from the photoresist onto the substrate. There are two different methods to achieve this goal: a subtractive process and an additive one^[9, 17].

In the subtractive method, first a material film is deposited on the substrate. Photolithography creates a positive image of the pattern and then etching removes the excess material leaving behind the desired structure. The additive method, on the other hand, uses photolithography to create first a negative image of the pattern and then to realize its positive version via selective deposition of material. Both these methods will be further developed with case studies later in this chapter.

Etching is one of the most crucial parts in fabrication. Selective etching creates the required polymer microstructure during the subtractive approach while it controls the material deposition in the additive one. In general etching is a method of removing material which is not protected under the photoresist. It can be done chemically, mechanically or with a combination of the two mechanisms.

Wet etching was initially the method of choice in the microelectronic industry. An acidic solution was used to erode the thin film not covered by the photoresist creating a selective 3D structure. Nevertheless, the method's isotropic nature usually resulted in an undercut profile damaging the overall resolution. Consequently, new dry etching approaches quickly became popular as they could provide etching in an

anisotropic way. Plasma etching, in particular, uses plasma (an ionized gas) to anisotropically and selectively etch only the patterned material and not the photoresist above it, allowing fabrication with sub-micrometer resolution. As dry techniques are easily automated and remove the need for toxic developers, it is not a surprise quickly rose to dominance ^[16].

Many different dry etching techniques have been developed, but among them reactive ion etching (RIE) offers the benefits of both the chemical and the physical etching worlds. RIE uses plasma to create ionized atoms which can be accelerated by an electrical field and cause a directional sputtering of the substrate. This is extremely important in giving anisotropy to the technique. The charged molecules gain kinetic energy which they transfer to the film in the collision, etching it vertically. At the same time they provide the energy for an etching reaction to take place which is selective due to its chemical nature.

The deposition of the material of interest, mentioned above, is done with a number of different techniques. Chemical Vapor Deposition (CVD), Physical Vapor Deposition (PVD), sputtering and electroplating are among them. Here we are going to focus on thermal evaporation as it widely used for metal film deposition and it will prove to be extremely useful for the fabrication of the organic devices that follows.

Stripping

The last step of the fabrication process is the removal of the remaining photoresist. That will create patterns by selectively discarding the evaporated material which was deposited on the photoresist while leaving the rest intact. The photoresist acts now as a sacrificial layer and is removed along with the metal layer on top of it, creating the desired metal profile. Photoresist stripping is usually performed with the help of organic solvents. Acetone is very commonly used for this task, along with other phenol-based commercial strippers. Nevertheless, environmental issues favor the use of dry stripping methods such as oxygen plasma. In any case, the ultimate criterion in the stripping approach is not to destroy the target material film. Especially for organic materials this criterion poses a number of extra difficulties due to incompatibilities with the majority of solvents.

1.2.4 Photolithography in polymer device fabrication

The previously presented steps of conventional photolithography could have theoretically been implemented in polymer device fabrication as well. The main challenge of organics, though, is the incompatibility issues between organic films and the solvents used during optical lithography. Unfortunately, the solvents employed for depositing, developing and removing photoresists usually have a destructive effect on organic materials (including dissolution, cracking, swelling and delamination of the polymer film^[9]). During the past years, two different but representative strategies that have been developed to overcome these limitations are presented here.

Sacrificial layer methods

An alternative way of patterning organic materials, developed by DeFranco and co-workers, is based on the use of a Poly(monochloro-p-xylylene (Parylene-C) sacrificial buffering layer^[9]. Parylene-C (a polymer widely used as a barrier layer) is employed to protect the organic film during each step of the photolithography fabrication (deposition, development and strip of the photoresist). After Parylene-C deposition, the formed film is inert and resistant enough to withstand a photolithography step on it.

From this point, two different fabrication methods (an additive and a subtractive one) lead, eventually, to the organic material patterning ^[9, 19]. For the subtractive method the developed photoresist serves as a mask to selectively etch and remove both the Parylene-C layer and the organic film under it. In the additive method, on the other hand, the photoresist acts as contact mask and an etching step leaves behind voids in the Parylene-C to be filled with the polymer. Both these approaches can give high quality patterned polymer films and are shown schematically in Figure 1.5.

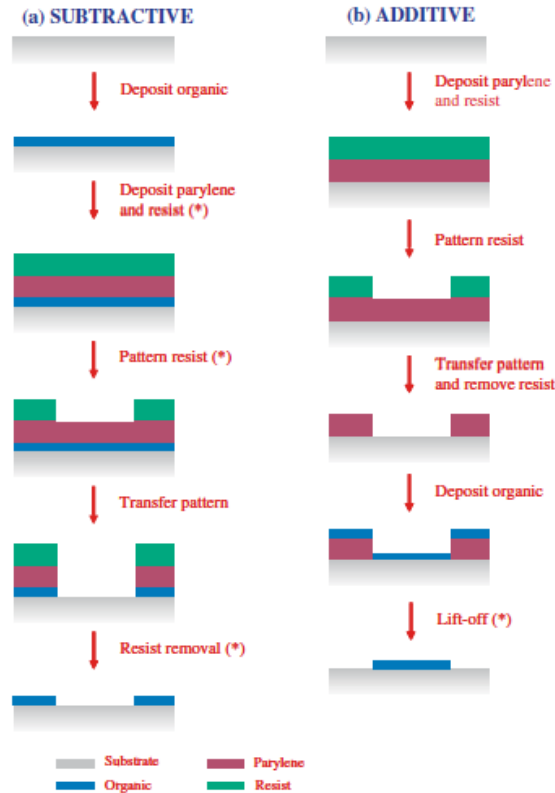


Figure 1.5: (a) Subtractive and (b) Additive fabrication approaches. The asterisks indicate the steps where the organics would be damaged during conventional photolithography. [Reproduced with permission from Ref.4]

The next two case studies are paradigms of the aforesaid additive and subtractive methods implemented in organic device fabrication. The active area of those devices is covered with a thin polymer (PEDOT: PSS) film while the electrodes and their wiring are gold patterned with the use of conventional photolithography techniques. Both methods are versatile, generic and can be used for direct patterning of polymer films in a variety of organic devices (polymer covered electrodes, organic transistors, etc.).

Subtractive patterning

A subtractive method that can result in high performing devices was presented in 2011 by D. Khodagholy and co-workers^[20]. In this approach PEDOT:PSS covered gold electrodes were fabricated on a 2 μ m Parylene-C film that served as a flexible substrate. Initially, gold electrodes, interconnects and pads were patterned on a Parylene-C film via standard photolithography. A second 2 μ m thick film of Parylene-

C was used to insulate the device while a second photolithography step followed by oxygen etching (RIE) opened windows over the recording sites and pads. The polymer (PEDOT:PSS) was deposited through spin casting and the devices were coated with a third (sacrificial) layer of Parylene-C. The final photolithography and etching step defined the PEDOT:PSS coated electrodes. Immersion of the device in deionized water promoted the removal of the Parylene-C sacrificial layer exposing the electrodes (Figure 1.6).

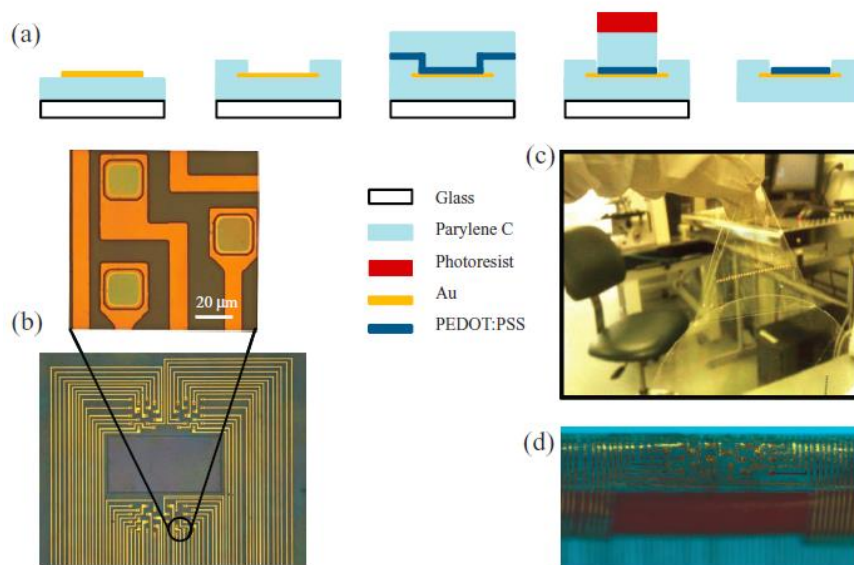


Figure 1.6: (a) The main steps of the fabrication process. The final array of electrodes is mounted on a Parylene-C substrate. (b) Optical image of the electrode array with a close up on three electrodes. (c) The electrode array can support the weight of a quartz wafer. (d) The array can conform to a cylinder of 2.2 mm radius. [Reproduced with permission from Reference 16]

The process success relies on the fact that the polymer film adheres better on gold than on the Parylene-C film above it. In addition, due to its hydrophobic character, DI water facilitates the sacrificial layer's peeling off without affecting the organic film's quality and conductivity. The conducting film's integrity is also guaranteed during the Parylene-C deposition process. The above points render the method generic, versatile and usable for different types of conducting polymers as they also become hydrophilic when doped.

Parylene-C plays a key role in the studied fabrication approach. It not only protects the organic film which is sensitive to solvents, but also offers electrical insulation for the device which is imperative for its functionality. Parylene-C is a

member of the greater Poly p-xylylene family and is produced with the substitution of one of the aromatic hydrogens by a chlorine atom (Figure 1.7).

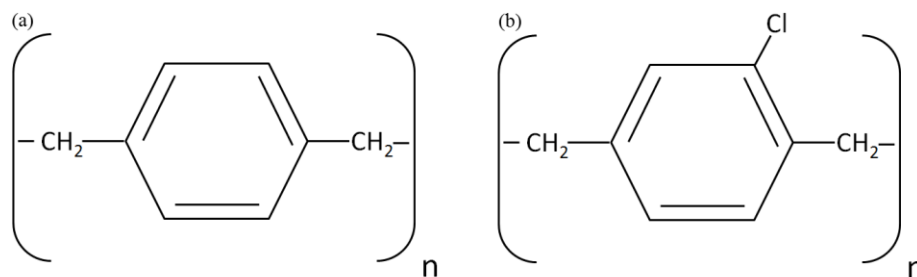


Figure 1.7: Chemical structure of (a) Poly (p-xylylene) and (b) (chloro-p-xylylene)

It has been extensively used in the past for coating purposes. It is a green chemistry polymer as it is chemically inert^[21] and needs no initiator for solvent free deposition as a coating film^[22]. Hence it can be easily deposited on and removed from the polymer films without causing their chemical deterioration^[20].

The material is deposited from its vapor phase via a CVD method proposed by Gorham. Its dimer is heated at 150°C (P= 1 Torr) creating the vapor phase of the material. A pyrolysis stage follows at 680°C (P= 0.5 Torr) that cracks the dimers to give birth to monomer units. The final polymerization step takes place on the device substrate at 25 °C (P= 0.5 Torr) resulting the formation of a thin polymer film^[22]. Most importantly, coating thickness can be controlled accurately and reproducibly through the amount of dimer used.

Additive patterning

An additive method of polymer patterning was presented by Sessolo and co-workers in 2013^[8]. Once more, gold electrodes, contact pads and their interconnections were patterned lithographically, on a glass substrate. The device was coated by a 2µm Parylene-C film which adhered on the substrate with the use of 3-(trimethoxysilyl)propyl methacrylate (-174 Silane). A soap solution was spin casted on Parylene-C to act as an anti-adhesive layer between the first and a second 2 µm Parylene-C (sacrificial) film. A photolithography and an etching step was used to open windows above the electrodes and the pads. After that, the polymer (PEDOT:PSS) was deposit by spin coating on the device and a final peel off step defined the final polymer device structure shown in Figure 1.8.

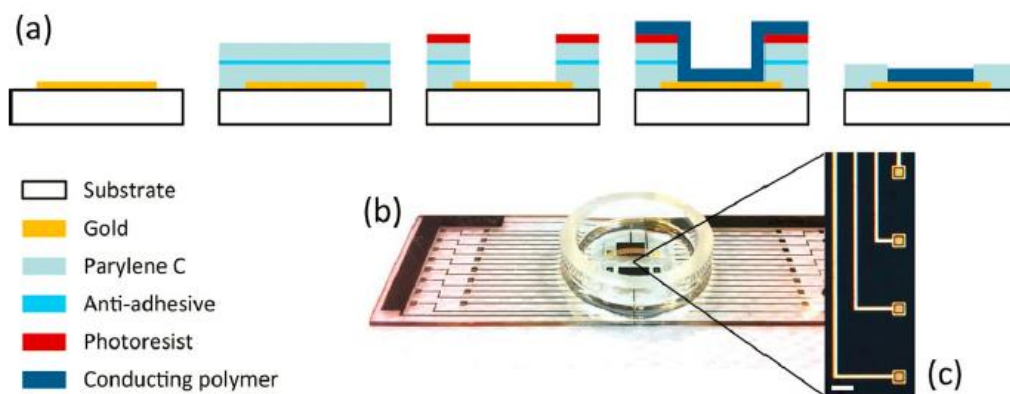


Figure 1.8: (a) The main steps of the fabrication process. The gold electrodes were first patterned lithographically and then Parylene-C was used for the device insulation. A second photolithography step followed by an etching step defines the well for the PEDOT:PSS deposition that follows. A mechanical peel off concludes the fabrication. (b) A Micro Electrode Array device fabricated on a glass slide (c) a close up of the PEDOT:PSS covered electrodes (scale bar 50 μm).[Reproduced with permission from Ref.3]

Once again, the method is generic and versatile, and it can be adapted regarding the desired device geometry. Moreover, different conducting polymers can be used as active layers as long as they can be deposited from solution.

Orthogonal photoresist method

A different way of dealing with the polymer patterning challenge comes with the utilization of orthogonal solvents. The term orthogonal refers to solvents in which the organic compounds are insoluble, a feature that allows not only the patterning of organic electronic materials but also their multilayer deposition.

Hydrofluoroethers (HFEs) , in particular belong to a class of solvents which, besides being nontoxic and environmental friendly, are also orthogonal to many organic materials^[23]. Consequently, they are ideal candidates for polymer patterning as long as a photoresist compatible with them is synthesized.

A photoresist like this was presented in 2009 by P.G. Taylor et al ^[10]. The HFE compatible material is a co-polymer composed of a highly fluorinated monomer **1** (3,3,4,4,5,5,6,6,7,7,8,8,9,9,10,10,10-Hepta-decafluorodecyl methacrylate) and a photosensitive monomer **2** (2-Nitro-benzyl methacrylate) (Fig 1.9). Its solubility can be modified after UV exposure from soluble to insoluble in HFEs solvents due to

structural changes to the photosensitive **2** part of the molecule, resulting in a negative tone photoresist. In addition, it is acid stable, a feature extremely useful when it is used to pattern acidic polymers.

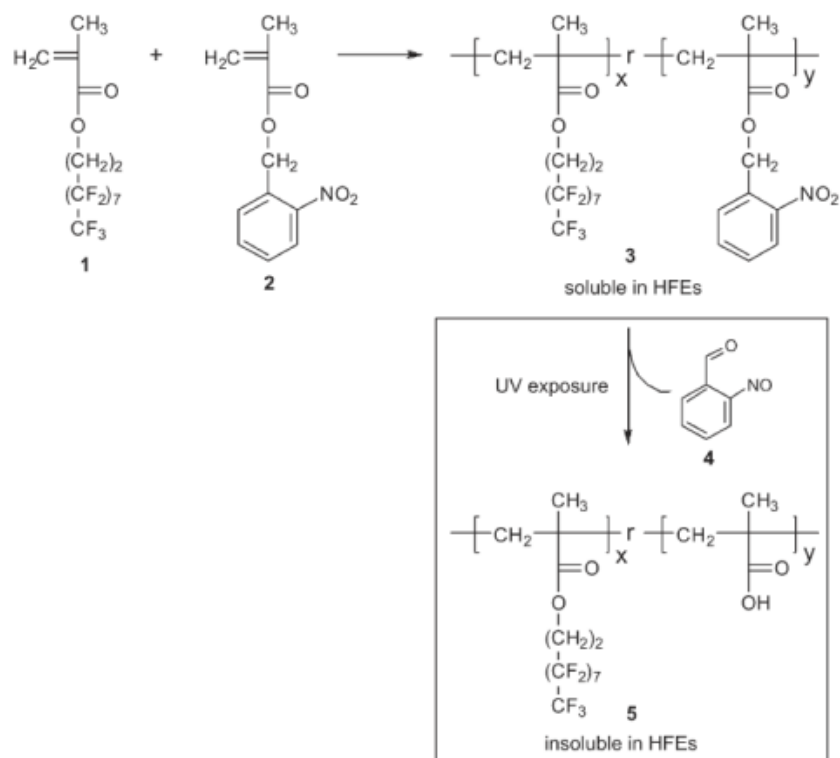


Figure 1.9: Synthesis of the HFE-soluble photosensitive co-polymer **3**. Exposure to UV light renders the polymer insoluble in HFEs. [Reproduced with permission from Reference 5]

As a proof of concept, a bottom contact organic thin field transistor was fabricated with a pentacene channel and PEDOT:PSS drain and source electrode by the same group. On a Si wafer, a 360 nm oxide was grown thermally just before PEDOT:PSS was spin cast and baked at 180°C for 10 min. Photoresist **3** was then spun on the PEDOT:PSS layer and patterned lithographically with HFE-7200 (an isomeric mixture of methyl nonafluorobutyl ether and methyl nonafluoroisobutyl ether) acting as its developer. The image was transferred on the PEDOT:PSS with oxygen etching and the remaining photoresist was lifted off in a propan-2-ol (10% by volume)/HFE-7100 mixture. Photoresist **3** was spun again on the patterned PEDOT:PSS film, this time followed by UV light exposure and a development step. Pentacene was thermally evaporated and the photoresist removal in the previously used solvents mixture ended up a pentacene channel connecting the PEDOT:PSS source and drain electrodes (Figure 1.10).

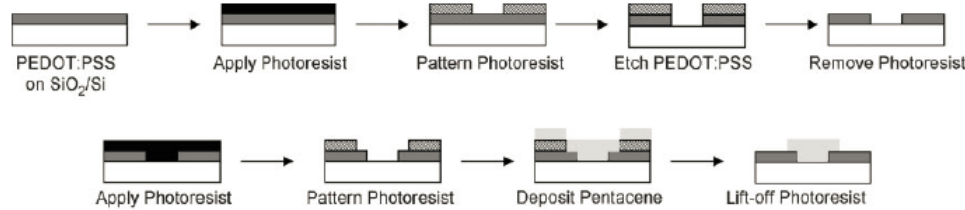
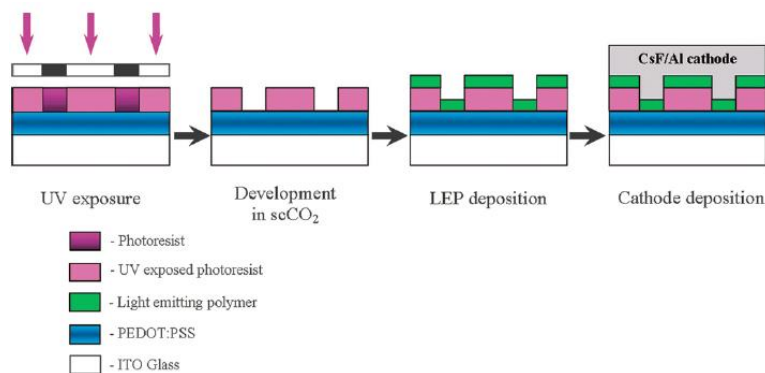


Figure 1.10. Main fabrication steps of the PEDOT:PSS/Pentacene bottom-contact Organic Thin Film Transistor. PEDOT:PSS was first spin cast on the substrate and patterned photolithographically with the use of the photoresist 3 as a developer and a following oxygen etching step. The process was repeated for the deposition of the pentacene film giving birth to the organic thin film transistor. [Reproduced with permission from Reference .5]

In a similar approach, H.S. Hwang and co-workers were able to pattern polymer materials using supercritical carbon dioxide (scCO₂) as solvent^[24] to fabricate an OLED. ScCO₂ is an environmental friendly fluid used in dry photolithography process (DPP) for resist stripping due to its physical and chemical advantages. Most importantly, it is a poor solvent for most ionic, high molecular weight and low pressure organic materials.

In their work, a light emitting polymer (LEP) was patterned on top of a PEDOT:PSS active layer. PEDOT:PSS was first spin cast on glass coated with indium tin oxide (ITO). A negative tone co-polymer was synthesized from 1H,1H,2H,2H-perfluorodecyl methacrylate (FDMA) and tert-butyl methacrylate (TBMA) and deposited on the PEDOT:PSS layer. After UV exposure, scCO₂ was used for the development followed by oxygen plasma cleaning treatment and a LEP spin casting step. A thermally deposited CsF(1nm)/Al(40nm) film completed the ITO/PEDOT:PSS(CH8000) /LEP/CsF/Al structure (Figure 1.11).

Figure 1.11: The main steps of the OLED fabrication process. PEDOT:PSS was spun on the substrate and a negative tone photoresist was used to pattern the LEP on top of PEDOT:PSS. The developer used was sCO₂ which is not harmful to the active material. A CsF(1nm)/Al(40nm) film completes the device fabrication. [Reproduced with permission from Reference 20]



1.3 Concepts of Neuroscience

Brain is, without any doubt, the most marvelous and remarkable organ in the human body. It is the center where the stream of environmental signals is sorted out to those events that are important for the survival or the well-being of the individual. Putting in a different way, it is the center where perception is organized and either is stored in the memory for future reference or is translated into an immediate action^[25].

Going a step further, brain is something more than just the center for moving and sensing functionality. It is the part of the body where processes like thinking and emotion creation take place, giving birth to the notion of consciousness. This is why Scientific American in 2014 named the new century the century of the brain. This is also why the new trend in science dictates large scales initiatives to facilitate recording and controlling brain activity as part of a greater effort to understand this extraordinary biological machine (e.g. “Human Brain Project”, “Brain Activity Map”). After all, the study of the brain is in its base the study of our own selves and mankind has always been fascinated by the idea knowing its inner world.

In practice, brain functionality is based on a very big number of interconnected nerve cells that form a complex information processing network. There are two main nerve cell classes participating in this task. The neural cells (or neurons) and the glia cells (or glia)^[25, 26]. (Some scientists will argue there are three if we count the blood vessels as well. Blood vessels’ main role is to provide the neural cells with glucose, the basic energy fuel)

1.3.1 Neurons

Neurons are the basic units of the brain. Inside the human brain we can find a little bit less than 100 billion individual neurons a number of the same order of magnitude with the number of stars in the Milky Way Galaxy. These neurons can be further classified to a thousand different types. Nevertheless, it is more the organization of them into different neuronal circuits that creates the complexity of the human behavior and less their variety. In other words, the same type of neurons can participate in different signaling function depending the way they are interconnected with other neural cells.

A typical neuron consists of four distinct parts:

1. The cell body (or soma)
2. The dendrites
3. The axon
4. The presynaptic terminals

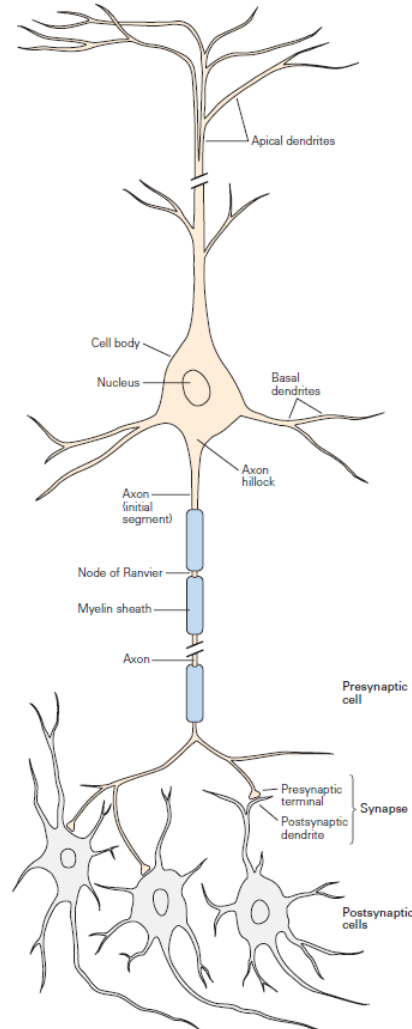


Figure 1.12 :Schematic of a typical neural cell^[27].

The cell body is the metabolic center of the cell and the part of the cell where the nucleus is located. As a consequence, this is where the protein synthesis takes place. There are two kinds of processes that arise out of the soma. The fine branching structure of many short dendrites and a single long axon. Dendrites' role is to receive information from other cells while the axon's to send signals to other cells. These signals are of electrical nature and propagate in the form of Action Potentials (AP). The term action potential refers to a fast membrane depolarization event (initially the inside of neuron membrane is negative in respect to the positive extracellular area) and a subsequent re- polarization. Nevertheless, neurons are not only electrical active

cells they are also secretory ones. They secrete molecules through their presynaptic terminals, the fourth of their distinct part. These molecules are called neurotransmitters and are the chemical substances that alters the electrical properties of the target cell by binding to special transmembrane proteins called neurotransmitter receptors^[25, 26]. The overall idea is that neurons transform the signal that they receive as a molecular input into an electrical one that can travel faster to the next neuron where it can be changed back to its chemical form before interacting with it.

Neuron can be classified into three major categories regarding their form. Thus we can talk about 1) Unipolar 2) Bipolar and 3) Multipolar neurons

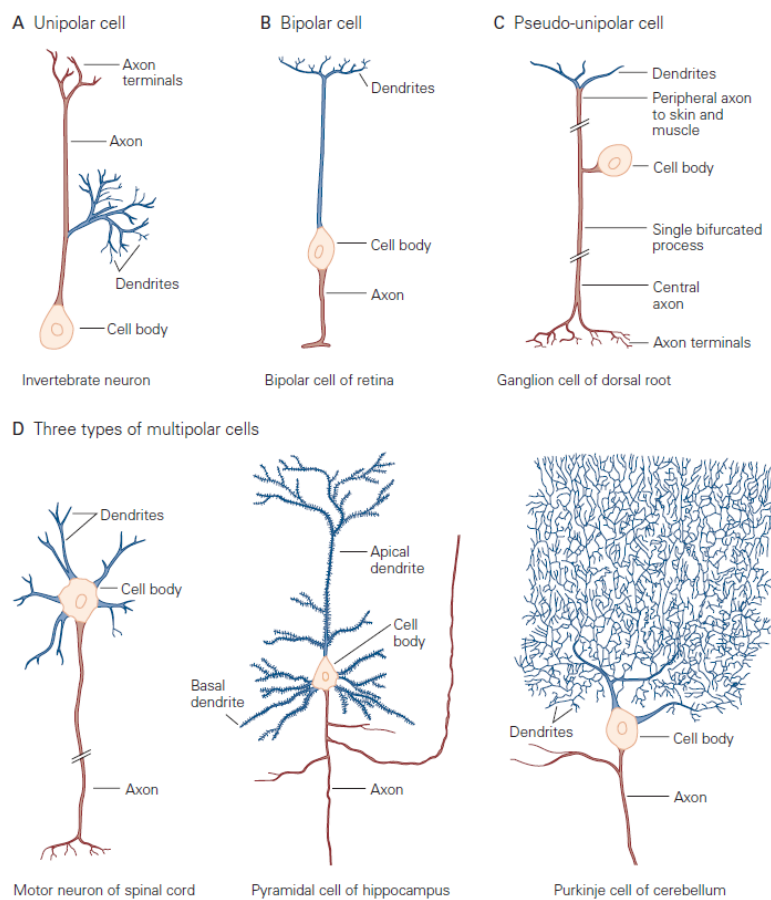


Figure 1.13 : Neural cell classification^[27].

This classification is based on the number of processes emerging from the cell body but it has significance in the neuron’s functionality as well. For example unipolar neurons are mainly found in the invertebrate nervous system and in the autonomic nervous system of the vertebrate animals. They have only one process which is later divided into an axon and a dendrite branch. Bipolar on the other hand,

are mainly sensory neurons with their dendritic part able to receive information from the periphery of the body while their axonal part forwards this information to the brain. A special subcategory of bipolar cells is the pseudo-unipolar which are the cells that transfer information of pain, pressure and touch to the spinal cord (DRG cells). Last but not least, multipolar neurons are the ones that we can find in abundance in the neuron system of the vertebrate kingdom .They have one axon and many dendrites which allows them to make a number of different connections with other neurons^[25].

1.3.2 Glia

The term glia ($\gamma\lambda\acute{\iota}\alpha$) comes from the Greek language and it means glue. It was conceived in 1895 by Rudolf Virchow as an effort to describe an “inactive substance” that holds the nerves together in the central nervous system ^[28]. Yet, glia does not really hold the neurons together. Instead, it surrounds them having a supporting to them role.

Glia cells are morphologically very different from the neurons as they do not have the typical soma-axon-dendrite structure of the later. In general, they present a remarkable diversity linked to their multi functionality and outnumber neurons by a factor of 2 to 10. Nevertheless, glia on vertebrates can be divided in two major categories. Microglia and Macroglia^[25].

Microglia are cells of the immune system while Macroglia has a slightly different more supporting role and is subdivided into Oligodendrocytes, Schwann cells and Astrocytes. For the first two (Oligodendrocytes and Schwann cells) there is not much of a dispute regarding their role. We know, today, that these are the cells that provide an insulating layer, called myelin, which is essential for the fast transfer of the electrical signals between the neurons.

Nevertheless, Astrocytes' role is still a mystery for the scientific community. We believe that their main function is to retain the central nervous system homeostasis^[28]. It is believed that they do not take part in information processing but they provide neural support in four ways ^[25] :

- 1) They separate cells and thus provide electrical insulation between neuronal groups.

- 2) They regulate the concentration of K^+ at the between the neuron space by absorbing the excess of the cation and a consequence ensure the quality of the signaling between the neuron cells.
- 3) They perform neurotransmitters' up taking from the synaptic clefts.
- 4) They secrete growth factors that nourish surrounding neurons.

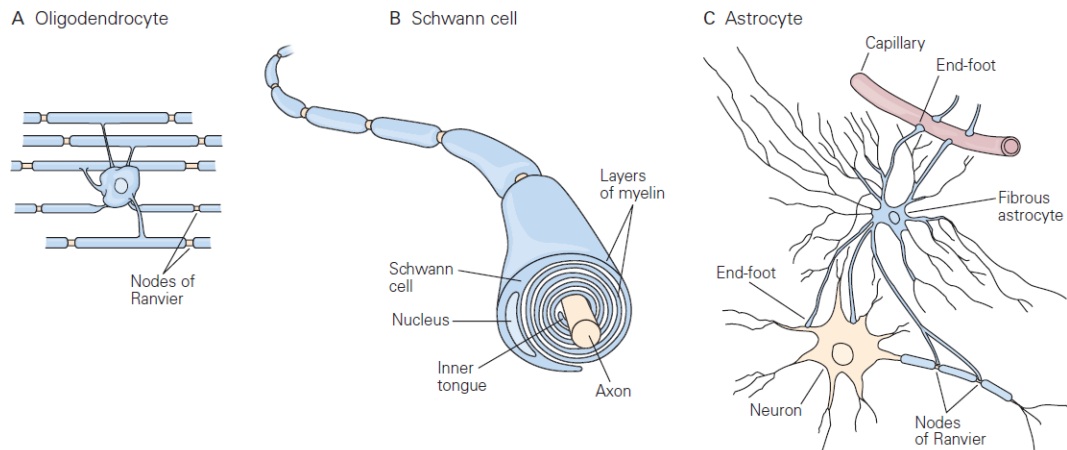


Figure 1.14: Glia cell classification^[27].

It is a common belief that astrocytes are not excitable cells. Nonetheless, it has been recently shown that the astrocyte membrane possess neurotransmitter receptors that could possibly trigger electrical and biochemical events inside the glial cells^[29]. This is something we try to explore in Chapter 6 of this thesis.

1.3.3 Action Potential

Neurons are using electrical signals to convey messages among them and to communicate. The basic unit that carries information from one neuron to another in the nervous system is called action potential (AP). An action potential is a fast, transient change in the membrane potential usually generated at a specialized part of the soma called the axon hillock, and which travels away from the cell body through the neuronal axon.

But how does the action potential is really generated? To answer this question we need to take a step back and study a bit the cell membrane physiology. The neuron cell membrane is a phospholipid bilayer which separates the interior of the cell from

the exterior. At the same time it creates a concentration gradient of some specific ions (most important of which is sodium Na^+ and potassium K^+) between the inside and the outside. This can be achieved through specialized transmembrane proteins. The proteins that create and maintain the concentration gradient are called active ion transporters (ion pumps) while other proteins that selectively allow ions to pass through them in a passive way are called ion channels. The ion channels can be either voltage or ligand gated. This means that they can respond either to changes in the voltage or to the binding of chemical molecules.

The role of the two kind of proteins is complementary as the transporters create a concentration gradient that could lead to ion flux through the ion channels and to electrical signal creation^[26].

Due to this unequally distribution of ions across the plasma membrane a membrane potential is generated which is called resting potential V_m . At rest, there is an excess of positive charges at the external of the membrane while the cytosol has an excess of negative ones giving rise to a negative value of about -70mV (by convention the potential outside the cell is zero). All of the neural signaling is happening when ion fluxes across the cell membrane causes fluctuations from this resting value^[25]. It is also worth noticing that at this point the concentration of sodium ions is greater in the outside of the cell than the inside while the concentration of potassium channels is in the inside.

Responding to external stimulus which is greater than a threshold value, the cell membrane becomes permeable to sodium ions (Na^+) which rush inside the neurons cytosol through the sodium ion channels. This causes the voltage in the inside to rise while the cell goes under a depolarization phase. The membrane voltage rises up to a value of approximately $+30\text{mV}$ when the sodium channels closes and the potassium channels open to allow an outward this time current. This time the membrane voltage drops to a negative value (repolarization phase).

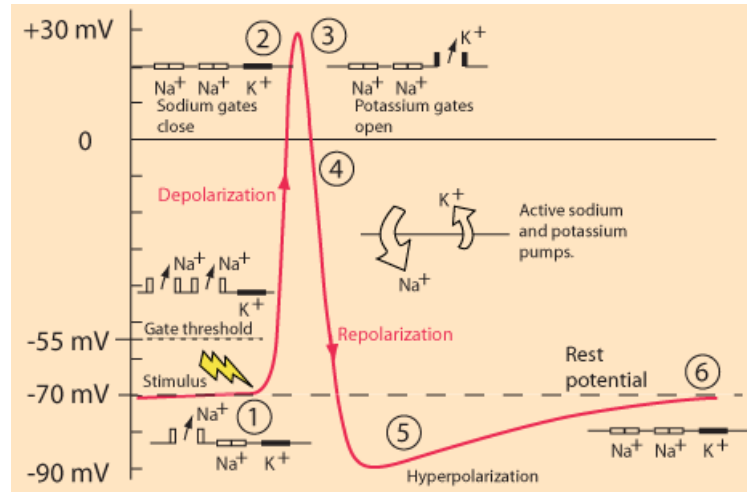


Figure 1.15: Plot of the phases of an action potential ^[30].

In most nerve cells, the potassium ion channels remain open even after the resting potential value is reached and potassium ions K^+ continue to rush out of the cell resulting in a membrane potential even more negative than the -70mV that can be measured at rest. This phase is called hyperpolarization phase (or undershoot) and defines the end of the action potential. Hyperpolarization is very important phase in information propagation. It prevents a neuron from receiving any stimulus and as a consequence from “firing” a new action potential (or makes it very difficult to do so by raising the activation threshold). In other words, it creates an absolute refractory period and/or a relative refractory period ensuring that no trigger will create an action potential travelling the opposite direction^[25, 30]. After hyperpolarization, Na^+/K^+ ion pumps will restore the membrane voltage to its resting potential value of -70 mV .

The time duration of the action potential last from 1-4 ms while the amplitude of the intracellular voltage fluctuation is about 100mV .

1.4 Concepts of Electrophysiology

Despite the fact that organic bioelectronics is a very broad field that embraces every possibly interaction between biology and electronics, electrical interfacing with the nervous systems is definitely one of most impressive and promising areas of scientific implementation.

Going back in time, the origins of this effort can be traced in the 18th Century when Luigi Galvani performed his, now considered to be pioneering, experiments.

Galvani was able to make the detached legs of a frog move just by applying a small electrical voltage to them creating the newborn field of electrophysiology.

In reality, the actual birth of the field should be located even earlier in the 1660 and the work of the Dutch microscopist and natural scientist Jan Swamerdamm and his neuromascular preparation ^[31]. Swamerdamm came real close to understand the nature of this interaction between nerves and muscles but it was no other than Isaac Newton who talked first about the idea of neural electrical signals. Nevertheless, he was convinced about the lack of appropriate experiments which could reveal the physical laws behind them. This experimental proof came 80 years later, in 1791 with the publishing of Galvani's work entitled "*De Viribus Electricitatis in Motu Musculari Commentarius*"^[31].

Electrophysiology is a compound word of Greek origin. It is made up of the word Ηλεκτρον (electron), φύση (nature,origin) and λόγος (study). It involves the study of the electrical properties of cells and tissues. It is performed with the measurement of either voltage or current and it can be applied in different scales. From a single ion channel and a cell to whole organs like the heart or the brain.

A broad categorization of the Electrophysiological techniques can make a distinction between *in vivo* and the *in vitro* preparations. *In vivo* are the techniques in which implantable probes are used to measure neural activity while the subject is still alive. In *in vitro* techniques on the other hand the recording devices are fabricated on glass and cell cultures or organs are placed on them. My work was exclusively based on *in vitro* recording techniques so I am going to give a small introduction on them leaving aside the *in vivo* approaches.

***In vitro* electrophysiology**

The *in vitro* electrophysiological approaches can be either intracellular or extracellular.

When intracellular recordings are performed a probe (microelectrode) penetrates the cell membrane and records the voltage (or the current) across the membrane. Typically it involves an electrode inside the cell and a reference electrode

outside of the cell. The technique was further developed by Cole, Hodgkin and Huxley resulting in the voltage clamp

Voltage clamp: In this approach a sharp microelectrode penetrates the cell membrane and “clamps” the voltage to a fixed value. The technique is based on the use of a voltage amplifier that holds the potential of the membrane fixed by injecting current inside the cell. This current is equal in amplitude and opposite in sign to those running out of the cell. These injected currents measure the ionic and capacitive currents flowing in and out of the neuron^[32]. A variation of voltage clamp is the current clamp.

Current clamp: In current clamp, on the other hand, the membrane’s voltage is left free to vary and is recorded as a response to a current stimulation applied to the cell by the recording electrode

Neher and Sakmann in 1976 developed the microelectrode intracellular method even further resulting in the Patch clamp approach.

Patch clamp: With the patch clamp technique a slightly different approach than before is followed. This time a glass pipette with a very small tip is used to form a very close contact with a part of the cell (patch) mostly by application of a small suction. This mode of the Patch Clamp technique is called “cell-attached” and is used to study the ion channels that are present in the patch. If more suction is applied then the patch is removed allowing the interaction between the inside of the cell and the micropipette. This is called “whole-cell” mode and allows the recording of voltage and currents originating from the entire cell.

In general, intracellular recordings allow ionic and synaptic conductance measurements along with subthreshold events which cannot be recorded with extracellular electrodes. Nevertheless, they cannot target multiple cells simultaneously and they are destructive for the under-studied neuron.

For the extracellular recordings the approach is different than the above. The goal is now to monitor the neural activity outside of the cell membrane. In practice, voltage variations are measured in a conductive extracellular field generated by a current flow with the help of an electrode placed as close as possible to the active neuron^[33]. This voltage is always measured in respect to a second electrode far away

from the first one ^[34]. The obtained signal is led to an operational amplifier and after that, usually, to an automated recording system.

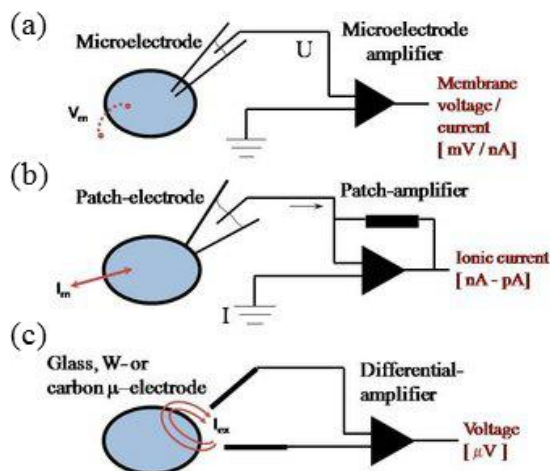


Figure 1.16: The *in vitro* recordings set ups. (a) Impaling microelectrode recording (b) Patch-clamp recording and (c) extracellularly microelectrode recording^[35].

The *in vitro* extracellular recording technique is usually easier to be implemented as it takes place in a controlled experimental environment. It is non-invasive and therefore ideal for chronic measurements as the under investigation neurons remain unharmed. It offers the privilege of synchronous recording from multiple sites allowing simultaneous recordings from multiple cells, something unachievable for the intracellular techniques. In addition, it is consistent with the 3Rs (Replacement, Reduction, Refinement) principle which dictates the less possible use of animals for experimental purposes due to ethical restrictions. Lastly, it is suitable both for basic research allowing a profound understanding of the neuronal signaling mechanism and for its technological implementation (e.g. drug screening platforms).

Its main drawback is the low amplitude of the signal that is targeted (typically about 100 μ V) due to its attenuation inside the extracellular space and the fact that it cannot record subthreshold events like post synaptic potentials ^[33].

Typically the extracellular recordings can be sorted into three categories. Single unit recordings, multi-unit recordings and Local Field Potential recordings.

If the extracellular recording electrode is small enough (about the size of a single neuron), then singlet-unit recordings are obtained. That means that action

potentials for a single neuron in the proximity of the extracellular electrode are recorded in a way very similar to the intracellular methods. Nevertheless, these APs are typically three orders of magnitude smaller in amplitude. In addition they usually show an inverse polarity in respect the intracellular recordings as extracellular electrodes sense the ion flux that creates the neural activity from a different angle.

If the size of the recording extracellular electrode is a bit bigger than the size of a single neuron then action potentials from more than one cell are recorded in a mode called multi-unit recording. In that case a process called spike sorting is usually applied. Spike sorting aims to distinguish the different action potentials coming from different cells.

Lastly, extracellular electrode can also record (Local) Field Potentials-LFPs. These are signals that are created by the sum of the activity of many single cells. These signals are typically slower than the action potentials (they present a frequency lower than 200Hz) and have a bigger amplitude (typically varies from a hundred of μV up to a few mV). Despite the fact that due their nature it is hard to locate the origin of the creation of LFP, they also present neurophysiological interest as they encode the dynamics and the function of the neural circuits.

References

- [1] R. M. Owens, G. G. Malliaras, MRS Bulletin 2010, 35, 449.
- [2] J. Rivnay, R. M. Owens, G. G. Malliaras, Chemistry of Materials 2014, 26, 679.
- [3] M. Berggren, A. Richter-Dahlfors, Advanced Materials 2007, 19, 3201.
- [4] Y. Kuwane, T. Masuda, T. Higashimura, Polym J 1980, 12, 387.
- [5] C. W. Tang, S. A. VanSlyke, Applied Physics Letters 1987, 51, 913.
- [6] G. Malliaras, R. Friend, Physics Today 2005, 58, 53.
- [7] S. R. Forrest, Nature 2004, 428, 911.
- [8] M. Sessolo, D. Khodagholy, J. Rivnay, F. Maddalena, M. Gleyzes, E. Steidl, B. Buisson, G. G. Malliaras, Advanced Materials 2013, 25, 2135.
- [9] J. A. DeFranco, B. S. Schmidt, M. Lipson, G. G. Malliaras, Organic Electronics 2006, 7, 22.
- [10] P. G. Taylor, J.-K. Lee, A. A. Zakhidov, M. Chatzichristidi, H. H. Fong, J. A. DeFranco, G. G. Malliaras, C. K. Ober, Advanced Materials 2009, 21, 2314.
- [11] J. Huang, R. Xia, Y. Kim, X. Wang, J. Dane, O. Hofmann, A. Mosley, A. J. de Mello, J. C. de Mello, D. D. C. Bradley, Journal of Materials Chemistry 2007, 17, 1043.
- [12] M. J. Madou, *Manufacturing Techniques for Microfabrication and Nanotechnology*, Taylor & Francis, 2011.
- [13] C. G. Willson, R. R. Dammel, A. Reiser, "Photoresist materials: a historical perspective", 1997.
- [14] B. Bahreyni, in *Fabrication and Design of Resonant Microdevices*, (Ed: B. Bahreyni), William Andrew Publishing, Norwich, NY 2009, 9.
- [15] H. J. Levinson, *Principles of Lithography*, Society of Photo Optical, 2005.
- [16] L. F. Thompson, C. G. Willson, M. J. Bowden, "Introduction to microlithography", Washington, DC, 1994.
- [17] C. Mack, *Fundamental Principles of Optical Lithography: The Science of Microfabrication*, Wiley, 2008.
- [18]
- [19] B. Ilic, H. G. Craighead, Biomedical Microdevices 2000, 2, 317; I. Kymissis, C. D. Dimitrakopoulos, S. Purushothaman, Journal of Vacuum Science & Technology B: Microelectronics and Nanometer Structures 2002, 20, 956.
- [20] D. Khodagholy, T. Doublet, M. Gurfinkel, P. Quilichini, E. Ismailova, P. Leleux, T. Herve, S. Sanaur, C. Bernard, G. G. Malliaras, Advanced Materials 2011, 23, H268.
- [21] T. Y. Chang, V. G. Yadav, S. De Leo, A. Mohedas, B. Rajalingam, C.-L. Chen, S. Selvarasah, M. R. Dokmeci, A. Khademhosseini, Langmuir 2007, 23, 11718.
- [22] J. B. Fortin, T.-M. Lu, Journal of Vacuum Science & Technology A 2000, 18, 2459.
- [23] A. A. Zakhidov, J.-K. Lee, H. H. Fong, J. A. DeFranco, M. Chatzichristidi, P. G. Taylor, C. K. Ober, G. G. Malliaras, Advanced Materials 2008, 20, 3481.
- [24] H. S. Hwang, A. A. Zakhidov, J.-K. Lee, X. Andre, J. A. DeFranco, H. H. Fong, A. B. Holmes, G. G. Malliaras, C. K. Ober, Journal of Materials Chemistry 2008, 18, 3087.
- [25] E. R. Kandel, J. H. Schwartz, T. M. Jessell, *Principles of neural science*, McGraw-Hill, Health Professions Division, New York 2000.
- [26] R. b. Donald H Edwards, The Quarterly Review of Biology 2006, 81, 86.

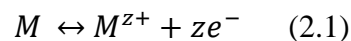
- [27] E. Kandel, J. Schwartz, *Principles of Neural Science, Fifth Edition*, McGraw-Hill Education, 2013.
- [28] P. R. Hof, G. Kidd, J. DeFelipe, J. de Vellis, M. A. Gama Sosa, G. A. Elder, B. D. Trapp, in *Fundamental Neuroscience (Fourth Edition)*, (Eds: D. Berg, F. E. Bloom, S. d. Lac, A. Ghosh, N. C. Spitzer), Academic Press, San Diego 2013, 41.
- [29] M. F. Bear, B. W. Connors, M. A. Paradiso, *Neuroscience : exploring the brain*, 2016.
- [30] <http://hyperphysics.phy-astr.gsu.edu/hbase/biology/actpot.html>
- [31] A. Verkhratsky, O. A. Krishtal, O. H. Petersen, *Pflugers Archiv : European journal of physiology* 2006, 453, 233.
- [32] M. Scanziani, M. Hausser, *Nature* 2009, 461, 930.
- [33] Y. Nam, B. C. Wheeler, *Crit Rev Biomed Eng* 2011, 39, 45.
- [34] V. L. Harvey, A. H. Dickenson, in *Encyclopedia of Psychopharmacology*, (Eds: P. I. Stolerman, H. L. Price), Springer Berlin Heidelberg, Berlin, Heidelberg 2010, 1.
- [35] http://www.scholarpedia.org/article/Intracellular_recording

Chapter 2: Biopotential Electrodes

2.1 Introduction

Up until today the gold standard for electrophysiology measurements has been the use of electrodes (usually referred to as Biopotential Electrodes). These electrodes are coupled with living tissue allowing biological activity recording or even electrical stimulation of living cells in an interactive pathway. Hence, electrodes act as a “transducer” that conveys a “message” from the world of biology to the world of electronics and vice versa. Their role should be even more appreciated if we take into consideration the profound differences between the two worlds. Living cells are soft, fragile, bendable and use ionic currents to communicate. Electronic read out systems on the other hand are rigid, hard, stiff and most importantly use conventional electronic current. Therefore, there is an imperative need of a device that can translate the ionic current to electronic current^[1].

Before moving further into the physics behind this “transduction” let us have a quick look on the nature of the electrodes. Electrodes are, essentially, pieces of metal dipped inside an electrolyte. The moment the electrode is immersed in an ionic conductor an electrode-electrolyte interface is formed. The phenomena taking place in such an interface can be extremely complicated. Nevertheless, in a basic first approximation, the metal dissolves inside the electrolyte and an equilibrium like the one described by equation (2.1) is formed. The phenomenon is called electrolysis.



In the above equations it is assumed that the metal M is immersed in an electrolyte that contains ions of the same metal. This results in the development of a potential since negative charges are accumulated on the metal surface compensated by positive charges in the electrolyte. This potential is called the half-cell potential.

In the above analysis, we have transfer of electrons and as a consequence an oxidation and reduction reaction occurs. These reactions are governed by Faraday’s

law and are called faradaic processes. The electrodes at which these process take place are called charge transfer electrodes or non-polarizable electrodes and behave as resistors^[2].

On the other hand when we consider the case during which non-charge transfer reactions occur then we are talking about ideally polarizable electrodes (IPE). These electrodes are considered to behaving like capacitors.

In reality, electrodes will have both a capacitive and a resistive character. The equivalent circuit of such an electrode consists of a resistor R_s in series with a resistor R that is itself in parallel to a capacitor C ($R_s-(R//C)$). (Figure 2.1)

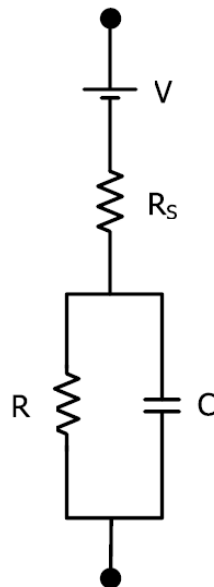


Figure 2.1: Equivalent circuit of a recording electrode inside an electrolyte bath. R_s refers to the solution resistance while R and C are the resistance (faradaic process) and the capacitance (non faradaic process) on the electrode. This equivalent circuit is called a Randels circuit and V represents the half-cell potential.

R_s refers to the solution resistance (to be more accurate this is called the spreading resistance and we will talk about it later in this chapter), while R and C are the resistance and the capacitance that correspond to the electrode. V is the half-cell potential of the interface between the electrode and the electrolyte. Biopotential signals are extracted from the differential between two electrodes; the recording electrode as presented above and a reference electrode. Let us have a look at how this potential is actually recorded. In order to do that we are going to use an IPE. As

already stated there is not such a thing as an ideal IPE since at high enough voltages any electrode can inject/extract electrons to/from molecules in the electrolyte. Nevertheless, noble metals like Pt, Au, Ir and others like Ta/Ta₂O₅ and TiN can act like IPEs over a limited range of applied voltages^[3].

Let us consider a metal IPE immersed in an electrolyte. There is no really charge exchange between the electrode and the electrolyte nevertheless other processes like absorption or desorption may take place. In the case where a small voltage is applied between the electrode and a reference electrode, and after redistribution of the ions inside the electrolyte, a negative ionic charge will appear close to the anode and a positive ionic charge will build up near the cathode. A transient current will flow for a short time until a steady state is reached.

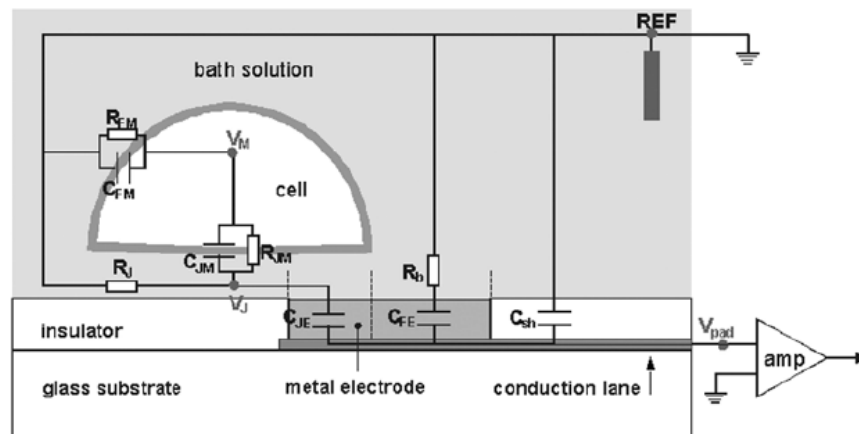


Figure 2.2: Schematic of the extracellular recording of a cell from a planar electrode. The recorded voltage is the difference between the metal electrode and the reference electrode^[4].

Now consider the case where cells are cultured inside the electrolyte (culture media) on top of the metal electrode. The cell soma will partially cover the electrode while the free part of the electrode will be in contact with the culture media and connected to the ground. A set potential is established and the amplifier records the sum of the potential from both the free electrode surface part and the membrane covered one. If we assume that the resistance of the media R_s is low enough to be neglected, then the relation between the voltage at the contact pad V_{pad} and in the cleft between cell membrane and the electrode V_J is given by the frequency-independent relationship (2.2)^[4].

$$\frac{V_{pad}}{V_J} = \frac{\frac{Q}{C_E + C_{sh}}}{\frac{Q}{C_{JE}}} = \frac{C_{JE}}{C_E + C_{sh}} \approx \frac{C_{JE}}{C_E} = \frac{A_{JE}}{A_E} \quad (2.2)$$

where C_{JE} is the capacitance of the covered electrode of area A_{JE} , C_E is the capacitance of the whole electrode with area A and C_{sh} is the shunt capacitance of the connecting lane. Given that $C_{sh} \ll C_E$ the recording signal amplitude depends linearly on the ratio of the covered electrode and the whole electrode area.

$$V_{pad} = V_J \times \frac{A_{JE}}{A_E} \quad (2.3)$$

The take away message is that this simplistic model, electrodes (with the use of ideal bandpass filters) can act as frequency independent voltage followers for the capacitive monitoring of cellular signals^[4].

2.2 Theoretical model of the neural recording

The recording principal of the cell generated electrical signal is based on the extracellular field theory^[5, 6]. A metal microelectrode of about the size of the electrogenic cell is placed as close as possible to the part of the cell that creates ionic current flow. This can be the soma or the axon hillock which generate action potentials that propagate to other passive parts of the cell (dendrites). This transmembrane ionic current consists of two components. A capacitive and a resistive one^[5, 6]:

$$J_m = J_{cap} + J_{res} = C_m \left(\frac{dV_m}{dt} \right) + G_m V_m \quad (2.4)$$

where V_m is the transmembrane potential, C_m is the membrane capacitance and G_m is the membrane conductance.

These currents can be modeled with the help of a distributed current dipole which generates extracellular field potentials ^[5, 7]. The sink of the dipole is located at the soma or the axon hillock (the place where the action potential is created) while the sources are distributed over dendrites. The relative position of the recording electrode with respect to the sink or the source of the dipole will affect the polarity of the recorded field potential (action potential).

The extracellular generated potential at a particular point P is given by:

$$V_e(P) = \frac{1}{4\pi\sigma} \sum_i \frac{J_i}{r_i} \Delta S_i \quad (2.5)$$

where σ is the conductivity of the extracellular medium, J_i is the current density over the i^{th} segment (positive for source, negative for sink), r_i is the distance from the i^{th} segment to point P and ΔS_i is the surface area of the i^{th} segment.

This is the voltage that can be detected and recorded by the extracellular metal electrodes with respect to a reference electrode located inside the bath solution (Figure 2.2).

Going back to the equivalent circuit of the electrode we can now model the metal potential probe with a capacitor (IPE) connected in series with a resistor representing the solution resistance R_s . V represents the half-cell potential as usual (Figure 2.3).



Figure 2.3: A simple equivalent circuit of an electrode consists of a resistor R_s in series with a capacitor C . R_s refers to the solution resistance while C is the capacitance (non faradaic process) on the electrode. V represents the half-cell potential.

This simple circuit can give us now a deeper understanding of the role of the capacitance on the recording of neural activity. Let us assume that the neuron in Figure 2.2 “fires” an action potential. That means that its cell membrane undergoes a fast depolarization/repolarization circle just like the way it has already been described in Sub-Chapter 1.3. In brief, a cascade of biological events, including the opening and closure of sodium and potassium channels, results in ionic currents in and out of the cell. It is the creation of these currents which produce the extracellular potentials of equation (2.5) that is recorded by the electrodes. Considering the equivalent circuit of Figure 2.3 this applied potential will cause a voltage drop across the resistor and the capacitor which is given by:

$$V = V_R + V_C = I \cdot |Z| \quad (2.6)$$

where Z is the complex impedance of the in-series combination of the resistor and the capacitor.

The complex impedance Z and its magnitude $|Z|$ are respectively equal to:

$$Z = R_s + \frac{1}{i\omega C} = R_s - \frac{1}{\omega C} i \quad (2.7)$$

$$|Z| = \sqrt{R_s^2 + \left(\frac{1}{\omega C}\right)^2} \quad (2.8)$$

where i is the imaginary unit ($i^2 = -1$) and ω is the angular frequency.

Therefore in the impedance term involved in the recording of a signal except for the resistive part, there is also a capacitive part related to the double layer capacitor created the moment the electrode is introduced inside the electrolyte bath.

What is really important is to understand the physical meaning behind each term in equations (2.7) and (2.8) and most importantly how these terms affect the quality of the recordings.

The greatest issue in every electrophysiological measurement is the noise that can camouflage the recorded biological signals. In general electrophysiological noise

can be defined as any unwanted signal that can add to the measured signal of interest^[8]. The origin of this noise can be biological (undifferentiated background action potentials/neural noise)^[3], instrumental (wires and recording amplifiers)^[9] or it can stem from the very same electrodes that were employed in the first place to couple the preparation with the recording system^[3, 10]. The latter noise source is the most interesting one to us as it links the physical characteristics of the electrodes with their ability to perform high quality measurements.

In particular, there is an inextricable connection between the electrodes impedance and the noise level acquired, as higher impedance electrodes are expected to have lower signal-to-noise ratio^[1, 3, 10]. Therefore, from a materials science point of view, the use of a material that minimizes the impedance value in (equation 2.8) would be extremely beneficial for improving the recording quality. A new pathway to this direction is provided by conducting polymers and their high capacitance values that they offer.

2.3 Conducting Polymer Coated Electrodes

Measuring the neuron cell activity is far from a trivial task as it poses a great number of challenges. To begin with, the amplitude, of the extracellular action potentials are much smaller than the magnitude of the intracellular ones as the created field potential by the membrane depolarization attenuates exponentially inside the extracellular space according to equation (2.4)^[1, 5]. As a result the recorded signals in the extracellular medium are on the order of $100\mu\text{V}$ ^[1, 11].

In addition, in order for high spatial resolution to be achieved the size of the recording (or stimulating) electrodes should be diminished to about the size of a single neural cell. It is exactly this area reduction that results in an impedance increase due to the inversely scaling of the capacitance C to the electrode size (equation 2.8). Hence, recording and stimulating, becomes harder and harder as the electrodes are made smaller and smaller.

Conducting polymers have emerged as a solution to this problem as they present a significantly reduction of impedance when used as electrode coatings. In addition, they offer means to bridge the mechanical properties mismatch between

metal electrodes and living tissue^[1]. Poly(3,4-ethylenedioxythiophene) polystyrene sulfonate (PEDOT:PSS), in particular, has become an archetype polymer for use in organic bioelectronics due to its unique features^[12].

Historically, PEDOT:PSS was not the first material to be used in the field. Electrodeposited polypyrrole (PPy) on metal electrodes was the initial conducting polymer of choice back in the early days. Nevertheless, PEDOT:PSS has established its position as more chemically and mechanically stable material^[13]. (Figure 2.4)

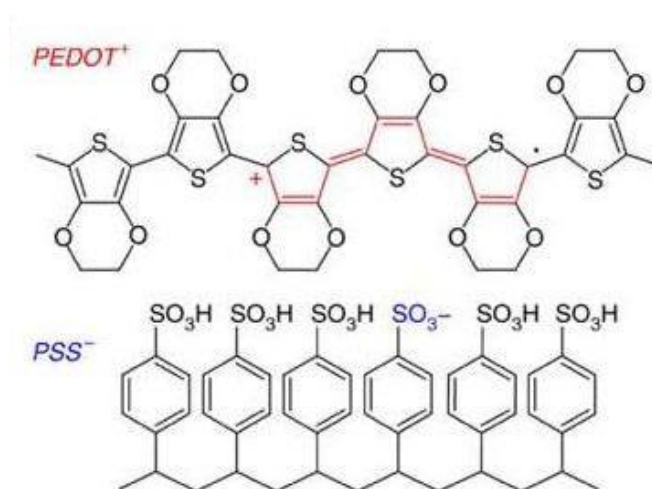


Figure 2.4: Chemical structure of PEDOT:PSS.

PEDOT is a conjugated polymer, hence a semiconductor, which is degenerately p-type doped by the sulfonate groups of the PSS chain. If we wanted to draw an analogy with silicon, PEDOT would be the silicon and the sulfonate ions would be the boron acceptors. The main differences are that doping is not done by substitution (the dopant is not introduced in the PEDOT chain, but near it), and the fact that the dopant is introduced in large quantities (there is more PSS than PEDOT in a typical formulation). Its conductivity can be very high as it can reach the order of 1000 S/cm^[12]. It is commercially available as an aqueous dispersion from which films can be formed through traditional techniques like spin coating (Chapter 1).

Nonetheless, with these fabrication approaches a crosslinker, usually 3-methacryloxypropyltrimethoxysilane (GOPS), is needed in order to prevent dissolution and delamination of the film in aqueous environments. Moreover, PEDOT:PSS films can also be formed through vapor phase deposition or electrochemical polymerization. Electrochemical deposition is of particular interest

due to the fabrication advantages it provides , as will be presented later in this chapter. The morphology of the created films plays an important role in the overall conductivity. It is believed that in the dispersion PEDOT and the excess PSS form a polyionic complex. The PEDOT-rich core is surrounded by a PSS-rich shell forming colloidal gel-like particles. After film formation those particles interconnect forming a hole transport network through the PEDOT-rich phase while the PSS-rich phase supports ion transport^[14]. Especially when it comes to electronic conductivity, addition of a co-solvent like ethylene glycol has been found to be beneficial as it facilitates the interconnection of the PEDOT rich phases leading to more efficient hole transport^[15].

Many studies have shown that the coating of metal electrodes with conducting polymers (such as PEDOT:PSS) results in lowering the electrodes impedance by approximately 2 orders of magnitude^[11] (Figure 2.5). The reason behind that is both the increase of the effective area due to the presence of the conductive polymer and the ion uptake inside the polymer film.

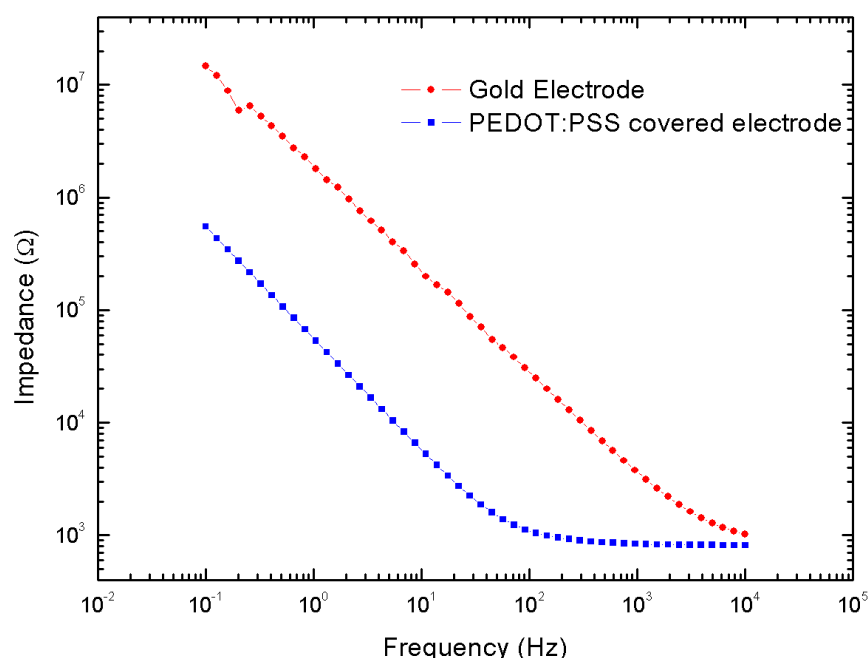


Figure 2.5: Impedance spectra comparison of a Gold and a PEDOT:PSS covered electrode. Both electrodes are 500μm x 500μm .PEDOT:PSS film thickness is about 350nm.

In order to study the physics behind the functionality of the polymer covered electrodes we need to consider how and where the interaction between them and the living tissue takes place. In brief, this sophisticated interplay involves charge carrier movement through many different interfaces. For example, if we imagine the metal (electrode) - conducting polymer – tissue stack we can easily identify the metal-conducting polymer and conducting polymer-tissue interfaces. In addition, there is a variety of charge carriers as the different materials conduct charge through different species and mechanisms. Metals, for example, move charge with electrons in the solid-state, while organics transport mostly via positive charges (holes or polarons) that move on the polymers' backbones. The picture gets even more complicated if we take into consideration the watery tissue environment. In that, charge transport involves both positive cations (Na^+ , K^+ , Ca^+) or negative anions (Cl^-). In any case, all of these complex charge exchanges occur at the formed interfaces^[16] therefore it is reasonable to assume that their microstructure and composition will greatly affect the overall biomedical device performance. Principally, it is expected that an increase in the effective surface due to the conductive polymer film formation, provides more opportunities for charge transfer to occur, a fact that lowers the device impedance^[11].

From another, different, perspective, the presence of the conducting polymer provides an effective capacitance that is substantial greater than the bare metal electrode. In order to calculate this effective capacitance of the data in Figure 2.5 we use a simple RC equivalent circuit. The value of C was determined to $1120\mu\text{F}/\text{cm}^2$ a value that is 30 times higher than the double layer capacitance of the IPE. This increase also implies an ion penetration inside the polymer film^[17].

2.4 Impedance Spectroscopy of PEDOT: PSS Coated Electrodes as a Function of Area

As stated before the impedance that a biopotential electrode presents inside the electrolyte is of great importance regarding its recording quality. As a consequence, the parameters that affect this value need to be thoroughly studied and determined in order for the optimal electrode geometry to be obtained during the experiments.

It has been asserted that the impedance of metal electrodes should scale inversely with the electrode area^[18]. In addition, some ideas regarding the effect of

the PEDOT:PSS film thickness has already been discussed in previous works resulting in thickness dependence of the measured impedance^[11]. Nevertheless, a full study taking into account every possible parameter that could affect the impedance value is not available but would be extremely useful. On the contrary, there have only been few systematic, detailed experimental studies of the effect of electrode area on the impedance of biopotential electrodes. We anticipated that these devices would enable studies of the impedance response as a function of frequency and to compare the performance of polymer coatings deposited under different conditions (such as spin-casting or electrodeposition). Therefore, in order to test all these parameters we designed and realized a device that incorporated electrodes of different areas and shapes (Figure. 2.6).

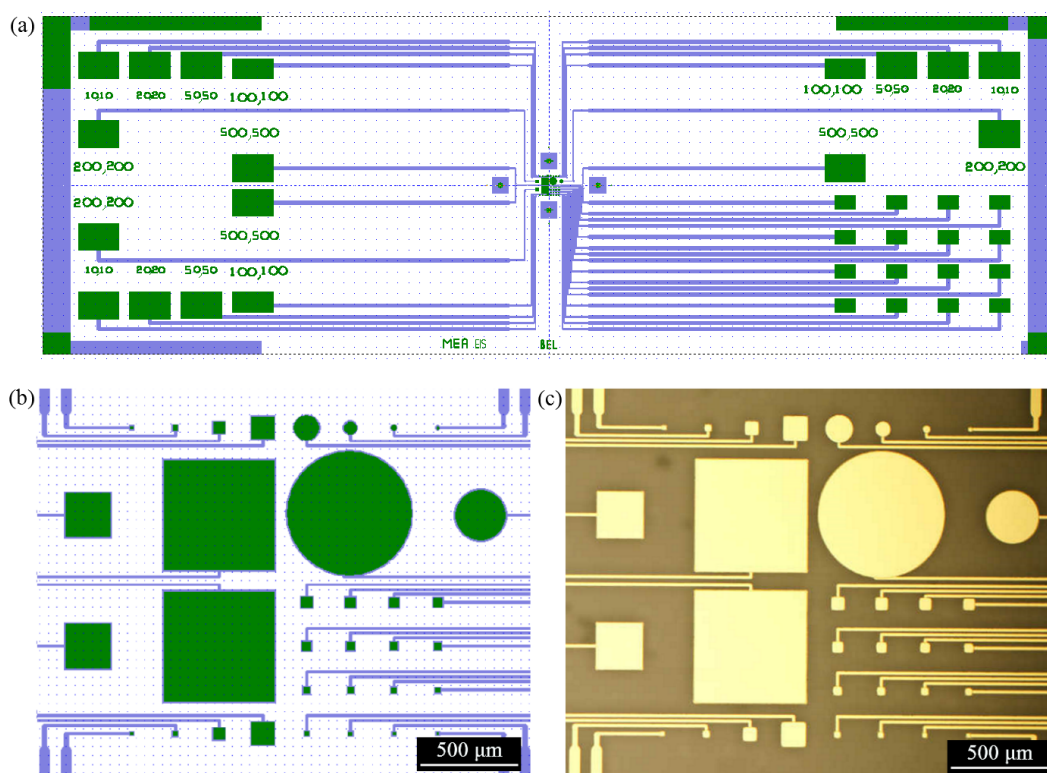


Figure 2.6: (a) The device layout and (b) a zoom in, in the active area. For the square electrodes sizes scale from 10 μm to 500 μm . There are also round -electrodes for testing the effect of the shape on the device performance. (c) The actual fabricated device in gold.

Figure 2.6 (c) presents the realized device in gold. The electrodes' area scaled from $10 \times 10 \mu\text{m}^2$ to $500 \times 500 \mu\text{m}^2$ (electrode's dimensions $10 \times 10 \mu\text{m}^2$, $20 \times 20 \mu\text{m}^2$, $50 \times 50 \mu\text{m}^2$, $100 \times 100 \mu\text{m}^2$, $200 \times 200 \mu\text{m}^2$ and $500 \times 500 \mu\text{m}^2$ with multiple electrodes on the same device for statistical reasons).

The initial motivation behind this work can be summarized in the following questions:

1. How does spun cast PEDOT:PSS/GOPS compare to electrodeposited PEDOT:PSS
2. Can we get a better understanding of the origin of impedance for better device optimization?
3. Do we see any impedance variations at high and low frequencies?
4. What is the role of the electrode shape and of the electrolyte?

Impedance spectra for the different electrode areas are presented in Figure 2.7

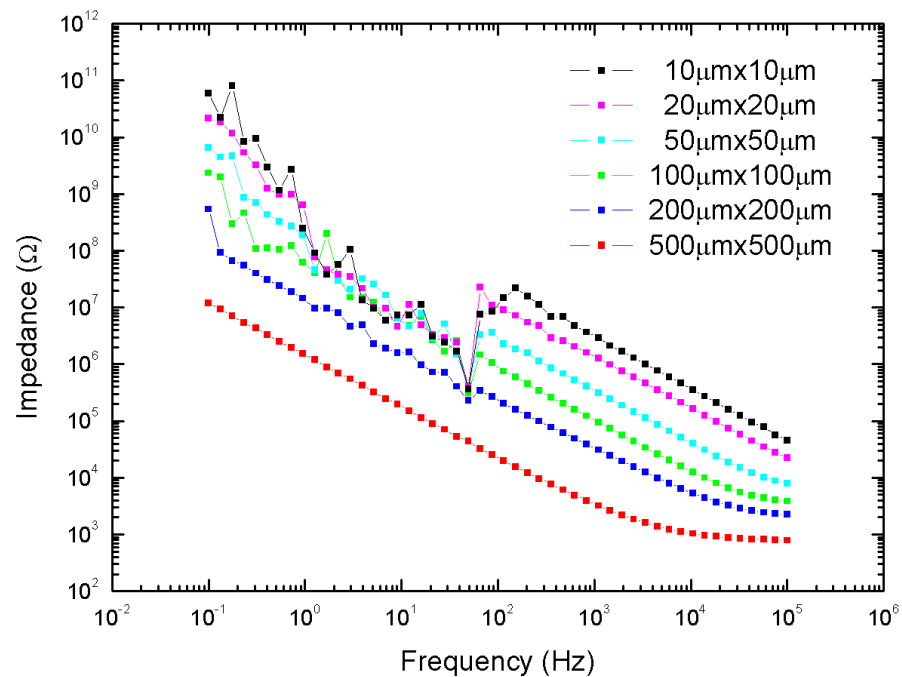


Figure 2.7: Impedance vs frequency plots for the different sized gold electrodes.

The plots for the different sized electrodes follow the expected trend. The larger electrodes ($500 \times 500 \mu\text{m}^2$) have the lower impedances while the smaller ones ($10 \times 10 \mu\text{m}^2$) shows the larger impedances. It is also worth noticing that there is a critical frequency f_c where a change in the plot slope is observed. The value of f_c moves to higher frequencies as the area of the electrode diminishes. The f_c s for electrodes smaller than $50 \mu\text{m} \times 50 \mu\text{m}$ appear at frequencies higher than 100 kHz. This frequency is a characteristic frequency that signifies a change in the mechanism behind the physical phenomenon that takes place. In this particular case, we have a change from a capacitive-dominated impedance ($Z_c = \frac{1}{i\omega C}$) to a resistive-dominated one ($Z_R = R$). The fact that the curves for the smaller electrodes are a bit disturbed is due to the noise that becomes more important for the smallest electrodes with the greater impedance values.

The above measurements served as control measurements for the experiments to come. An identical device covered with an approximately 350 nm thin layer of PEDOT:PSS was fabricated and the impedance spectra for those electrodes is presented in Figure 2.8. Again, the trend is similar, with the bigger electrodes presenting smaller impedances. Nevertheless, the impedance values for the same area electrodes are significantly smaller for the covered in comparison with the bare ones.

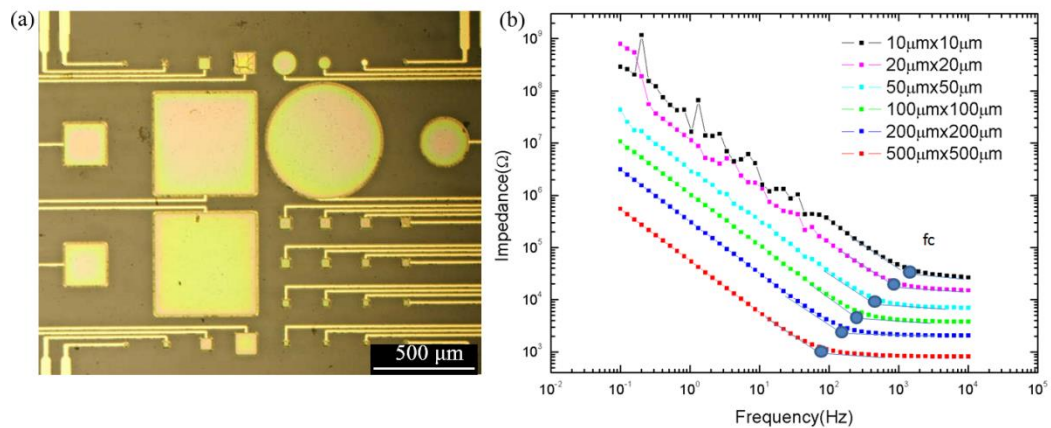


Figure 2.8: (a) Optical microscope picture of the PEDOT:PSS covered electrodes. (b) Impedance spectrum of the same electrodes. f_c denotes the critical frequency where a change in the slope is induced.

This is attributed to the effect of the conducting polymer film which alters the spectrum profile by both lowering the impedance value and moving the curves to

lower frequencies (the characteristic f_c is recorded at lower frequencies). As discussed above, this is due to the porous open structure of the PEDOT:PSS that provides a greater effective area for the charges to be transferred through. In other words, the capacitance of the film C is dramatically increased. Since the value of the spreading resistance R_s is not significantly changed, the transition frequency f_c occurs at lower frequencies.

Up until this point, everything is as theory predicts. Nevertheless, for electrodes of different area we expect the impedance Z to be inversely proportional to A , where A is the electrode area. As a consequence, the quantity that should characterize a material (in our case PEDOT:PSS) should be the product $A \cdot Z$ and this product should normalize all of the different electrodes impedance curves to one master curve^[19].

Figure 2.9 shows this normalization attempt. The impedance for each electrode was multiplied with the corresponding area and then plotted vs frequency.

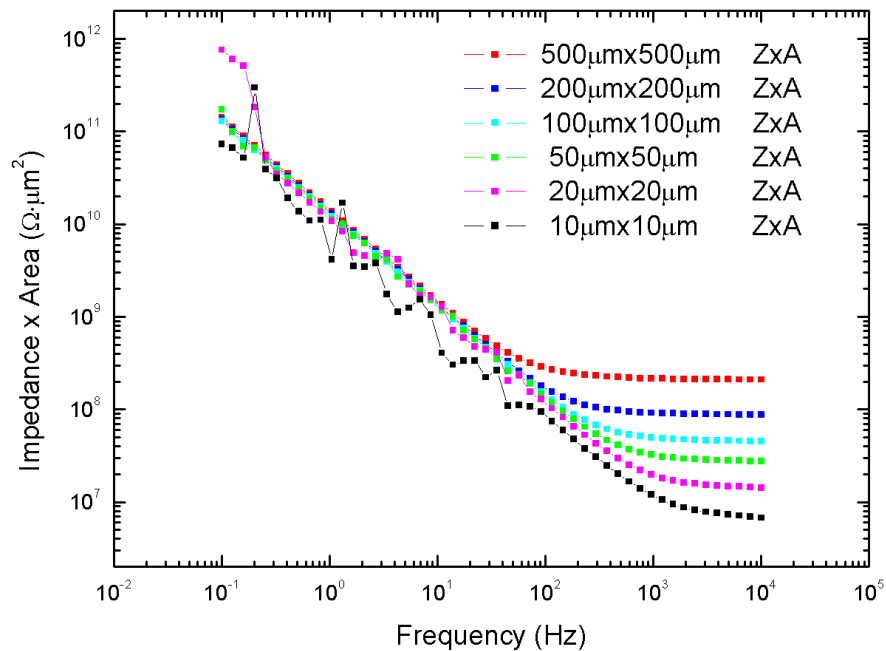


Figure 2.9: Impedance normalization with the electrode area. The product impedance x area is plotted vs frequency for every electrode size.

Interestingly, the expected master curve did not show up. Even if we considered having some overlap in the lower frequency regime, in the high frequency regime there is an obvious mismatch between impedance curves. The results above made us think that obviously multiplying impedance with the area is not the right way to go as there is a mechanism involved in the phenomenon that remained hidden through this approach.

In order to crack this problem we had to go back to the fundamentals of the impedance spectroscopy. Trying to model our system we used the equivalent circuit of Figure 2.3 as it was the simplest one that could adequately fit the experimental data, with a resistor R_s in series with a capacitor C . The resistor R_s is called the spreading resistance and is the resistance encountered by current spreading out into the solution, under the assumption that the counter electrode is infinitely large and the working electrode is surrounded by electrolyte ^[20, 21]. The capacitor C is the double layer capacitance formed at the interface between the metal electrode and the electrolyte.

At low frequencies the capacitive term is the one which dominates as in the equation 2.3 the angular frequency ω in the denominator of the fraction ($\frac{1}{\omega C}$) results in a large value. In the high frequency regime, though, the fraction of the capacitive contribution goes to zero leaving behind the value of the resistance R_s . This value is frequency independent as it is a function only of the electrolyte used and the size of the electrode.

In theory the value of the R_s for a square electrode should be $R_s = \frac{\rho \ln 4}{\pi l}$ ^[21] where ρ is the solution resistivity and l the square's side. Capacitance on the other hand should scale with area A since $C = \epsilon \epsilon_0 \frac{A}{d}$

Playing around with equations we have

$$\tau = RC \text{ and } f = \frac{1}{2\pi\tau} = \frac{1}{2\pi R C} \quad (2.8)$$

so if $R_s \sim \frac{1}{A^{1/2}}$ and $C \sim A$ then

$$f \sim A^{-1/2} \quad (2.9)$$

Indeed if we plot R_s , f_c and C versus area we get Figure 2.10 where the values of R_s and C are fitting parameter to the measured data.

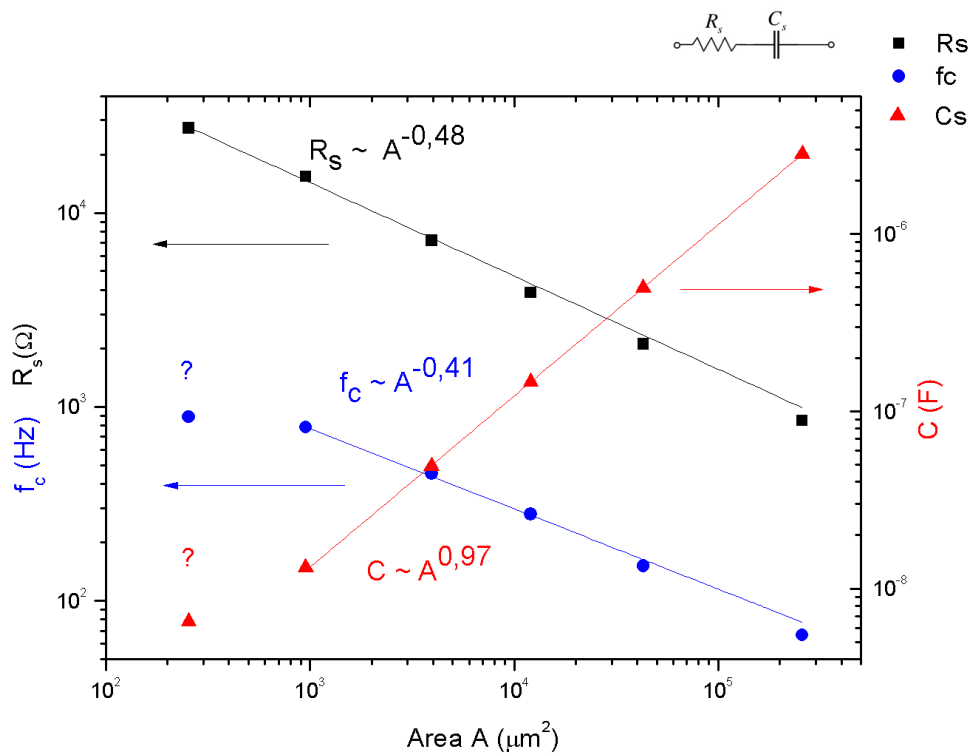


Figure 2.10: Spreading resistance R_s , critical frequency f_c and Capacitance F as a function of electrodes area.

As depicted in the plot of Figure 2.10 R_s scales as $A^{-0.48}$ while C scales as $A^{0.97}$. f_c seems to scale with $A^{-0.41}$ while it was anticipated to scale with $A^{-0.5}$. We believe that this has to do with the experimental uncertainty when we calculate the real electrode area. This area is usually a bit bigger than the originally designed one on the mask due to fabrication issues (mask's resolution, over etching effects etc). This phenomenon is more intense in the smaller electrodes so the real area value is not the same with the nominal designed one. That is why during the fitting in the above Figure 2.10 the smallest electrodes were noted with question marks. Nevertheless the overall trend is as expected.

The question is now how can these values help us perform the intended impedance spectra normalization.

Let us consider equation $|Z| = \sqrt{R_s^2 + \left(\frac{1}{\omega C}\right)^2}$ (2.7) again. For $\omega \rightarrow +\infty$ we focus on the higher frequency resistive part and impedance Z becomes $\lim_{\omega \rightarrow \infty} Z = \lim_{\omega \rightarrow \infty} \sqrt{R_s^2 + \left(\frac{1}{\omega C}\right)^2} = \sqrt{R_s^2} = R_s$ which is a constant value. That means dividing every curve with its corresponding value of R_s will shift it on the y axis normalizing it to 1. On the other hand, dividing frequency f with the critical frequency f_c will move each plot on the same spot on the frequency axis. Therefore, a normalization using Z/R_s and f/f_c might do the job and that is what we tried.

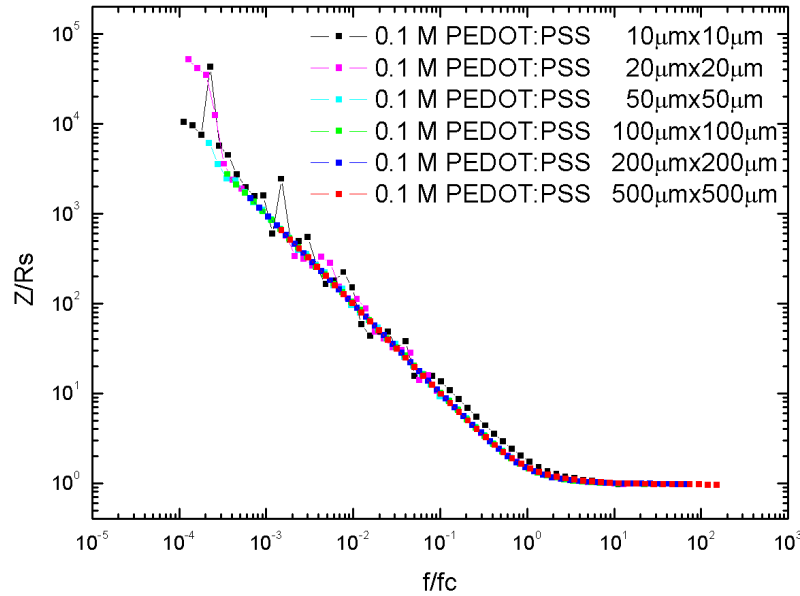


Figure 2.11: Master curve of the Impedance spectra for different solution concentrations.

The electrolyte used for these measurements was NaCl 0,1M and the results imply the existence of a consistent mechanism for transport, regardless the area of the used electrode. Of course, the area changes the position of the curve on the axis making the phenomenon faster (higher frequencies) or slower (lower frequencies) depending the time needed for the capacitor to be charged; nevertheless this can be predicted if we take into account the electrode's area.

In order to test our hypothesis we decided to make extra experiments using different conditions. In particular we tested the effect of:

- Electrode shape
- PEDOT:PSS thickness
- Electrolyte concentration
- Electrode material (Gold electrodes vs the PEDOT:PSS covered ones)
- PEDOT coating deposition methods (spin-coating vs. electrodeposition)

Electrode Shape

In order to test the effect of the electrode shape to the overall device performance we incorporated both square and round electrodes on the same device. Special care was taken to ensure that the areas of the different shaped electrodes are identical (or as close as possible). Impedance spectroscopy measurements performed on those electrodes and indicative results for two different sized electrodes are presented in Figure 2.12 ($10000 \mu\text{m}^2$ and $250000 \mu\text{m}^2$).

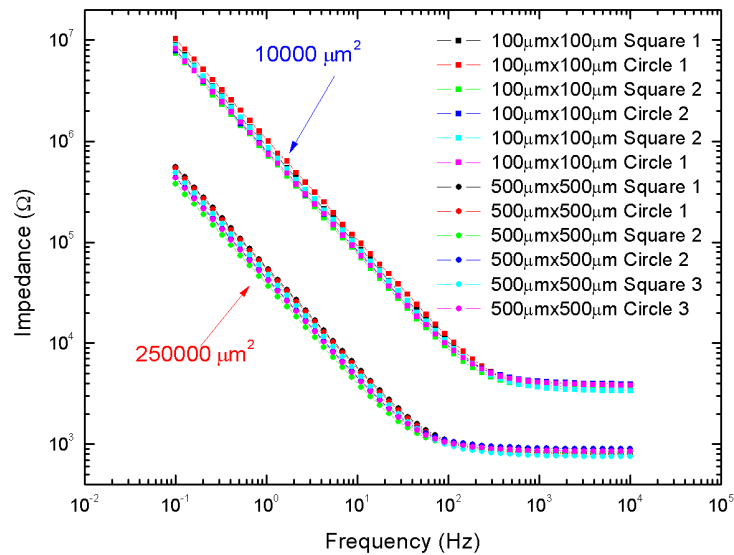


Figure 2.12: Impedance spectroscopy for two different electrode areas and shapes.

From the figure above is clear that the impedance value is not significantly affected by the shape (round or square) of the electrode as the measurements are identical for electrodes of same size and different shape. In the experiment, multiple electrodes were used for statistical reasons.

PEDOT: PSS Thickness

Then we tried to test the effect of the PEDOT:PSS film thickness to the impedance. We tested two electrode sizes (500 $\mu\text{m} \times 500 \mu\text{m}$ and 200 $\mu\text{m} \times 200 \mu\text{m}$) and three different film thicknesses (100 nm, 350 nm, and 550 nm) (Figure 2.13). The high frequency regime is the same for every thickness as it refers to the solution spreading resistance R_s , a function of the area and the solution characteristics. The low frequency regime though is different as it depends on the formed capacitance that changes according the film deposition.

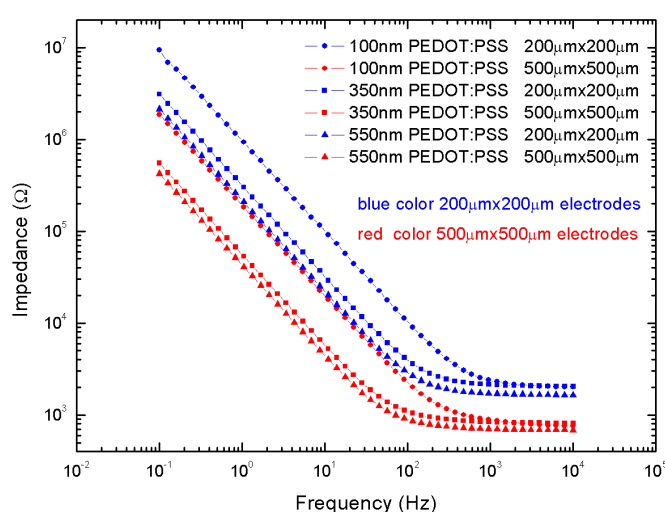


Figure 2.13: Impedance vs frequency for three different PEDOT:PSS film thicknesses and two different electrode areas.

Electrolyte Concentration

Then we tried to study the effect of different electrolyte concentration on the impedance spectra of the electrodes. Figure 2.14 depicts the results obtained by comparing the impedance of the same electrode on different solution concentrations. For the measurements we used NaCl solutions of 0.1 M, 0.01 M and 0.001M.

Interestingly, for the same electrode size the impedance in the low frequency regime seemed to collapse on each other for all the sizes. Keeping in mind that this part of the spectra is dominated by the double capacitance this can be explained by the

fact that the size of the electrode is the same regardless of the electrolyte concentration. The system also shows that with less concentrated electrolytes the transition frequency f_c becomes smaller. What is also interesting is the fact that the part of the spectrum of the high frequency regime is different for the different concentrations. This is attributed to the fact that it refers to the solution resistance R_s which depends on the number of charges in the electrolyte (concentration). The plots are getting noisier for the small size electrodes as expected.

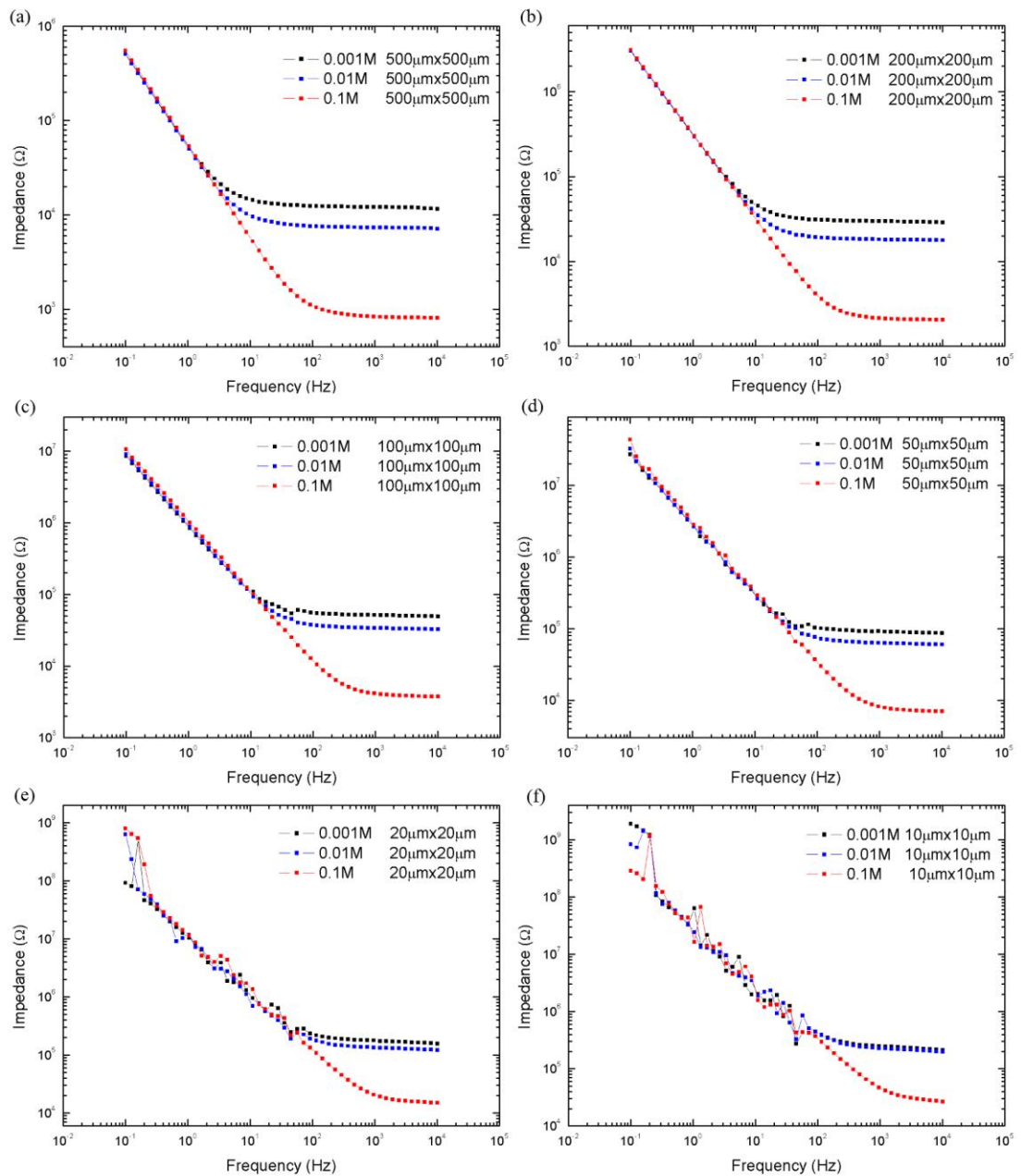


Figure 2.14: Impedance vs frequency for three different electrolyte concentrations (0,1M , 0,01M and 0,001M NaCl).

Gathering all these thoughts together it seemed that the initial idea of the normalization would also apply for these conditions. Indeed Figure 2.15 shows that the master curve is the same one for every possible condition

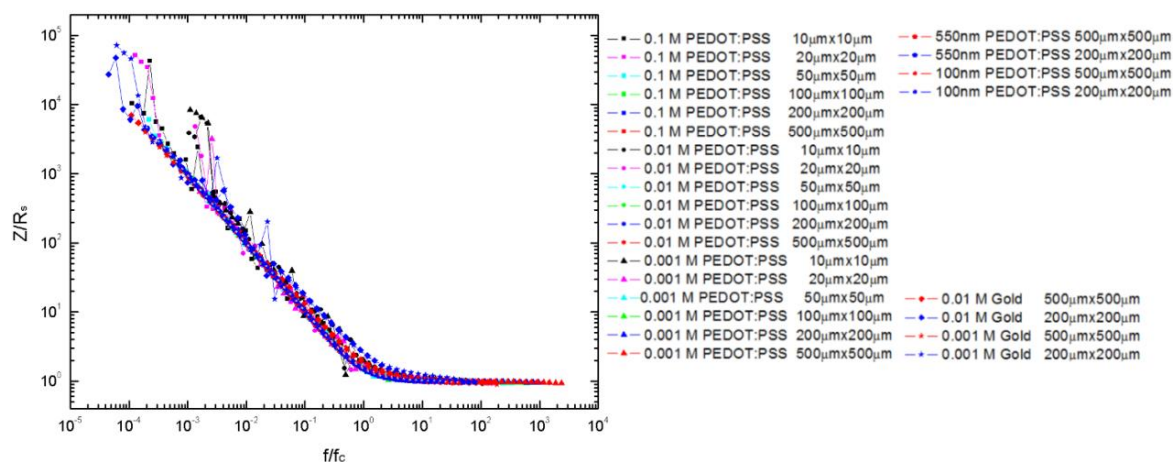


Figure 2.15: Impedance vs frequency master curve.

The way we would like to interpret this is that there is one consistent mechanism for charge transport at the electrode-electrolyte interface that is depicted in the master curve. This phenomenon consists of two mechanisms that involve a drop of potential due to the spreading resistance R_s and the capacitive charging of the film. Regardless of the electrode size, the material of the electrode or even the electrolyte concentration used, everything can be normalized to one single master curve that should make it possible to better predict the system behavior in advance provided that we know the chosen conditions.

2.5 Electrodeposition

As discussed in Chapter 1, device fabrication is a complicated process that involves a lot of different steps. The most important of all though, is the formation of the conducting polymer film itself. So far in our lab the standard fabrication process used has been the PEDOT:PSS film formation through spin casting. It is a rather easy to implement way of depositing films which gives precise control over the film thickness and quality. Nevertheless, depositing film in a way like this comes with certain drawbacks the most important of which is the film delamination in aqueous environments. In order to tackle this issue what has usually been used is a silane (3-methacryloxypropyltrimethoxysilane) GOPS compound inside the spun dispersion. GOPS is a surface adhesion promoter and a polymer cross-linking agent that enhances film stability. The tradeoff is the potential penalty in the films conductivity due to its presence. In addition, with this technique it is rather difficult to address individual electrodes through spin coating so sacrificial layers methods should be employed in order for the device to be fabricated.

Nevertheless, other approaches have also been used by other groups for PEDOT:PSS patterning. Electrodeposition of the film is particularly interesting and offers a number of advantages. The process is based on the polymerization of the EDOT monomers on the underlying electrode and the subsequent formation of the PEDOT polymer film. This is realized either in a galvanostatic (constant current) or a potentiostatic (constant voltage) mode. If PSS⁻ anion (polyelectrolyte) also used the final film is the doped polymer (PEDOT:PSS).

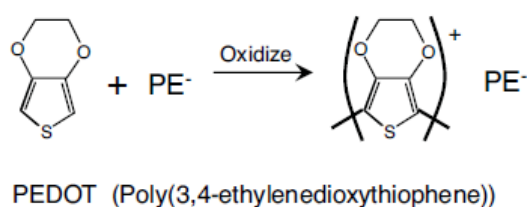


Figure 2.16: Schematics of the electrochemical polymerization of EDOT to PEDOT^[1].

Figure 2.16 shows the electrochemically driven polymerization of the monomer EDOT towards PEDOT^[1]. The applied current to the monomer solution

oxidizes the EDOT monomers forming cationic radicals that eventually leads to polymerization. The total electrical charge provided through the electrode drives the polymerization reaction, giving films of defined composition, thickness and microstructure.^[1]

In general, it is a controlled deposition technique directly onto the electrode from aqueous solution and with operating voltage around $\sim 1V$. It creates soft, fuzzy and bioactive conducting polymers that favor charge transfer (both electronically and ionically), a fact of extreme importance for biological interactions.

As in the case of the spin-cast PEDOT:PSS/GOPS film, the presence of the polymer reduce the electrode's impedance and facilitates better recordings. In addition, the use of GOPs is no longer needed and as a consequence no conductivity penalty is taken. Furthermore, each electrode can be addressed individually and consequently devices with electrode coatings of different thickness can be fabricated on the same chip.

What would be of extreme importance is a comparison between PEDOT:PSS films on electrodes of same geometry but of different synthesis and processing. Our initial goal was to determine if there are any impedance variations at either high or low temporal frequencies. For this reason, we used the previous testing mask and made devices with the same PEDOT:PSS film thickness fabricated with different methods (spun cast vs electrodeposited). Reflected light optical microscope pictures of those devices are shown in Figure 2.17

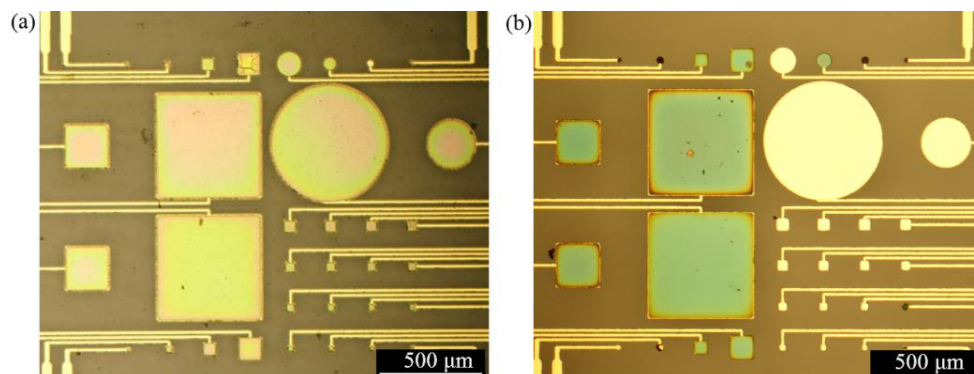


Figure 2.17: Microscope pictures of (a) a device with a spun cast PEDOT:PSS film (b) an electrodeposit PEDOT:PSS film.

The colors reveal the presence of the PEDOT:PSS film on both devices. The deposition parameters were chosen carefully in order for the film thicknesses to be the same (~350 nm) regardless the fabrication process. It is worth noticing the non-covered electrodes on Figure 2.17 (b). This is one of the biggest advantages of electrodeposition as it allows individual electrodes to be addressed separately. It also allows for electrode fabrication with different polymer coating thicknesses on the same chip. The scanning electron microscopy (SEM) images of the 500 μm x 500 μm electrode are presented in Figure 2.18.

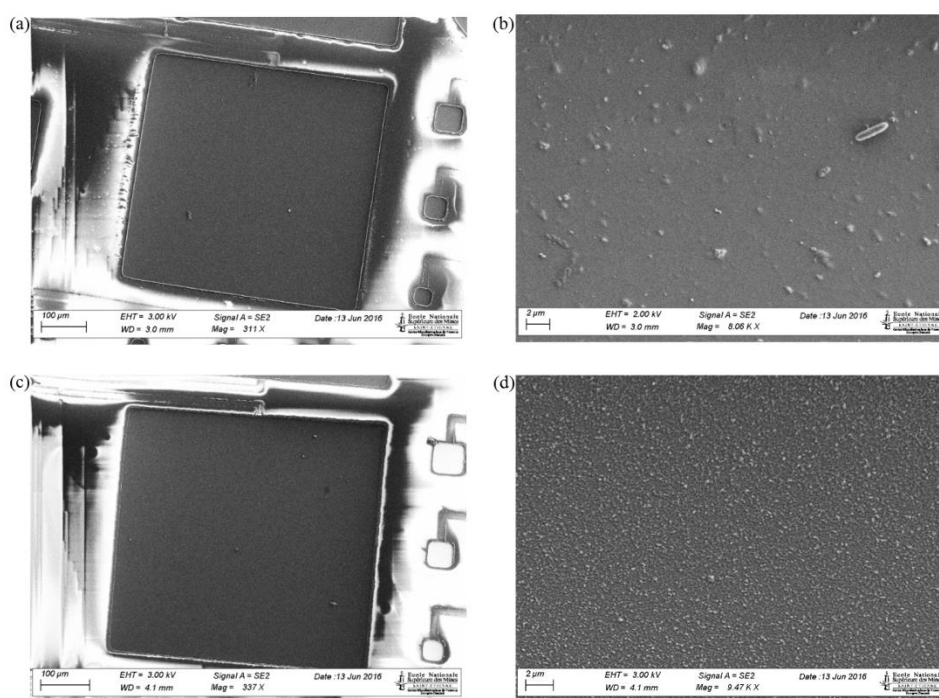


Figure 2.18: SEM images of the spun cast and the electrodeposit PEDOT:PSS films (a) Spun cast film on a gold electrode and (b) a higher resolution picture of it. (c) Electrodeposited film on a gold electrode and (d) a higher resolution picture of it.

Comparing Figures 2.18 (b) and Figures 2.18 (d) we see that there seems to be a subtle difference in the surface morphology between the two approaches. Electrodeposition creates a somewhat rougher surface more likely due to way the film is created. Probably, the energy given electrically to the monomers in order to initialize and to maintain the polymerization reaction affects the overall morphology. Nevertheless, what is the really important parameter in our case is the impedance spectra profile of the electrodes and how this changes depending the fabrication method (Figure 2.19).

Interestingly, the GOPS/PEDOT spun cast films show only slightly less capacitive (higher Z) values than electropolymerized PEDOT films of similar thickness. This result is indicative that the two approaches seem to be nearly equivalent in terms of the resulting impedance of the films.

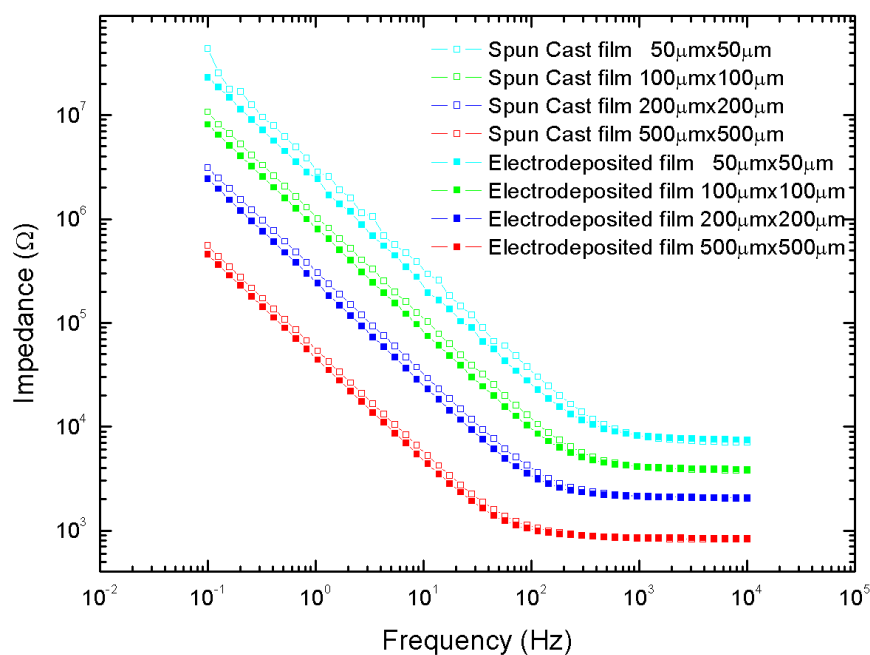


Figure 2.19: The Comparison of PEDOT:PSS/GOPS spun cast films vs the electrodeposit films yields identical Impedance values.

2.6 Conclusions

In this chapter we studied the device physics behind the biopotential electrodes, which are extremely important tools for electrophysiological measurements. Engineering those devices means choosing the right geometrical characteristics that would optimize their performance and result in better quality recordings. Nevertheless, this requires answering, first, some fundamental questions like how can we understand better the origin of impedance for future device optimization? How does impedance scale with electrode area and what is the role of the electrode shape, electrolyte and, conducting polymer film thickness? And how do spun cast PEDOT:PSS films compare to electrochemically deposit ones?

The experiments done in this project tried to enlighten all these aspects providing answers to some of the above questions creating at the same time new ones as typically happens in research.

In conclusion, we were gratified to see that electrodes with systematic variations in their area (A) provided us with a useful tool to examine the origins of electrode behavior. We were also happy to see that the simplest possible (2-element) model with a capacitor C (electrolyte – film interface) and a resistor R_s (electrolyte spreading resistance) in series can adequately describe the electrochemical impedance spectra data obtained during the experiments.

The results showed that impedance scales with area, with a capacitance C that is proportional to the electrode area and a spreading resistance R_s that is proportional to electrode size L . The characteristic frequency $f_c = \frac{1}{2\pi RC}$ also scales as $A^{-1/2}$ (or $1/L$) and can be used with R_s in plots to normalize the impedance into master curves (of Z/R_s vs f/f_c).

Changing the electrolyte concentration lowers R_s without affecting C . We believe that this has to do with the two separate mechanisms we see in the impedance spectra. One is correlated with the capacitance dominating in the lower frequency regime and the other is the resistive behavior in the higher frequency regime. Changes in the electrolyte concentrations can be translated into changes in the charges with the ability to move inside the electrolyte a fact that echoes in changes in the resistance R_s .

Nevertheless, this change does not seem to affect the charging process of the double layer capacitor formed.

Regarding the PEDOT:PSS/GOPS spun cast films vs the electrodeposited ones of similar thickness, it seems as that they first show a slightly less capacitive part (higher impedance). This is likely due to the somewhat disconnected pathways for charge transport that are formed in the spun cast film and the resistance provided by the addition of GOPS. However, it is reassuring that the transport properties of the spun cast and electrodeposited films are not so different, for films of equivalent thickness.

After the theoretical study of the physics behind the recording electrodes the next two chapters provide implementation of the acquired knowledge in electrophysiological measurements. Chapter 3 presents electrical activity measurement of Hippocampal cell cultures while Chapter 4 deals with electrophysiology on pancreatic cell islets.

References

- [1] D. H. Kim, S. Richardson-Burns, L. Povlich, M. R. Abidian, S. Spanninga, J. L. Hendricks, D. C. Martin, in *Indwelling Neural Implants: Strategies for Contending with the In Vivo Environment*, (Ed: W. M. Reichert), CRC Press/Taylor & Francis Taylor & Francis Group, LLC., Boca Raton (FL) 2008.
- [2] A. J. Bard, L. R. Faulkner, *Electrochemical Methods: Fundamentals and Applications*, Wiley, 2000; R. F. Yazıcıoğlu, (Eds: C. v. Hoof, R. Puers), Springer, [Dordrecht] : 2009.
- [3] S. F. Cogan, *Annu Rev Biomed Eng* 2008, 10, 275.
- [4] M. Taketani, M. Baudry, *Advances in Network Electrophysiology: Using Multi-Electrode Arrays*, Springer, 2006.
- [5] Y. Nam, B. C. Wheeler, *Crit Rev Biomed Eng* 2011, 39, 45.
- [6] D. R. Humphrey, E. M. Schmidt, in *Neurophysiological Techniques: Applications to Neural Systems*, (Eds: A. A. Boulton, G. B. Baker, C. H. Vanderwolf), Humana Press, Totowa, NJ 1990, 1.
- [7] G. Buzsaki, C. A. Anastassiou, C. Koch, *Nature reviews. Neuroscience* 2012, 13, 407.
- [8] J. Rettinger, S. Schwarz, W. Schwarz, in *Electrophysiology : Basics, Modern Approaches and Applications*, Springer International Publishing, Cham 2016, 23.
- [9] L. L. C. Molecular Devices, 2012.
- [10] C. M. Lopez, M. Welkenhuysen, S. Musa, W. Eberle, C. Bartic, R. Puers, G. Gielen, *Conference proceedings : ... Annual International Conference of the IEEE Engineering in Medicine and Biology Society. IEEE Engineering in Medicine and Biology Society. Annual Conference 2012*, 2012, 759.
- [11] M. Sessolo, D. Khodagholy, J. Rivnay, F. Maddalena, M. Gleyzes, E. Steidl, B. Buisson, G. G. Malliaras, *Advanced Materials* 2013, 25, 2135.
- [12] A. Elschner, *PEDOT : principles and applications of an intrinsically conductive polymer*, CRC Press, Boca Raton, FL 2011.
- [13] M. Asplund, T. Nyberg, O. Inganas, *Polymer Chemistry* 2010, 1, 1374.
- [14] A. M. Nardes, M. Kemerink, R. A. J. Janssen, J. A. M. Bastiaansen, N. M. M. Kiggen, B. M. W. Langeveld, A. J. J. M. van Breemen, M. M. de Kok, *Advanced Materials* 2007, 19, 1196.
- [15] S. Ashizawa, R. Horikawa, H. Okuzaki, *Synthetic Metals* 2005, 153, 5.
- [16] D. R. Merrill, M. Bikson, J. G. Jefferys, *J Neurosci Methods* 2005, 141, 171.
- [17] J. Rivnay, P. Leleux, M. Ferro, M. Sessolo, A. Williamson, D. A. Koutsouras, D. Khodagholy, M. Ramuz, X. Strakosas, R. M. Owens, C. Benar, J.-M. Badier, C. Bernard, G. G. Malliaras, *Science Advances* 2015, 1.
- [18] A. R. Abdur Rahman, D. T. Price, S. Bhansali, *Sensors and Actuators B: Chemical* 2007, 127, 89.
- [19] D. C. Martin, G. G. Malliaras, *ChemElectroChem* 2016, 3, 686.
- [20] J. Newman, *Journal of The Electrochemical Society* 1966, 113, 501; M. R. Abidian, D. C. Martin, *Biomaterials* 2008, 29, 1273.
- [21] W. Franks, I. Schenker, P. Schmutz, A. Hierlemann, *IEEE transactions on bio-medical engineering* 2005, 52, 1295.

Chapter 3: *In vitro* PEDOT:PSS Microelectrode Arrays for hippocampal cell culture electrophysiological recordings

3.1 Abstract

Despite its importance in neuroscience, neuron signal recording can be a challenging task mostly due to difficulties in the coupling between conventional electronics and neurons. Lately, conducting polymers have emerged as one of the most promising candidates for the next generation devices in neural activity recording due to their unique features. Nevertheless, the interaction between living tissue and conducting polymer devices is far from being something trivial, as special care needs to be taken in order for the latter to be rendered a suitable environment for cell culturing. In this work, we demonstrate the use of a Poly(3,4 ethylenedioxythiophene) : poly(styrenesulfonate) (PEDOT:PSS) platform of a multi electrode array (MEA) capable for *in vitro* measurements. With those PEDOT:PSS coated electrodes we were able to record neural activity, such as action potentials (APs), from *primary fetal rat hippocampal neurons*. Our results demonstrate that PEDOT:PSS dramatically improves the resolution of electrophysiology while a biofunctionalization technique ensures the biocompatibility of our devices with living cells.

3.2 Experiment-Results

Neural signals play a major part in central nervous system physiology while their role is also essential in the understanding of neurological disorders. This is the reason why a lot of effort has been devoted lately to the difficult task of recording and interpreting these signals through high tech platforms that allow the interplay between biological systems and electronic devices. *In vivo* experiments have been already successful in establishing a way of communication between brain regions and artificial recording sites giving rise to new approaches in diagnostics and treatment of various pathologies, promising, at the same time, to replace ineffective pharmacotherapies. Pacemakers and cochlear implants are perfect examples of those devices ^[1-3] allowing dreams for even closer and more sophisticated ways of human-machine interaction.

Nevertheless, *in vitro* devices are still playing an important role in modern neuroscience as they are the most efficient, easy to implement and reliable way to perform experiments either on neuronal cell cultures or on brain slices. Further development of the *in vivo* applications must, inevitably, rely first on similar experiments performed *in vitro* that would allow a more profound understanding of the neuronal signaling mechanism. In addition, *in vitro* models are of great importance in modern drug discovery as they induce a more biological-driven approach in drug development in accordance with the new trend in pharmacological research that dictates the *in vivo* experiments restriction due to ethical reasons. In particular, today's necessity is the development of alternative approaches to animal testing, consistent with the 3Rs (Replacement, Reduction, Refinement) principle. Replacement refers to methods of avoiding or replacing the use of animals in research, Reduction to methods of minimizing the number of animals used and Refinement to mitigating animals' suffering and promoting its welfare. Lastly, REACH regulation is an extra driving force as it demands the evaluation of the toxicity of more than 30000 chemical substances – weighting more than 1 ton a year – produced by or imported to the European Union. Taking into account that many diseases/disorders, including the neurodegenerative ones, are thought today to be caused by environmental toxins, the need for the development of high-throughput screening technics is imperative^[4].

For the above reasons, *in vitro* platforms gather great interest among the scientific community. Especially microelectrode arrays (MEAs) are one of the most essential tools in the study of neuronal networks. They allow the fabrication of planar recording sites on top of which cell can be cultured or brain slices can be easily placed^[5-7]. Stimulation and/or recording from these devices can be performed with great efficiency while their patterning technic provides the ability to control the position of the electrode with respect to the under study neural network. Drug testing is one of the obvious uses of those platforms, as the study of the effect of different chemical agents on neurons is of great importance. However, the acquisition of those signals can be a challenging task mostly due to difficulties in the coupling between conventional electronics and biological systems. Commercial available metal MEAs have been extensively used during the past years, yet the need of scaling down these electrodes to the size of single neurons becomes more and more imperative nowadays. The reason is that smaller sized electrodes allow localized neuron stimulation and high temporal resolution recordings. The drawback of electrode miniaturization, though, is the deterioration of their ability to record and stimulate, mostly due to increase of the impedance at the interface between electrolyte and electrode. This can be attributed to a decrease of the interfacial capacitance which is proportional to the active electrode area^[8]. Furthermore, an extra difficulty, of cell cultures on devices is posed by the need for the creation of a suitable , for them, environment to survive and to proliferate^[9] , a task far from being a trivial one. The alternative could be the use of brain slices, an approach that comes, though, with the disadvantage of a few micrometers thick layer of dead cells between the active cells and the recording sites, a fact that renders the activity recording even more challenging.

Lately, conducting polymers have emerged as one of the most promising candidates for the next generation devices in neural activity recording both *in vitro* and *in vivo*^[10-12]. Poly(3,4-ethylenedioxythiophene):poly(styrenesulfonate) (PEDOT:PSS) ,in particular, has the unique ability to conduct both electronic and ionic carriers, offering a highly performing platform of communication between biological systems and electronics^[13-16]. It shows extremely low impedance in physiological environments due to the combination of high electrical conductivity and ion permeability while it is considered to be biocompatible as PEDOT based devices have been already used for *in vivo* chronic recordings^[17]. Furthermore, PEDOT:PSS

coated microelectrode arrays demonstrate ease of processability and chemical tunability in contrast with their inorganic counterparts^[18].

It has already been reported that hippocampal cell cultures show a great variety of neural activity. Local field potentials (LFPs) and action potentials (AP or spikes) are the two that gather the greatest interest of the scientific community. The former are created by the contribution of multiple sources of neural activity^[19]. They are slow events (typically 1-200 Hz) and their amplitude varies from a few hundreds of μV up to a few mV. The latter are faster events (typical 1 kHz) with extracellular amplitude of around 100 μV since they are generated from single neurons^[20-24]. These action potentials characteristics (high frequency, low amplitude) make their extracellular recording a challenging task as they can be easily camouflaged inside the background noise level of the sensing device. Nevertheless, their role in neural communication is central as they realize the cell-to-cell signal propagation and as a consequence their detection is imperative in modern neurophysiology research. PEDOT:PSS coated MEAs are a useful tool in this recording assignment as they provide us with a state of the art tool that could increase the recordings quality.

Moreover, a bio functionalization treatment of our device is essential for establishing a cell compatible interface on our recording sites^[9, 25]. This is why the polypeptide poly-L-lysine (PLL) was added on the device's active area^[9]. The presence of PLL on our *in vitro* platform make it suitable for cell culturing. Thus, it allows the study of hippocampal cell activity by ensuring the neural cell survival and growth.

In this work we report electrophysiological measurements from *in vitro* MEAs that are biofunctionalized in order to be compatible with cell cultures. Using PEDOT:PSS coated electrodes we were able to record single units from *primary hippocampal neuron cells*. Our results, demonstrate that PEDOT: PSS dramatically improves the resolution of electrophysiology and paves the way for the use of active devices such as OEECTs in neural recordings. Furthermore, the PEDOT:PSS devices presented here provide a vehicle for fundamental research in life sciences, facilitate the study of neural activity, open new horizons in understanding the central nervous system physiology and neuropathology and prove their potential to be used for drug screening purposes.

Figure 3.1(a) shows a close-up of a cell culture on a conducting polymer coated MEA. The MEA consists of a 32 gold electrode grid. Each recording site has a $10 \times 10 \mu\text{m}^2$ active area covered by a thin film of about 350 nm of PEDOT:PSS and is exposed to the culture medium and the neural network (Supplementary Figure S1).

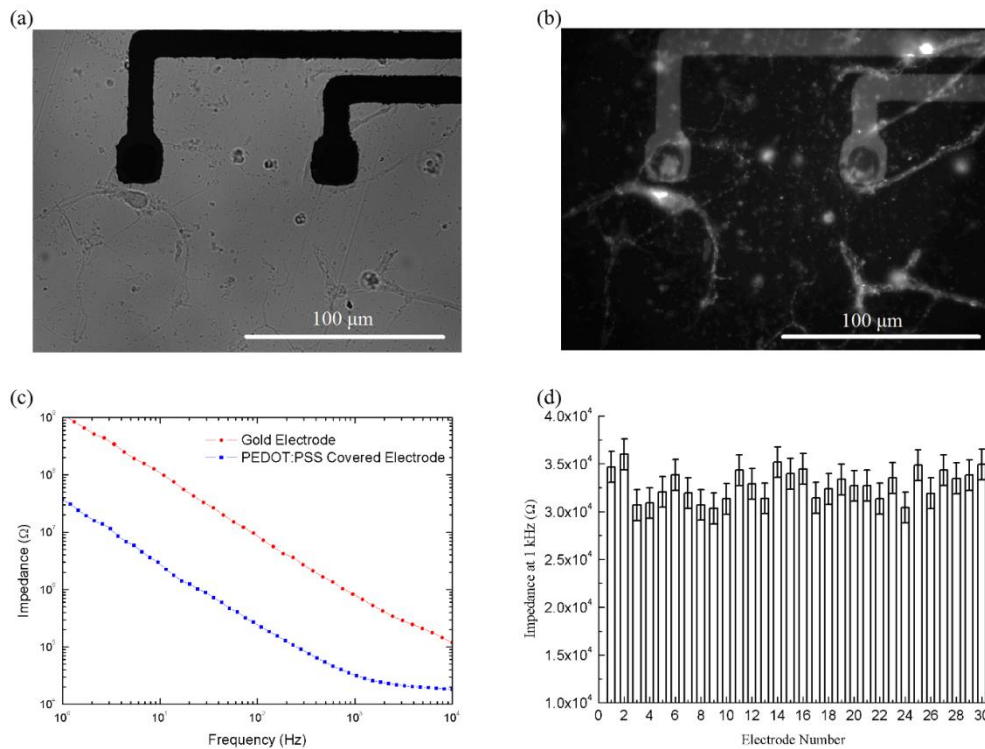


Figure 3.1: Biocompatibility assessment and device characterization. (a) Micrograph of a hippocampal cell culture on the PEDOT:PSS electrodes and (b) a vital dye stained neurons (4-Di-2-ASP) picture of the same electrodes and culture. (c) Bode plot of a PEDOT:PSS coated electrode and a gold electrode of the same area.(d) Impedance value at 1 kHz of 30 PEDOT:PSS coated electrodes randomly selected out of 4 different devices.

When a cell is placed in the proximity of the electrode and fires an action potential, it is sensed by the recording site and is translated into a peak emerging out of the noise background. The quality of the recordings depends on both the quality of the cell culture (ion channel expression, ion cell density, cell size, cell density) and on the quality of the bioelectrode (lower impedance means better recording quality). Figure 3.1(b) documents the biocompatibility of our devices as the vital dye 4-Di-2-ASP used, stains the mitochondria of living neurons hence asserting the viability and functionality of the neuronal cultures lying on the recording device. Figure 1(c) on the

other hand depicts the contribution of PEDOT:PSS to the recording quality. As previously reported, coating a metal electrode with a polymer lowers its impedance by about two orders of magnitude^[17]. This fact is attributed both to an increase of the effective area of the electrode and to the ion uptake in the polymer film. As lower impedance of the recording site results in a lower background noise level (Supplementary Figure S1 (d)) the signal-to-noise ratio (SNR) of a PEDOT:PSS coated electrode is higher than the one of the bare electrode. In our case, the value of the electrode's impedance at 1 kHz is as low as $32.8 \text{ k}\Omega \pm 600 \text{ }\Omega$ (mean value) consistent with previous reports^[13, 14]. The background noise is $\pm 3 \mu\text{V}$ peak to peak ($1.36 \mu\text{V}$ RMS) (Supplementary Figure S1 (d)). Furthermore, the previously reported fabrication method used for those electrodes^[14], results in electrodes with reproducible values of impedance as shown in Figure 1(d).

Hippocampal cells were successfully cultured on the active area of our conducting polymer MEA (Supplementary Figure S3.2) for at least 21 days. In fact, three weeks *in vitro* allows the network to become spontaneously active. The cell cultures were tested for their excitability through a standard, well established technique presented in Figure 3.2(a). More specifically, patch clamp recordings were performed on 21DIV (days *in vitro*) cell cultures and on multiple hippocampal cells. Bursts of action potentials of 150 mV of amplitude were successfully recorded validating the ability of our devices to sustain neural culturing Figure 2(b). The next step was the extracellular recordings. A cell culture was grown again on a device and extracellular recordings performed with a conducting polymer MEA. The cell covered electrode (marked as number 5 in Figure 2(c)) was recording the extracellular spontaneous activity in contrast with the uncovered electrodes around it (Figure 3.2 (c-d)). Time-frequency analysis revealed the frequency content of the high-pass filtered ($f_c = 200 \text{ Hz}$) signal. The recorded spikes showed a frequency around 1 kHz, which is the typical value for hippocampal cell APs. The time trace of the same recordings presents the extracellular action potentials in the time domain displaying spikes originated, putatively, from multiple cells. (Figure 3.2(e)).

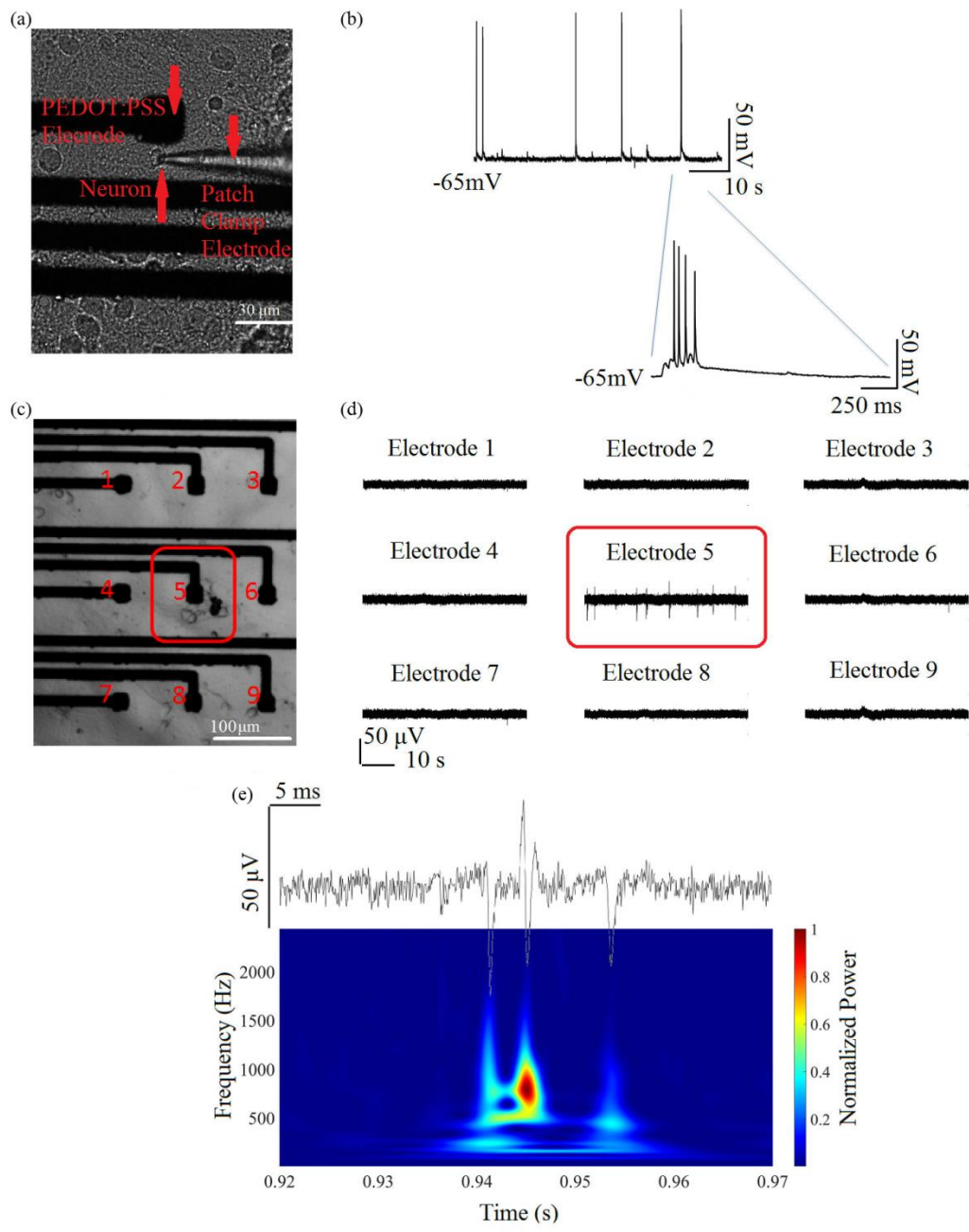


Figure 3.2: Electrophysiological recordings from cell cultures with different recording methods (a) Picture of a patch clamp electrode sealed at the surface of the membrane of a hippocampal neuron (21DIV) and (b) the subsequent recordings. The expanded trace below depicts a burst of action potentials. (c) Infrared DIC micrograph of the cell culture on top of the recording device and (d) extracellular recordings of a hippocampal cell culture. The picture shows the coverage of electrode number 5 with cells. As a consequence, the covered electrode records the extracellular activity while the non-covered ones around it do not (e) Time-frequency analysis of a short period of the previous extracellular recordings. The signal was high passed at 200Hz and the analysis shows peaks of activity around 1 kHz (referred to as neuronal action potential frequency in the literature) exactly at the time instant when the cell activity occurs in the time domain.

For further validating the biological origin of the recorded signal from our MEAs and for further testing, their potential in pharmacological application, we used drugs in order to alter the neural activity as a response to different external chemical stimulations (Figure 3.3).

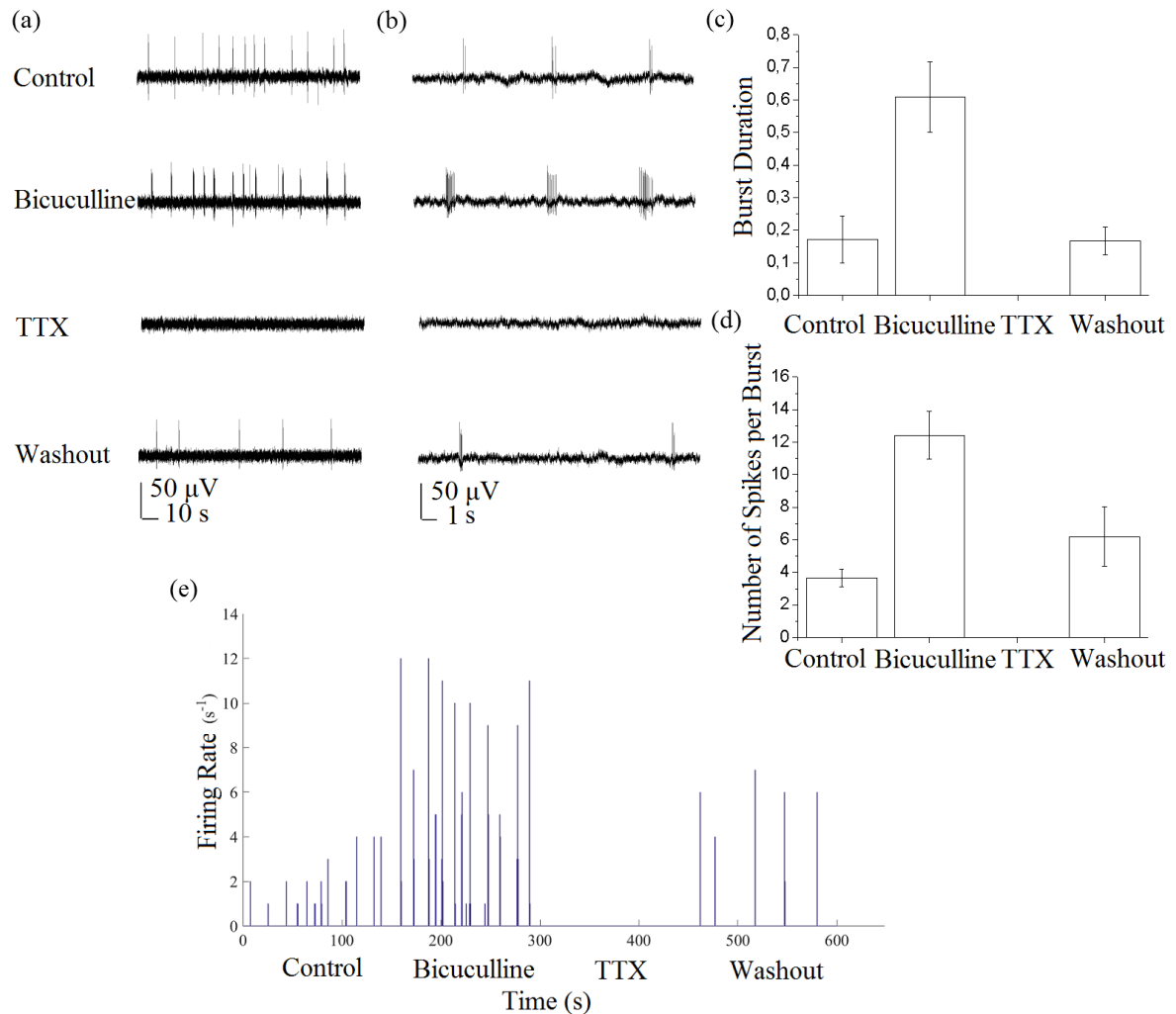


Figure 3.3: Drug modulation of the extracellular activity. (a) Electrophysiological recordings for different chemical conditions. The initial spontaneous cell activity was modified by the application of bicuculline. TTX suppressed any activity while the activity recovered after a wash out phase. (b) The smaller time scale depicts better the changes in the firing rate (number of spikes per second) during each condition (c-d) Quantification of the experimental results. The recorded burst duration and the number of spike per burst increased and decreased corresponding to chemical stimulation. (d) Firing rate profile evaluated over 600s of activity under different conditions (bin size = 500ms).

During the experiment different pharmacological conditions with time duration of 2.5 minutes each, were employed. Figure 3.3 (a-b) depicts the recorded activity under those conditions and for different time scales. The spontaneous activity (referred to as control) shows the initial firing ability of the cells. Bicuculline (3 μ M)

was consequently perfused in the recording chamber. Bicuculline is a blocker of the ionotropic GABA_A receptor. It mimics epilepsy by blocking the receptors' inhibitory action resulting in an increased cell activity in the form of bursts of spikes as previously reported ^[26]. Indeed, the initial number of recorded cell activity increased after drug application. Tetrodotoxin (TTX-15 μ M) was then employed in order to prove the biological origin of the recordings. TTX is a neurotoxin which inhibits action potential firing by binding to the voltage gated sodium channels and blocking the passage of sodium ions, which are mandatory for the creation of an action potential. As a result, the presence of TTX in the recording chamber resulted in the extinction of cell activity as presented in Figure 3.3(a-b). TTX sodium channel inhibition is reversible, so washing out both drugs (bicuculline and TTX) and restoring the cell environment to normal recording solution resulted in the cell activity recovery in the form of spike trains. The above qualitative analysis is followed by a quantitative one in Figures 3(c-f) with the study of the burst duration, the number of spikes per burst and the firing rate in each condition. Figure 3.3(c) presents the mean burst duration for different drug conditions. The initial duration of almost 0.20 s ($0.17 \text{ s} \pm 0.07 \text{ s}$) for the spontaneous activity (which is referred to as control) increased up to 0.60 s ($0.61 \text{ s} \pm 0.11 \text{ s}$) with the use of bicuculline and dropped to zero after the perfusion of TTX. Interestingly, the drug wash out phase restored the duration to almost 0.20 s ($0.17 \text{ s} \pm 0.04 \text{ s}$) again. Figure 3.3(d) presents the change in the mean number of spikes per burst. As expected, the initial average number of 3.60 ± 0.54 spikes per burst increased to 12.42 ± 1.47 spikes per bursts after the use of bicuculline, before returning to 6.20 ± 1.84 spikes per burst after the washing step. The use of TTX in between had set this value to zero.

Another way to characterize a neuronal activity is the firing rate of the cells and how it changes throughout the experiment. Firing rate (FR) is defined as the number of spikes recorded by the electrode over a small time interval T ^[27]. The smaller the interval, the better the firing rate simulates the instantaneous firing rate (IFR). In our case the time interval was set to $T = 500\text{ms}$ and it resulted the histogram presented in Figure 3.3(f). As expected, the initial firing rate in control conditions was tripled after the use of bicuculline. TTX set the firing rate to zero as the cell activity was blocked and reinduced after the drugs washout.

Similar experiments performed with the use of a different drug and other chemical agents (4-Aminopyridine and KCl solutions). They also resulted changes in the firing rate of the cells (Supplementary Figure S3.3).

3.3 Conclusions

In conclusion, high quality measurements of neural activity from hippocampal neuron cell cultures were performed with our *in vitro* PEDOT:PSS MEAs. The conducting polymer coated electrodes were fabricated with the use of a versatile technic previously used for similar fabrications^[14]. A biofunctionalization technique was also performed in order for cell cultures to grow on our devices which were electrically characterized before, through impedance spectroscopy. The low impedance values of the electrodes were essential for the high quality measurements of the neural activity. These recordings prove the efficiency of our recording devices as a tool for fundamental research in the life sciences field and especially in *in vitro* electrophysiology. The use of various drugs resulted in cell activity modification, paving the way for the use of our electrodes as a drug screening platform during pharmacology tests.

3.4 Experimental Section

3.4.1 Microelectrode Arrays fabrication: The Microelectrode Array was fabricated in a previously reported way^[14]. It includes the deposition and patterning of metal (Gold), Parylene-C and PEDOT:PSS on a glass substrate. The substrate (a 25 mm x 75 mm glass slide) was thoroughly cleaned by sonication in a soap bath for 15 minutes followed by a 15 minutes sonication in a mixture of Aceton/Isopropanon (1:1). S1813 photoresist was spun on the substrate before exposed to UV light with the use of a SUSS MJB4 contact aligner and a chromium mask (1st Photolithography step). The exposed parts of the photoresists were then developed in a MF-26 developer bath and a 10 nm of Chromium/100 nm of Gold deposition step in a metal evaporator followed. Lift-off in a 1:1 mixture of solvents (Acetone/Isopropanol), removed the excess of gold creating the desired gold electrode pattern on the substrate. Two layers of Parylene – C , 2 μm each, were deposited with the help of a SCS Labcoater. Between the two layers commercial available soap solution 1%

(Micro-90) was deposited in order to act as an anti-adhesive layer. At the same time, between the first layer and the substrate a 3-(trimethoxysilyl)propyl methacrylate (A-174 Silane) acted as an adhesive promoter. A second photoresist (AZ 9260) was then spun and a second photolithography step took place. Reactive Ion Etching (RIE) with plasma O₂ (Oxford 80 Plasmalab plus) resulted in window opening on top of the electrodes. A peeling-off of the sacrificial second Parylene-C layer defined the active area of the recording site after PEDOT:PSS solution was spun cast. The devices were then baked at 140 °C for 1h and were immersed in D.I. water over night so that any excess of low molecular weight compounds inside the dispersion to be removed.

For the PEDOT:PSS films preparation, 38 mL of PEDOT:PSS aqueous dispersion (Clevios PH -1000) were mixed with 2 mL of ethylene glycol (conductivity enhancement), 50µL of 4-dodecylbenzenesulfonic acid (DBSA) that helps film formation and 0.4 mL of 3-methacryloxypropyltrimethoxysilane (GOPS) which is a surface adhesion promoter and a polymer cross-linking agent that enhance film stability of in aqueous environments.

3.4.2 Preparation of the rat hippocampal cell cultures: Primary hippocampal cell cultures were performed from embryonic day 18-Wistar rats. Hippocampi were collected in Hanks' balanced salt solution, dissociated with trypsin and plated at a density of 12105 cells/cm² on poly-L-lysine coated wells. The hippocampal neurons were cultured in Neurobasal supplemented with 2% B-27, 1% penicillin-streptomycin and 0.3% glutamine in a humidified atmosphere containing 5% CO₂ at 37°C. All animal experiments were carried out according to the animal care and experimentation committee rules approved by CNRS, France. A vital fluorescent dye (4-Di-2-ASP, 3µM, Sigma-Aldrich) was used to stain living neurons and assert the viability of the culturing process on the electronic devices. Cultures were immersed for 15 min with a warm (37°C) solution of the dye, then abundantly rinsed with the recording extracellular solution.

3.4.3 Electrical and electrophysiological recordings:

MEAs electrical characterization: Impedance measurements were performed with a potentiostat (Autolab PGSTAT128N) in a three electrodes configuration. An Ag/AgCl

electrode was used as the reference electrode, a Pt electrode was the counter electrode while the MEA's electrodes were the working electrodes.

Extracellular recordings: During the electrophysiological recordings a 3D printed holder was used in order to facilitate the access to all electrodes. The holder was printed with the use of a 3D printer Model EDEN 260V from Stratasys. All data were recorded with a multichannel amplifier chip RHD2132 (INTAN technologies US) which was connected to the MEA through the 3D printed holder. The sampling rate was set to 20 kS/s and the recordings were analysed in Matlab (Mathworks) with custom-written tools. A Morlet wavelet analysis was used for the frequency content determination of the recordings in Figure 2 (e).

Statistical analysis: Data are reported in the text as mean values \pm confidence with the level of significance set at $P < 0.05$ (t-student).

Patch clamp : Whole-cell recordings were performed using an Axopatch200B amplifier (Axon Instruments, Axon Digidata 1550) under visual control (InfraRed Differential Interference Contrast (DIC), Microscope, Zeiss Examiner A1; camera, Jenoptik ProgRes MF) and patch microelectrodes (1.5 mm OD, borosilicate filament glass, BF150 from WPI); PP-830 electrode puller, Narishige) filled with (in mM): potassium chloride, 140; N-2-hydroxyethylpiperazine-N-2-ethanesulphonic acid (HEPES), 10; ethylene glycol-bis(b-aminoethylether)-N,N,N', N-tetraacetic acid (EGTA), 10; MgCl₂, 1; CaCl₂, 1; and Mg-ATP, 4 / Na₂-GTP, 0.4 added the day of the experiment (pH 7.4 with KOH). Pipettes (4-6 M Ω) were directed onto neurons using a motorized Sutter microdrive (ROE200, Sutter Instrument Co). The offset between the reference electrode and the patch pipette was zeroed when touching the recording chamber extracellular medium (in mM: NaCl, 140; KCl, 3; Hepes, 10; glucose, 10; CaCl₂, 2.5; MgCl₂, 1; pH 7.4 with NaOH). The reference electrode was an Ag/AgCl wire connected to the extracellular solution. The resting membrane potential values ranged from -53 to -68mV and were not corrected for junction potential. Selected neurons had gigaohm seals (typically 1-5 G Ω) and a stable resting membrane potential. In current-clamp mode output bandwidth was set at 10 kHz and series resistance was not adjusted. After membrane rupture with a negative pressure the input resistance ranged 340 M Ω to 1.5 G Ω . Selected neurons had an access resistance < 15 M Ω that was not compensated for.

References

- [1] W. T. Abraham, W. G. Fisher, A. L. Smith, D. B. Delurgio, A. R. Leon, E. Loh, D. Z. Kocovic, M. Packer, A. L. Clavell, D. L. Hayes, M. Ellestad, R. J. Trupp, J. Underwood, F. Pickering, C. Truex, P. McAtee, J. Messenger, *The New England journal of medicine* 2002, 346, 1845.
- [2] G. M. Clark, *Philos. Trans. R. Soc. Lond. B Biol. Sci.* 2006, 361, 791.
- [3] G. M. Clark, *Hearing Research* 2015, 322, 4.
- [4] J. Rivnay, R. M. Owens, G. G. Malliaras, *Chemistry of Materials* 2014, 26, 679.
- [5] J. Pine, *J Neurosci Methods* 1980, 2, 19.
- [6] D. A. Borkholder, J. Bao, N. I. Maluf, E. R. Perl, G. T. Kovacs, *J Neurosci Methods* 1997, 77, 61.
- [7] E. M. Steidl, E. Neveu, D. Bertrand, B. Buisson, *Brain Res* 2006, 1096, 70.
- [8] A. R. Abdur Rahman, D. T. Price, S. Bhansali, *Sensors and Actuators B: Chemical* 2007, 127, 89.
- [9] Y. Nam, B. C. Wheeler, *Crit Rev Biomed Eng* 2011, 39, 45.
- [10] X. Cui, V. A. Lee, Y. Raphael, J. A. Wiler, J. F. Hetke, D. J. Anderson, D. C. Martin, *Journal of biomedical materials research* 2001, 56, 261.
- [11] R. A. Green, N. H. Lovell, G. G. Wallace, L. A. Poole-Warren, *Biomaterials* 2008, 29, 3393.
- [12] M. R. Abidian, J. M. Corey, D. R. Kipke, D. C. Martin, *Small* 2010, 6, 421.
- [13] K. A. Ludwig, N. B. Langhals, M. D. Joseph, S. M. Richardson-Burns, J. L. Hendricks, D. R. Kipke, *J Neural Eng* 2011, 8, 014001.
- [14] M. Sessolo, D. Khodagholy, J. Rivnay, F. Maddalena, M. Gleyzes, E. Steidl, B. Buisson, G. G. Malliaras, *Advanced Materials* 2013, 25, 2135.
- [15] D. Khodagholy, T. Doublet, P. Quilichini, M. Gurfinkel, P. Leleux, A. Ghestem, E. Ismailova, T. Herve, S. Sanaur, C. Bernard, G. G. Malliaras, *Nat Commun* 2013, 4, 1575.
- [16] D. A. Koutsouras, P. Leleux, M. Ramuz, J. Rivnay, G. G. Malliaras, "Organic electrochemical transistors for BioMEMS applications", presented at *2014 IEEE International Electron Devices Meeting*, 15-17 Dec. 2014, 2014.
- [17] D. H. Kim, S. Richardson-Burns, L. Povlich, M. R. Abidian, S. Spanninga, J. L. Hendricks, D. C. Martin, in *Indwelling Neural Implants: Strategies for Contending with the In Vivo Environment*, (Ed: W. M. Reichert), CRC Press/Taylor & Francis Taylor & Francis Group, LLC., Boca Raton (FL) 2008.
- [18] G. Malliaras, R. Friend, *Physics Today* 2005, 58, 53.
- [19] G. Buzsaki, C. A. Anastassiou, C. Koch, *Nature reviews. Neuroscience* 2012, 13, 407.
- [20] Y. Jimbo, *Archives italiennes de biologie* 2007, 145, 289.
- [21] T. Tateno, Y. Jimbo, H. P. Robinson, *Neuroscience* 2005, 134, 425.
- [22] G. Buzsáki, M. Penttonen, Z. Nádasdy, A. Bragin, *Proc. Natl. Acad. Sci. U. S. A.* 1996, 93, 9921.
- [23] Z. Qiao, K. Xie, K. Liu, 2014, 2014, 626108.
- [24] M. Chiappalone, A. Vato, M. B. Tedesco, M. Marcoli, F. Davide, S. Martinoia, *Biosensors & bioelectronics* 2003, 18, 627.
- [25] C. Vallejo-Giraldo, A. Kelly, M. J. Biggs, *Drug discovery today* 2014, 19, 88.
- [26] F. J. Arnold, F. Hofmann, C. P. Bengtson, M. Wittmann, P. Vanhoutte, H. Bading, *The Journal of physiology* 2005, 564, 3.
- [27] T. T. Kanagasabapathi, P. Massobrio, R. A. Barone, M. Tedesco, S. Martinoia, W. J. Wadman, M. M. Dece, *J Neural Eng* 2012, 9, 036010.
- [28] Z. Yang, Q. Zhao, E. Keefer, W. Liu, in *Advances in Neural Information Processing Systems 22*, (Eds: Y. Bengio, D. Schuurmans, J. Lafferty, C. K. I. Williams, A. Culotta), 2009, 2160.

Supplementary Information

Device layout and noise level

Figure S3.1 presents the electrode array layout used during the experiments. The device consists of two separate 32 electrode MEAs built on the same glass slide each one of which can be addressed separately (from the left and the right side of the device). The horizontal and the vertical spacing of the grid is $100\ \mu\text{m}$ while each recording site has a $10\ \times 10\ \mu\text{m}^2$ PEDOT:PSS area. The lower impedance of the polymer coated electrode in comparison to a bare gold electrode results in lower noise level a fact linked to better quality measurements. The background noise is $\pm 3\ \mu\text{V}$ peak to peak and the RMS $1.36\ \mu\text{V}$.

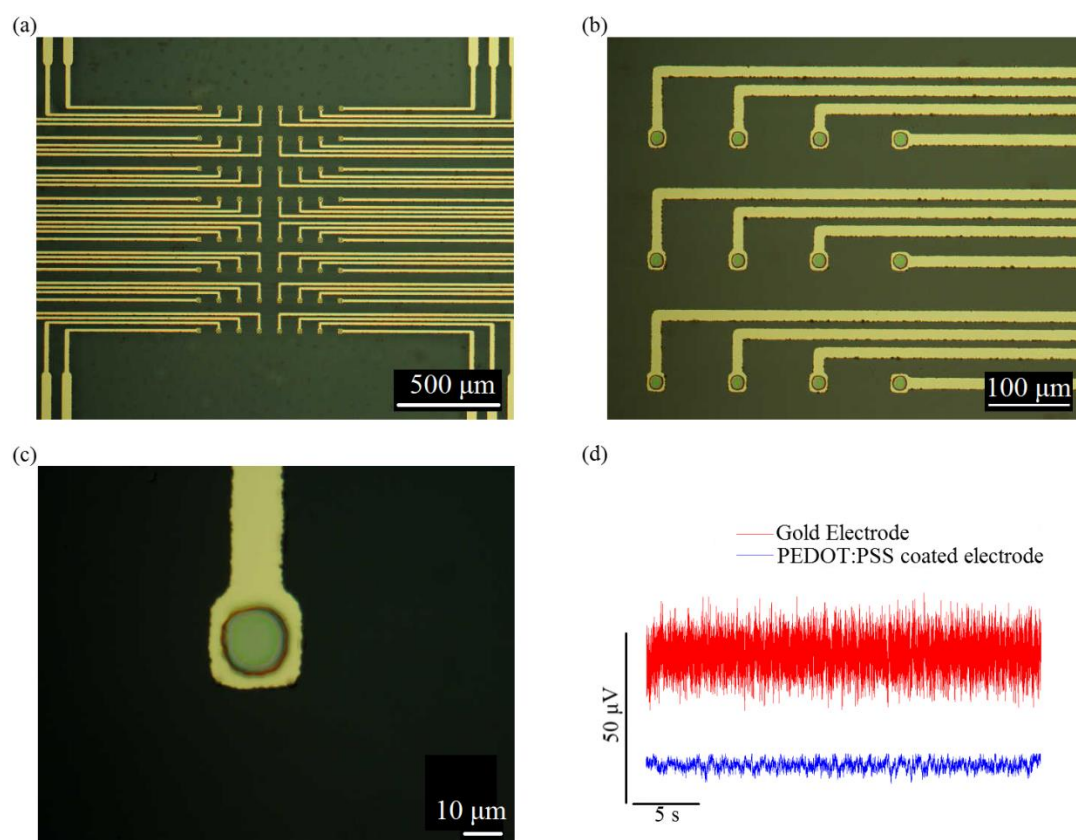


Figure S3.1: (a) Active area of the PEDOT:PSS covered MEA. Each device consists of two separately addressed grids of 32 electrodes. (b) A close up of the MEA and (c) A $10\ \mu\text{m} \times 10\ \mu\text{m}$ single electrode (nominal dimensions). (d) Noise level of a PEDOT:PSS gold electrode and a bare electrode of the same area (measurements in 0.1M NaCl solution).

MEAs biocompatibility assessment

Pictures of the hippocampal cell cultures used in this work. A vital dye (4-Di-2-ASP) was used to assert the device biocompatibility. 4-Di-2-ASP is a fluorescence dye that targets the mitochondria of living neuronal cells and stains them in contrast to non-living ones.

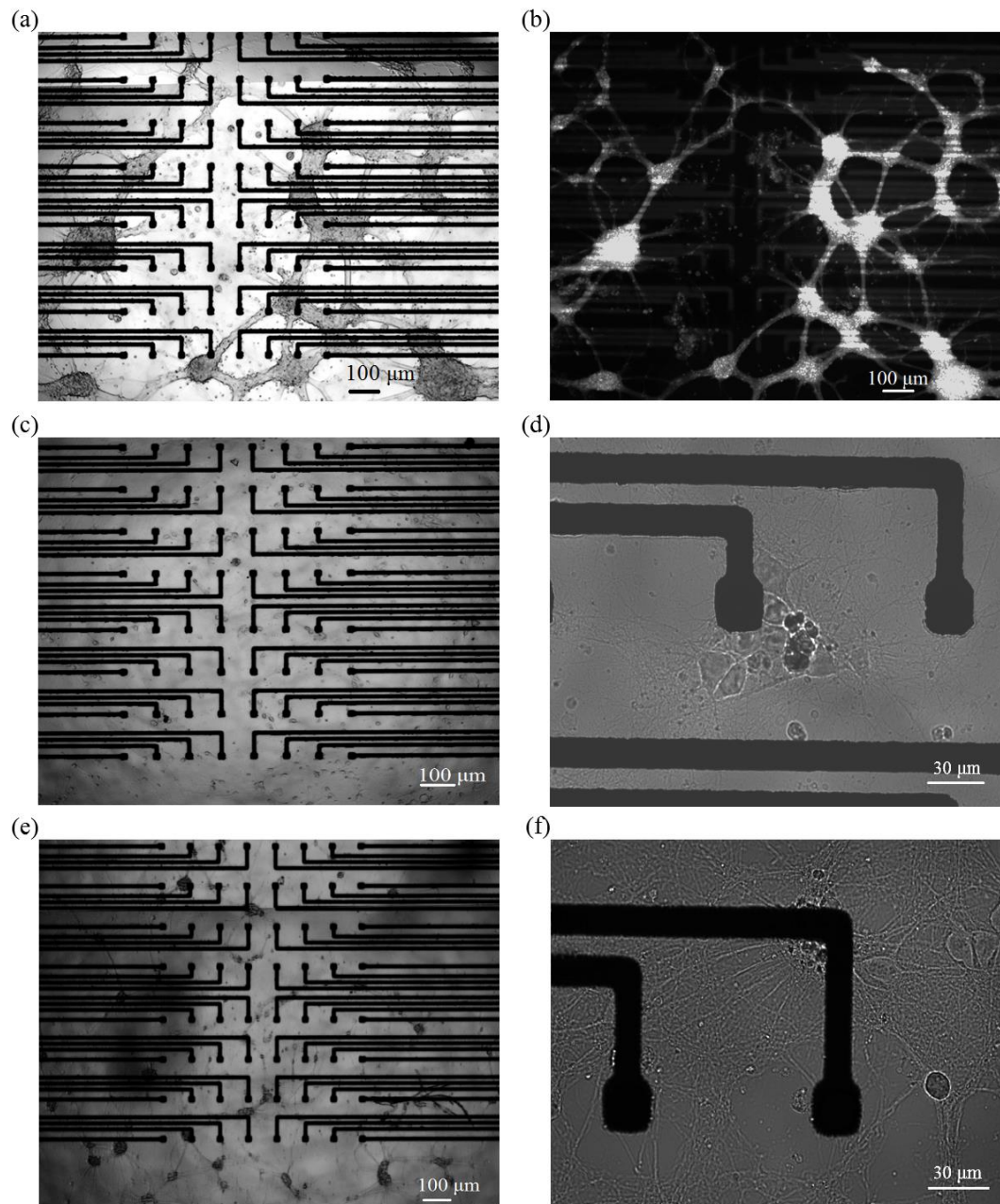


Figure S3.2: Biocompatibility assessment of the MEAs. (a) Microscope (Infrared DIC) picture of hippocampal cell cultures on a MEA device and (b) a stained image of the same culture (4-Di-2-ASP). (c) The neuronal cell culture used for the electrophysiology measurements presented in Figure 3.2 (d) Electrode number 5 of Figure 3.2 (c) covered with neurons. (e) The neuronal cell culture used for the electrophysiological measurements presented in Figure 3.3 and (f) a close up of the recording electrode.

Recordings from multiple electrodes and for different conditions

Figure S3.3 shows recordings from multiple electrodes from the cell culture used in Figure 3.3. Each recording condition lasted for 60 seconds. Except bicuculline and TTX, 4-Aminopyridine (4-AP)(3 μM) and a KCl solution (100 μM) were also used. 4-AP is a relatively selective blocker of voltage-activated K^+ channels and is used to generate seizures (status epilepticus) in animal models for the evaluation of anti-seizure agents. KCl is a salt that cause depolarization of the membrane preventing its repolarization. When applied extracellularly, induces long lasting action potential firing.

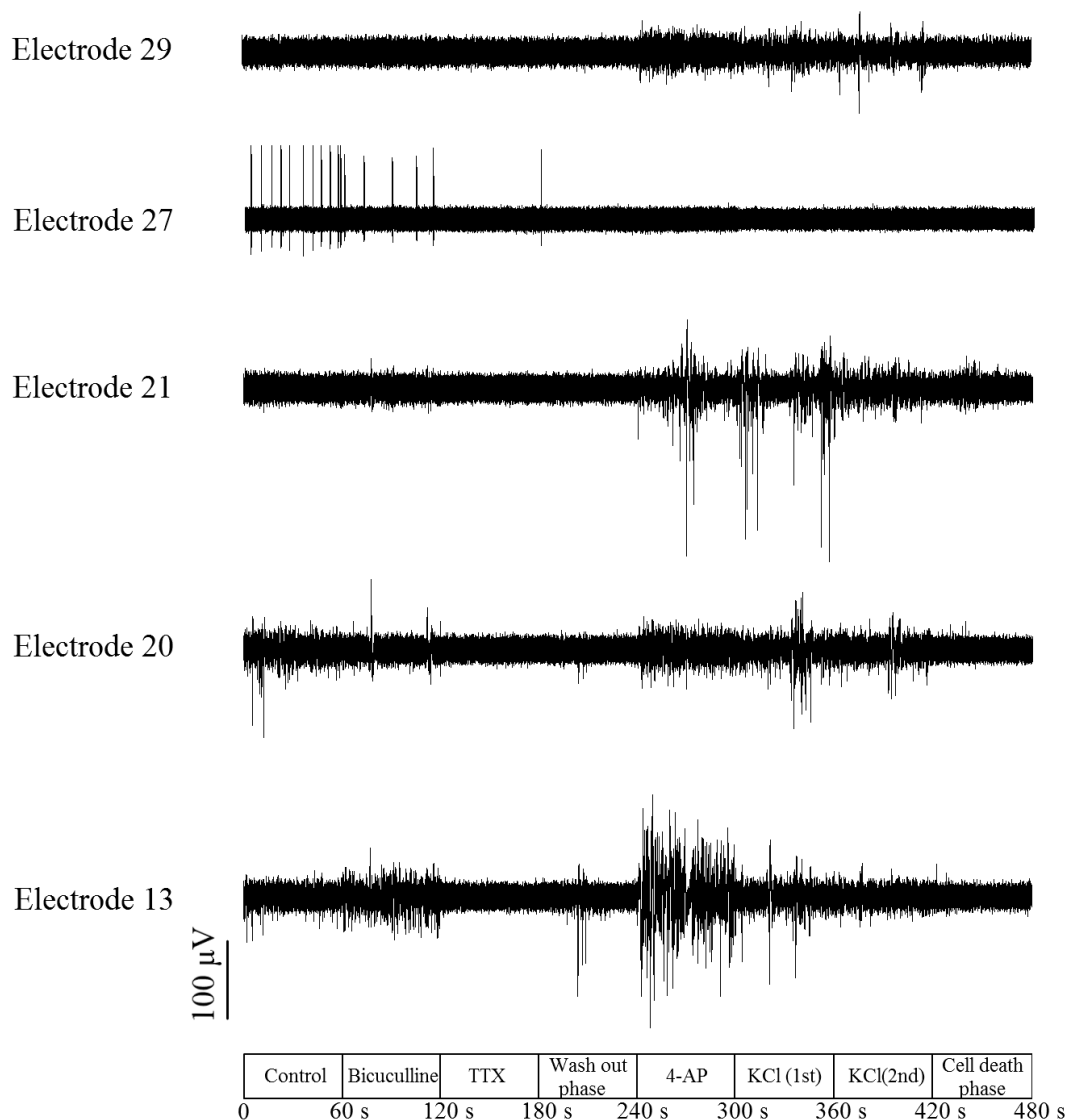


Figure S3.3: The initial spontaneous firing activity on different channels was increased after bicuculline application ($t=60$ s) and was blocked in the presence of the neurotoxin TTX ($t=120$ s). The activity recovered after a wash out phase ($t=180$ s). Application of 3 μM of 4-Aminopyridine (4-AP) at $t=240$ s modified the general firing activity as observed from multiple recording sites. KCl solution also affected the recording activity until its high levels (second dose-200 μM) became toxic causing cell death. The toxic effect comes mainly from the influx of a huge amount of calcium after prolonged depolarization of the cell membrane.

Chapter 4: A PEDOT:PSS *in vitro* Platform for Pancreatic Islet Cell Electrophysiology

4.1 Abstract

Pancreatic cells play a crucial part in preserving nutrient homeostasis in human body. Having been extensively studied during the past years, today they are considered to be ideal nutrient sensors as they possess a twofold role. They, both, store and secrete insulin (beta cells) and glucagon (alpha cells), the two hormones that regulate the blood glucose level. In the case of beta cells, an increase in glycaemia results in membrane depolarization and insulin secretion. Recording these electrophysiological signals is of extreme importance for decoding the endogenous algorithms used in pancreas islets to attain homeostasis. Nevertheless, this task is rather challenging due to the coupling incompatibilities at the level where electronic materials meet the biological soft tissue.

Lately, conducting polymers have gained increasing attention by the scientific community due to their potential to bridge the gap between electronics and biology. Especially, Poly(3,4-ethylenedioxythiophene):poly(styrenesulfonate) (PEDOT:PSS) offers a new approach in bioelectronic devices mostly to its unique feature to conduct both electronically and ionically. Moreover, it has the advantages of being easy processable and chemically tunable over its inorganic counterparts. In this work, we present a PEDOT:PSS covered microelectrode array (MEA) platform for real-time monitoring of pancreatic cell activity as response to glucose, adrenaline and multiple environmental factors. With this platform we were able to record slow potentials (SP) and action potentials (AP) from mouse and human islet cells.

Our results verify that PEDOT:PSS dramatically improves the quality of passive electrode recordings and paves the way of using conducting polymers for elucidating pancreatic cells physiology.

4.2 Experiment – Results

Pancreas islets cells play a pivotal role in retaining the nutrient homeostasis as being both sensors and reservoirs of insulin, the main hormone of blood glucose regulation. Beta cells in particular, which make up 65-80% of the total islet cells, are the hormone's main secreting sites of pancreas. They are able to sense, uptake and metabolize glucose in a metabolic pathway that involves many different steps and which is controlled by a number of different hormones. During this multistep process, an increase of ATP concentration leads to ATP-dependent potassium channels (K_{ATP}) closure, a phenomenon that causes the cell membrane to depolarize. It is exactly this membrane depolarization that triggers the opening of voltage-dependent Ca^{2+} channels resulting in a calcium influx and an ultimately insulin exocytosis^[1]. Hormones (like adrenaline) and drugs (like glibenclamide and nifedipine) can bind to transmembrane proteins affecting the inward and outward cation current through the membrane and hence altering the insulin secretion status^[2]. That is the reason why monitoring pancreatic cells electrophysiological activity, is a first integrative read-out of insulin demand^[3].

Since insulin secretion from beta cells and their membrane depolarization are deeply correlated, recording and studying electrophysiological data is of extreme importance for two reasons. Firstly, it gives an insight into the endogenous algorithms these cells use to communicate and secondly can be used to detect abnormalities during pathological conditions like diabetes^[4]. Consequently, a platform that would allow continuous monitoring of this activity would be an extremely useful asset both in therapy and sensing.

Nevertheless, recording these electrical signals possess a great challenge mostly due to incompatibilities in the coupling between electronic materials and biological soft tissue. In addition, most of the already existing electrophysiological approaches require invasive techniques (e.g. patch clamp) which are destructive for the cell membrane. Those techniques share a rather complicated set up, can target only individual cells and can be implemented for limited time only^[5]. Extracellular recordings on multielectrode arrays (MEAs) on the other hand, preserve the under study cells intact and allow the simultaneous data acquisition from many different cells for an extended period of time. Its main drawback, though, is the low signal to noise ratio due to attenuation of the recorded electric field inside the extracellular conductive media^{[5] [6] [7] [8] [9]}.

In this work, we present an *in vitro* PEDOT:PSS platform for Pancreatic Islet Cell extracellular electrophysiology. Recently, conducting polymers have become extremely popular among the scientific community as one of the most promising candidates for the next generation biology interfacing devices, both *in vitro* and *in vivo*^[10]. Especially, Poly(3,4-ethylenedioxythiophene):poly(styrenesulfonate) (PEDOT:PSS) has the unique feature to conduct both electronically and ionically, offering a new pathway of interaction between biological systems and electronics^[11]. Thus, during the performed experiments we take advantage of the low impedance that the PEDOT:PSS covered electrodes offer, in order to improve the quality of the recorded biological signals. To the best of our knowledge, that is the first time that a conducting organic polymer multielectrode array (MEA) has been used to monitor the activity of this kind of cells.

In Figure 4.1(a), it is presented a microscope picture of a mouse pancreatic islet cell culture on a 32 (8x4) MEA. The cell coverage is limited to the top right corner of the device resulting in 11 fully covered PEDOT:PSS electrodes. The rest of the electrodes are poorly or non-covered at all, serving as control electrodes for the upcoming data analysis. The electrical characterization of the PEDOT:PSS covered electrodes that were used during the measurements is presented in Figure 1(b). The electrodes were fabricated in a previous published photo lithographically way^[12]. Characterization confirms the fact that the use of a conductive polymer coating lowers the impedance by more than two order of magnitude compared to bare gold electrodes^[11] ^[13]. Furthermore, conducting polymer coated MEAs present lower impedance even when are compared to commercially available TiN ones. This leads to better quality recordings keeping the background noise level extremely low (Supplementary S4.1)

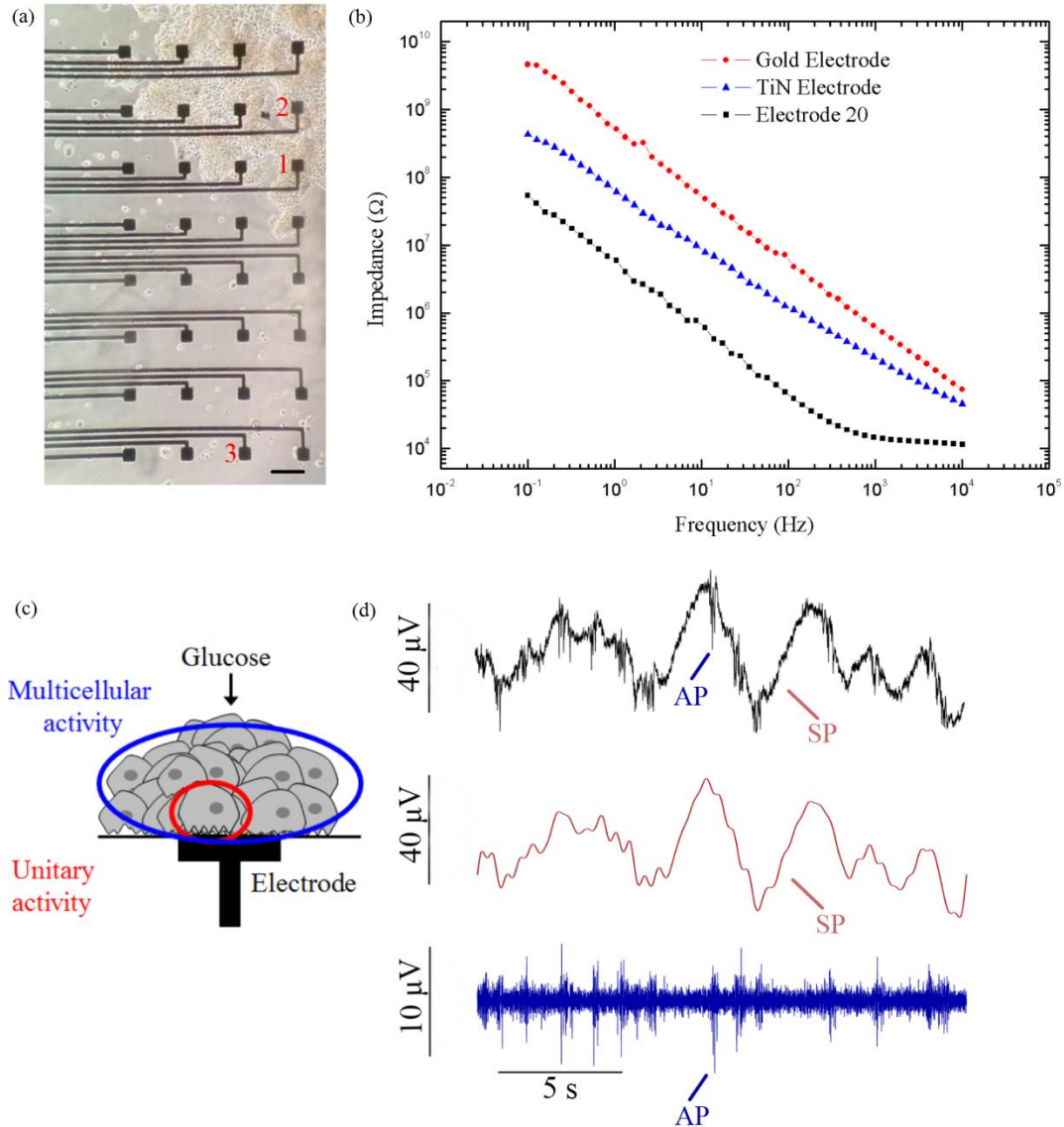


Figure 4.1: (a) A microscope image of a mouse islet cell culture on top of the PEDOT:PSS MEA. Electrodes 1 and 2 are selected as representatives of the cell covered electrodes. Electrode 3 at the bottom serves as a non-covered control electrode (scale bar 100μm). (b) Impedance spectroscopy of a PEDOT:PSS electrode vs a gold and a TiN commercial one of the same area. (c) Schematic representation of a mouse islet on top of a recording electrode. An action potential (AP) is the unitary activity of a single beta cell when excited with high glucose. A multicellular activity, on the other hand, is the superposition of signals coming from a large population of cells resulting in a slow potential (SP). (d) High temporal resolution image of recordings from Electrode 1, showing fast action potentials superimposed on a slow potential bearing wave. The cells were triggered with high glucose concentration (15mM-G15). The overall signal can be broken down to fast events (AP) (2-700Hz band pass filtering) and slow oscillations (SP) (2 Hz low pass filtering).

On top of these electrodes the pancreatic cells were cultured forming islets similar to the ones presented in the schematic of Figure 4.1(c). Their membrane depolarization creates extracellular field potentials which can be sensed by the electrodes of the MEA that lie beneath. The activity of a single cell is called action

potential (AP)^[14] and it is a fast event of small amplitude (30-100ms in duration, 10-50 μV in amplitude). The superposition of these events coming from a greater number of cells (multicellular activity) is recorded as slow potentials (SP)^[3] which are slower and greater in amplitude signals (400-1500 ms in duration, 40 μV -1.2mV in amplitude). Representative recordings from the above cell culture are presented in Figure 4.1(d). Electrodes are marked with numbers in order to render their distinction easier during data analysis. The fact that the MEA was not uniformly covered gave us the privilege of using the uncovered electrodes as control ones. Electrode number 1, for example, is a well-covered one and consequently it should provide electrophysiological recordings during the measurement. Indeed, high concentration of glucose (15mM) inside the culturing chamber resulted in the recordings presented in Figure 4.1(d). Slow potentials (SPs) ,0.5Hz in frequency, were resolved by our *in vitro* platform corresponding to the multicellular activity of the islet cells seeded on the MEA. In reality, the recorded signal is the superposition of two distinct electrophysiological signals. Thus, when the slow oscillations are filtered out by a Butterworth high pass filter (with a 2 Hz upper cut off frequency) rapid spikes of small amplitude (40-60ms duration, 10-50 μV) is what is left behind. These fast events are due to the activity of unitary cells that happen to be in the close proximity of the recording electrode and are called action potentials (APs). What is important for the PEDOT:PSS platform is that fast events could be recorded with an efficiency of almost 100% on active electrodes in contrast with the $32.2\pm 3.7\%$ ($n=20$ experiments) of commercial MEAs^[3](Supplementary S4.2). In addition, the platform was able to detect both kinds of activities (slow potentials and action potentials) without the need of complex algorithms for their extraction^[14].

The electrophysiological activity could be recorded on all the active electrodes while the uncovered ones remained silent (Supplementary S4.2). Nevertheless, the biological origin of the recorded signals was still to be verified and that is why chemical agents, which could alter this activity, were employed (Figure 4.2).

Figure 4.2(a) monitors the progress of the experiment in time and under the use of chemical agents that can suppress or induce electrophysiological activity on pancreatic cell islets. Four different recording and a control condition were employed, namely: 1) Low glucose concentration-G3 (3mmol/l) (control condition) 2) High glucose concentration-G15 (15mmol/l) 3) G15+adrenaline (5 $\mu\text{mol/l}$) 4) G15 +

clibenclamide (0.1 μ mol/l) 5) G15+nifedipine (25 μ mol/l). Each recording condition lasted for 5 minutes.

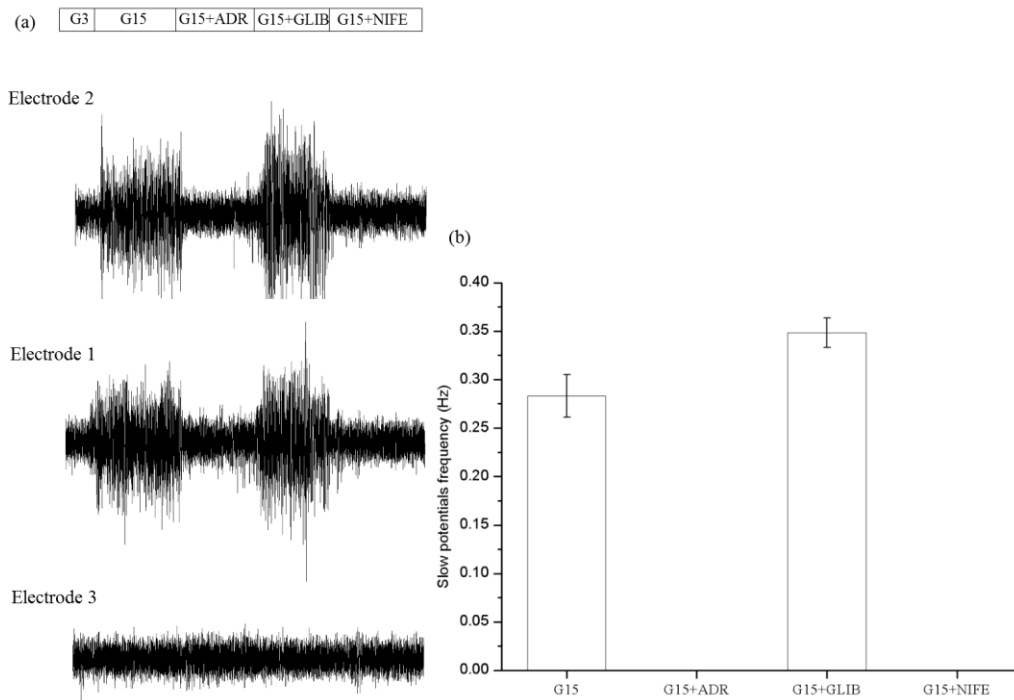


Figure 4.2: (a) Monitoring the pancreatic islet cells reaction for 4 different recording conditions. The initial low glucose (3mM-G3) zero activity is increased with the use of high glucose concentration (15mM-G15). Adrenaline reversibly suppresses the activity which was to be re-induced with the use of the drug clenbuterol. Nifedipine as a Ca^{2+} blocker permanently suppresses the activity. (b) The frequency of slow potentials (events per second) in response to high glucose concentration, adrenaline, glibenclamide and nifedipine.

The experiment started with an initial low glucose concentration of 3mM (G3) which served as a control condition and during which no activity was recorded. After 2 minutes glucose concentration was raised to 15mM (G15). The extra polysaccharide inside the culturing chamber increased the activity of beta cells resulting in slow potentials of about 40 μ V in amplitude (peak-to-peak). The hormone adrenaline has a transient inhibitive effect on beta cells activity as it reversibly suppresses it [3, 14, 15]. After the use of 5mM of the hormone the next five minutes showed a suppression of beta cells activity as anticipated by the literature [3].

Our next goal was to re-induce activity as prove of the claim that the recorder signals were biological events and consequently a response to chemical stimulation.

Glibenclamide is an antidiabetic drug that belongs in the class of sulfonylureas and is a known beta cell activator. It acts by blocking the K-ATP channels located in the cell membrane inducing electrophysiological activity recorded as slow potentials and action potentials. The frequency of the events is now even higher than the G15 condition as the synergic action of high glucose and glibenclamide pushes the cells to their activity limits. However, the non-covered control electrode remained not influenced by the presence of the drug.

Our final condition induces the drug nifedipine inside the culture chamber. Nifedipine, is an inhibitor of the voltage-gated calcium channels and as a result it permanently suppress the activity of pancreas islet cells. Indeed, as illustrated in Figure 4.2(a), after injection of 25 μ M of the drug, the activity is suppressed permanently in every recording channel of the platform.

Quantification of the resulting action of every chemical agent on cells is depicted in Figure 4.2(b). The bar graph shows the change in the number of slow potential events per second (frequency) as a response to different chemical conditions. The electrical activity of mouse islets increased from zero to 0.28 ± 0.02 Hz when glucose concentration increased was raised from 3mM to 15mM in the culture chamber. The frequency drops dramatically (but reversibly) to zero with the introduction of the hormone adrenaline and it recovers in an even higher level (0.35 ± 0.01 Hz) after the use of glibenclamide. The frequency drops to zero again with nifedipine.

The above are further elucidated in the higher resolution traces of a part of the recorded data in Figure 4.3. Traces from electrodes number 1 and 2 are compared to the control electrode number 3 which is free of cells. Figure 4.3(a) presents the three traces for a high glucose concentration (G15). Electrodes 1 and 2 recorded slow waves created from beta cells as response to the polysaccharide as well as fast activity coming from single cells and which is depicted as action potentials. Electrode 3 recorded only background noise. What is also worth noticing is that APs were mainly present during the falling than the rising phase as previously reported^[3].

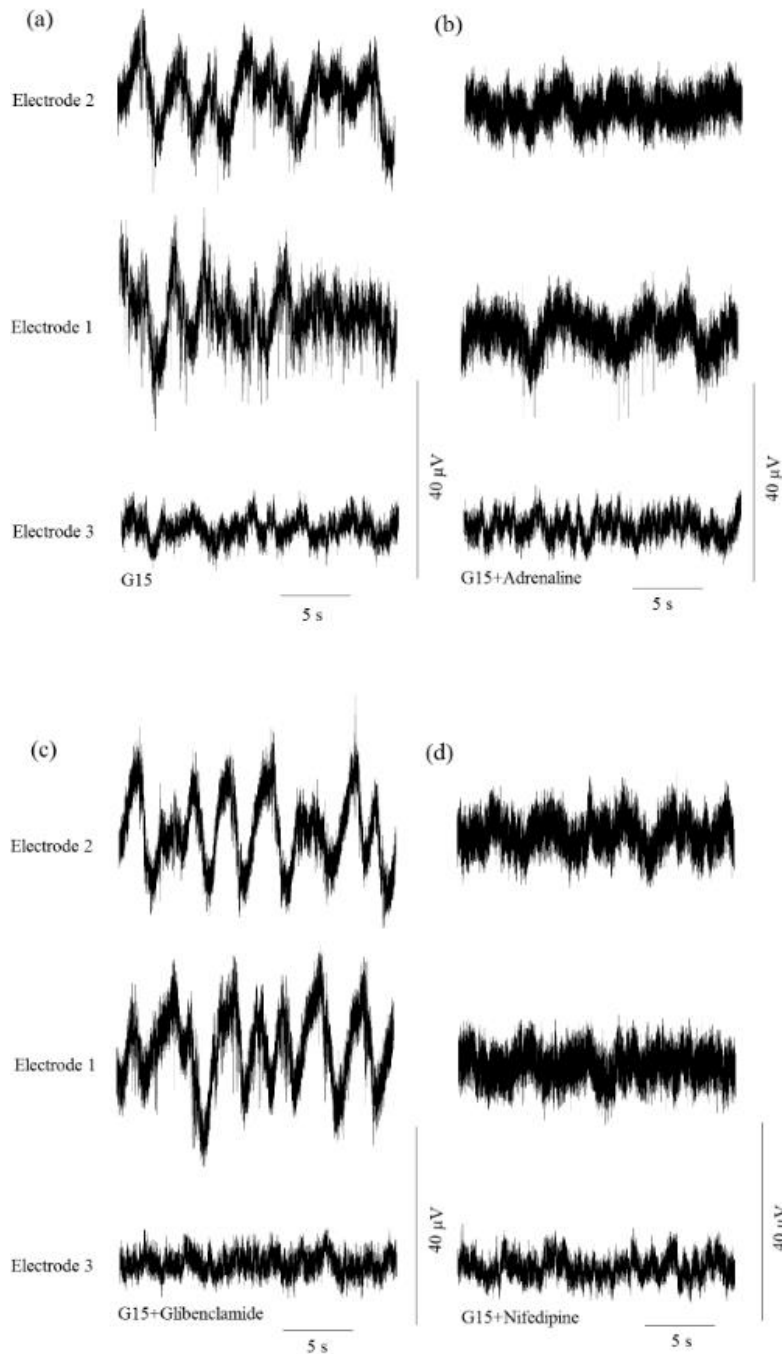


Figure 4.3: (a)-(d) Higher temporal resolution of 3 representative electrode recordings. Electrodes 1 and 2 were well covered electrodes while electrode 3 was a non-covered (control) one. (a) The covered electrodes 1 and 2 recorded biological activity (both slow waves and action potentials) under the presence of 15mM of glucose (G15). Control electrode 3 did not show any activity (b) Adrenaline reversibly suppressed beta cell activity on both electrodes 1 and 2. The remaining fast events on electrode 2 are attributed to alpha cells (c) Glibenclimide re-induced the activity to beta cells islets that covered electrodes 1 and 2. Control electrode 3 remained silent. (d) The drug nifedipine permanently suppressed the activity on all electrodes

Adrenaline is a stress hormone that has been reported to reversibly inhibit activity in beta cells^[3]. As a consequence, implementation of 5 μ M of adrenaline, temporarily suppressed the slow waves of beta cells as shown in Figure 4.3(b). Nevertheless, adrenaline acts differently on alpha cells, which are also cultured together with beta cells but in smaller portions making up only ~20% of the total islets cells. In particular, the stress hormone is a well-known alpha cell stimulator resulting in action potentials as the one shown on electrode 1 (Figure 4.3(b)). This behaviour is indicative of the adrenaline and glucose effect on alpha and beta cells. Glucose on high concentrations (15mM) induced slow potentials on beta cells inhibiting alpha cell activity. Adrenaline on the other hand transiently suppressed beta cells activity activating alpha cells at the same time.

The final two conditions included the use of the drugs glibenclamide and nifedipine. Glibenclamide was initially used to re induced the activity as depicted in Figure 4.3(c). The synergy of the drug with the high Glucose concentration (G15) resulted in the re appearance of the slow waves due to the re activation of beta cells. The observed action potentials on top of slow oscillations are now originating from single cell activity of beta cells since for those conditions, alpha cells are again silent. Finally, nifedipine was the last condition to be tested. The Ca²⁺ blocker permanently suppressed every cell activity^[3, 16] resulting in the flat lines presented in Figure 4.3(d).

Going a step further similar experiments were also performed with human pancreas islets (cells were taken from two different donors). Figure 4.4(a) presents examples of SPs induced by 15 mM of glucose and inhibited by adrenaline. Figure 4.4(b) on the other hand examples APs induced by 15 mM of glucose and inhibited by nifedipine.

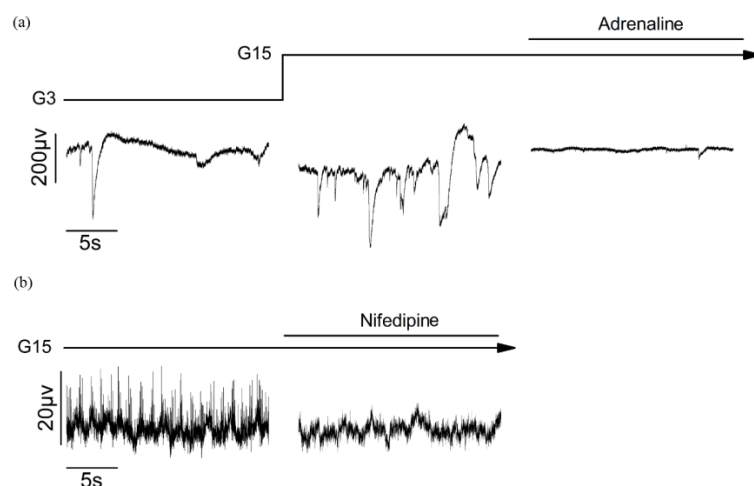


Figure 4.4: Electrophysiological recordings from two different human donor (a) and (b)

The significance of these measurements can be found on the ability of the PEDOT:PSS electrodes to successfully record oscillations from human islets. Taking into account the role of those oscillations in pathological condition like lipotoxicity or type two diabetes, those recordings pave the way for new *in vitro* diagnostic platforms based on PEDOT:PSS.

4.3 Conclusions

In this work, we have developed a PEDOT:PSS based platform capable of recording electrophysiological signals from pancreatic islet cells. These signals were directly connected to glucose concentration revealing their link with endogenous metabolic algorithms. Particularly, the recorded slow potentials and action potentials at elevated glucose concentrations are attributed to beta cell physiology revealing their role in nutrient homeostasis. Low glucose concentration, on the other hand, resulted in action potentials originated from alpha cells which role is associated with the synthesis and the secretion of the hormone glucagon at these concentrations of the polysaccharide.

The use of MEA for electrophysiology measurements comes with the advantage of a non-invasive technique that leaves the understudy cells intact and allows monitoring of their activity for extended periods of time. In addition, the numerous recording sites provide us with a large amount of data obtained from many different cell islets simultaneously. Nevertheless, the greatest issue that MEA

technology has to face is the low signal to noise ratio as a result of the attenuation the signal suffers inside the extracellular space^[5]. PEDOT:PSS , a mixed ionic/electronic organic semiconductor , is the material of choice for dealing with this problem. A thin layer of the organic material lowers the impedance of gold electrodes by a factor of 100 due to the increase of the electrode's geometric surface area (GSA). As a consequence, it improves the quality of the measurements resulting in recording of both action potentials and slow waves without the need of complex algorithms for their extraction^[14]. More importantly, the PEDOT: PSS platform is capable of recording both signals (SP+AP) with an efficiency of almost 100% on active electrodes vs only $32.2 \pm 3.7\%$ ($n=20$) for commercial MEAs ^[3] (Supplementary S2). That means that on every single electrode that was covered with cell islets and on which slow potentials were recorded (active electrodes), action potentials were also recorded at the same time. We believe that this feature is the result of the lower impedance that the PEDOT:PSS electrode has to offer and especially of the low background noise that comes with that. These findings are even more notable if we take under consideration the easy , reliable and reproducible way by which the PEDOT:PSS covered electrodes are fabricated^[12] . Lastly, the presence of the PEDOT:PSS polymer is also a great plus of the platform as due to its versatile chemistry it can be easily bio functionalized and chemically modified, a fact that can pave new ways for even more versatile devices.

4.4 Experimental Section

4.4.1 Device Fabrication: The devices were fabricated in a previously reported way^[12]. A 25 mm x 75 mm glass slide was used as a substrate which was thoroughly cleaned in a 1:1 Acetone/Isopropanol solvent mixture. The gold electrodes were patterned on top of the glass slide in a standard photolithographic technique with the use of S1813 photoresist, subsequent UV light exposure and development in MF-26 developer. The resulted gold electrodes were of 100nm of thickness while a 10 nm thick Cr layer between them and the substrate was chosen to act as an adhesive promoter. Both metals were deposit via standard metal evaporation. Thereinafter, two layers of Parylene-C (with the second serving as a sacrificial one in a later stage) were deposited for the device encapsulation, with an antiadhesive soap layer in between. A second photolithography step was used to pattern the electrode's active area with the

use of AZ 9260 photoresist and a subsequent development step in AZ developer. Reactive Ion Etching with O₂ plasma created openings in Parylene-C before the PEDOT: PSS suspension was spun on the device. A final peel-off step of the second Parylene-C sacrificial layer defined the conducting material covered electrode area. The devices were hard baked for 60 minutes at 140°C and immersed in D.I water over night for the removal of any low molecular weight compounds of the PEDOT:PSS dispersion. The PEDOT: PSS formulation used is as follows: 38 mL of PEDOT: PSS aqueous dispersion (Clevios PH -1000) were mixed with 2 mL of ethylene glycol (for conductivity enhancement), 50 µL of 4-dodecylbenzenesulfonic acid (DBSA) that helps the film formation and 0.4 mL of 3-methacryloxypropyltrimethoxysilane (GOPS) which is a surface adhesion promoter and a polymer cross-linking agent that enhance film stability in aqueous environments.

4.4.2 Islets isolation and cell culture: Before cell culturing the devices were plasma treated for 2 minutes to render them hydrophilic (the plasma treatment was 9.82 W/L -27.5 W in a 2.8 L chamber). After plasma treatment Matrigel solution (diluted 40µL in 2ml culture solution) was pipetted onto the MEA and the devices were incubated for an hour at room temperature. A washing step with cold culture media once and with room temperature water twice followed. The MEAs were dried and the cells were added in a set volume of 1mL to the center of the devices exactly on top of the active (recording) area. The cells adhesion lasts 3 days.

4.4.3 Device characterization and electrophysiological recordings: After fabrication the devices were characterized with the help of a potentiostat (Autolab PGSSTAT128N) in a three electrode configuration. The impedance spectra were obtained in 0.1M NaCl solution. The PEDOT:PSS covered electrodes served as the working electrode while a Pt and an Ag/AgCl electrode were used as counter and reference electrode respectively. The measurements were performed with the use of an INTAN RHD2132 32-channels amplifier chip with unipolar inputs (Intan Technologies) at a sampling rate of 10 kS/s. The data were analyzed with custom-written Matlab (Mathworks) codes and with the use of Spike 2 software.

References

- [1] F. M. Ashcroft, P. Rorsman, *Cell* 2012, 148, 1160.
- [2] B. Ahren, *Diabetologia* 2000, 43, 393.
- [3] F. Lebreton, A. Pirog, I. Belouah, D. Bosco, T. Berney, P. Meda, Y. Bornat, B. Catargi, S. Renaud, M. Raoux, J. Lang, *Diabetologia* 2015, 58, 1291.
- [4] N. Porksen, M. Hollingdal, C. Juhl, P. Butler, J. D. Veldhuis, O. Schmitz, *Diabetes* 2002, 51 Suppl 1, S245.
- [5] M. E. Spira, A. Hai, *Nat Nano* 2013, 8, 83.
- [6] G. Buzsaki, C. A. Anastassiou, C. Koch, *Nature reviews. Neuroscience* 2012, 13, 407.
- [7] T. Pfeiffer, U. Kraushaar, M. Dufer, S. Schonecker, D. Haspel, E. Gunther, G. Drews, P. Krippel-Drews, *Pflugers Archiv : European journal of physiology* 2011, 462, 835.
- [8] Q. Zhang, J. Galvanovskis, F. Abdulkader, C. J. Partridge, S. O. Gopel, L. Eliasson, P. Rorsman, *Philosophical transactions. Series A, Mathematical, physical, and engineering sciences* 2008, 366, 3503.
- [9] S. Schonecker, U. Kraushaar, M. Dufer, A. Sahr, C. Hardtner, E. Guenther, R. Walther, U. Lendeckel, W. Barthlen, P. Krippel-Drews, G. Drews, *Integrative biology : quantitative biosciences from nano to macro* 2014, 6, 540.
- [10] J. Rivnay, R. M. Owens, G. G. Malliaras, *Chemistry of Materials* 2014, 26, 679.
- [11] D. H. Kim, S. Richardson-Burns, L. Povlich, M. R. Abidian, S. Spanninga, J. L. Hendricks, D. C. Martin, in *Indwelling Neural Implants: Strategies for Contending with the In Vivo Environment*, (Ed: W. M. Reichert), CRC Press/Taylor & Francis Taylor & Francis Group, LLC., Boca Raton (FL) 2008.
- [12] M. Sessolo, D. Khodagholy, J. Rivnay, F. Maddalena, M. Gleyzes, E. Steidl, B. Buisson, G. G. Malliaras, *Advanced Materials* 2013, 25, 2135.
- [13] K. A. Ludwig, N. B. Langhals, M. D. Joseph, S. M. Richardson-Burns, J. L. Hendricks, D. R. Kipke, *J Neural Eng* 2011, 8, 014001.
- [14] M. Raoux, Y. Bornat, A. Quotb, B. Catargi, S. Renaud, J. Lang, *The Journal of physiology* 2012, 590, 1085.
- [15] Y. Z. De Marinis, A. Salehi, C. E. Ward, Q. Zhang, F. Abdulkader, M. Bengtsson, O. Braha, M. Braun, R. Ramracheya, S. Amisten, A. M. Habib, Y. Moritoh, E. Zhang, F. Reimann, A. H. Rosengren, T. Shibasaki, F. Gribble, E. Renstrom, S. Seino, L. Eliasson, P. Rorsman, *Cell Metab* 2010, 11, 543.
- [16] E. Pedraza, A. Karajic, M. Raoux, R. Perrier, A. Pirog, F. Lebreton, S. Arbault, J. Gaitan, S. Renaud, A. Kuhn, J. Lang, *Lab on a Chip* 2015, 15, 3880.

Supplementary Information

A. Device Characterization

The PEDOT:PSS covered electrodes were fabricated with a previous published method. The device's 32 electrodes showed identical impedance spectrum as presented in Figure S4.1(a) for 12 randomly selected electrodes measured on the same device. Similar tests were performed on different devices resulting always similar impedance spectrum for the PEDOT:PSS electrodes. Most importantly the conductive polymer layer on top of gold, lowers the impedance of the electrode by almost two orders of magnitude improving the quality of the measurements. The value of the impedance is about 13 k Ω for all the electrodes at 1 kHz. The resulting background noise is presented in Figure S4.1(b). The noise level is +/- 7.5 μ V peak-to-peak. This value is comparable or lower to previous published data of polymer covered electrodes.

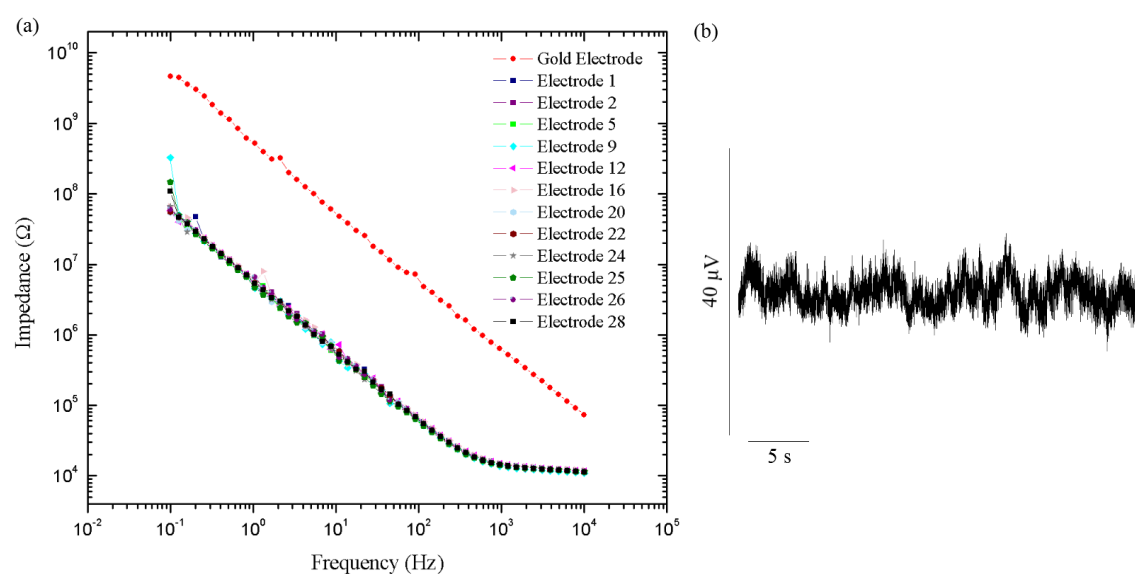


Figure S4.1: (a) Impedance spectrum comparison of 12 randomly selected PEDOT:PSS covered electrodes. All electrodes present identical impedance spectrum with lower values than the same sized gold electrode (control) (b) Resulting background noise level of +/- 7.5 μ V peak-to-peak.

B. Action Potentials recordings

The PEDOT:PSS platform is capable of recording action potential in all active electrodes. That means that every electrode that is covered with cells and records slow oscillations records at the same time fast activity (action potentials). Previous studies with commercial electrodes presented only 33% of action potential detection over active electrodes. Figure S4.1(a) shows a microscope image of the islet cell culture with all the electrodes marked with numbers for facilitation of the data analysis. Figure S4.2(b) presents simultaneously recordings from 11 channels that were covered with islets (high glucose concentration of 15mM was used). For those electrodes that clearly resolve slow waves (electrodes 31, 30, 29, 18, 16, 15, 1) spikes are also identified.

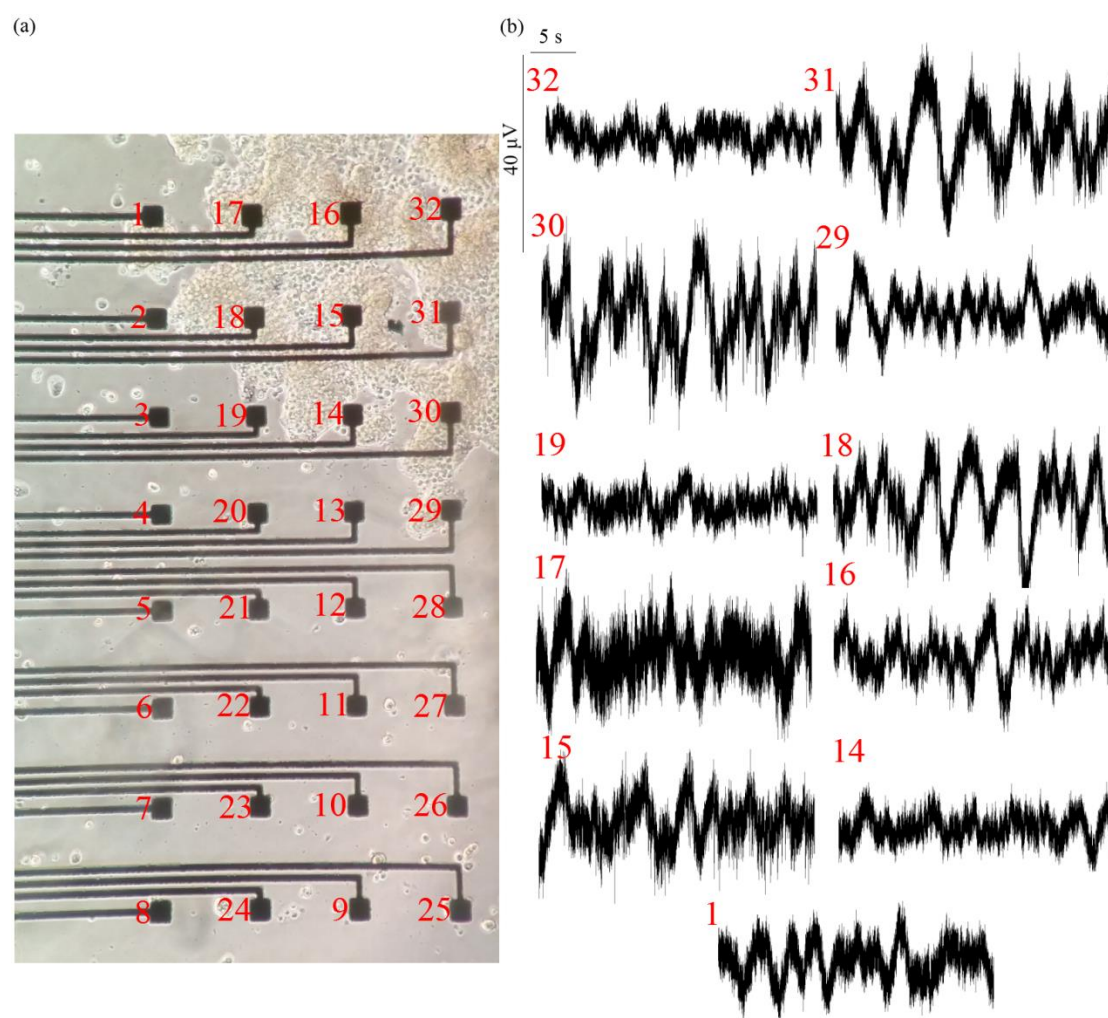


Figure S4.2: (a) A microscope picture of the mouse islet cells on the PEDOT:PSS MEA. The electrodes have been numbered for facilitating data analysis (b) Electrodes numbered 1,14,15,16,17,18,19,29,30,31,32 are covered electrodes. In every electrode that can clearly record slow waves, action potentials are also recorded (electrodes 31, 30, 29, 18, 16, 15, 1).

Chapter 5: Organic Electrochemical Transistors

The part 5.2 of this chapter is based on the collaborative work between BEL and Electronics lab of Department of Physics of Aristotle University in Thessaloniki (Greece). This collaboration resulted in the Master Thesis of Petros Sideris under the supervision of Professor Sytlianos Siskos entitled “**Verilog-A Modelling of Organic Electrochemical Transistors and Read-out Instrumentation**”

5.1 Introduction

Up until now, we have studied the case of conductive polymer covered biopotential electrodes and the advantages they offer in electrophysiology. Nevertheless, electrodes are passive devices and as such, they do not offer any amplification on the recorded activity which is by definition small in terms of amplitude. Consequently, external amplification with sophisticated electronics is needed for the proper signal acquisition. The price to be paid for that is the noise that is picked up from the used circuitry components and the resulting deterioration of the measurement quality. Amplifying transducers, offer a solution to this as they promise to amplify the bio signal just at the point where it is created circumventing the noise problem.

Organic Electrochemical Transistor (OECT) is an electrochemical organic device that could play the role of the above mentioned transducer. The first OECT was introduced in 1984 by White et al. ^[1]. The device innovation is found in the absence of an oxide separating gate and channel. What White succeeded in, was to modulate the current of a polypyrrole film by applying a gate voltage through an electrolyte offering an alternative to the Organic Field Effect Transistor (OFET). Lately, PEDOT:PSS has become the organic material of choice for the channel due to its unique features (chemical stability, high transconductance, biocompatibility etc.)

In brief, the device operation principle can be summarized as follows. The conductivity of a PEDOT:PSS film can be changed through the process of electrochemical doping. According to this process, ions from an electrolyte are injected into the film and change the hole density not just under the surface, but throughout the entire volume of the film. Injection of cations, for example, will lead

to hole extraction (through a metal electrode) and dedope the film (it is worth noting that the PSS chain “holds” the sulfonate ions in position, so that they do not diffuse into the electrolyte). This process is analogous to compensation doping of silicon, but takes place at room temperature and by applying a small bias. A ramification of this phenomenon is that the effective capacitance at the interface between a conducting polymer film and an electrolyte scales with film volume, rather than area, and can therefore reach very large values. OEECTs take advantage of this mechanism to deliver a large transconductance. An OEECT consist of a PEDOT:PSS channel, in contact with an electrolyte (Figure 5.1), and with source and drain electrodes that measure the (hole) drain current.

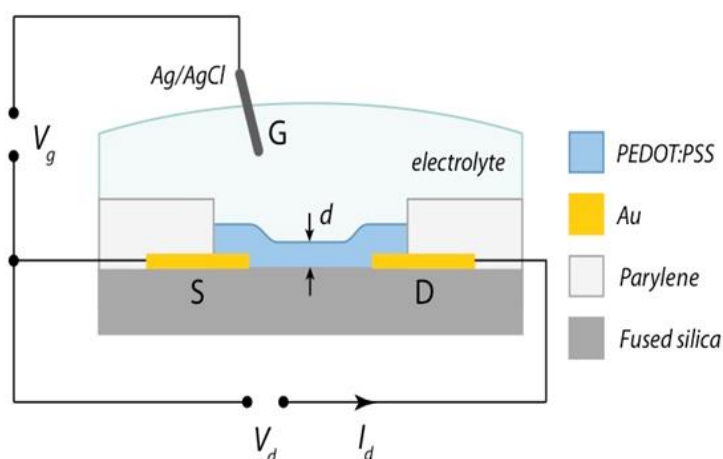


Figure 5.1: Schematics of an organic electrochemical transistor with a PEDOT:PSS channel, Au source and drain electrodes, and a Ag/AgCl gate electrode. The substrate (fused silica) can be replaced by a flexible plastic foil, while Parylene-C is used to insulate the contacts from the electrolyte.

A change in the electrical potential at the interface between the electrolyte and the polymer film drive ions in and out of the channel and changes the conductivity of the latter, thereby modulating the drain current^[2]. As the entire volume of the channel participates in the current modulation process, OEECTs exhibit a very large transconductance (in the mS range)^[3]. As such, they can be very useful for transducing signals of biological origin^[4]. For this purpose, the voltage applied at the gate is held constant, and a biological phenomenon is used to modulate the potential at the electrolyte/channel interface. This phenomenon can be, for example, the electrical activity of a neural network in the brain, or an electron transfer reaction due to a redox enzyme^[5]. Finally, we should note that simple voltage amplifiers have been

fabricated using OEECTs, offering >50 dB of power amplification for low frequency signals^[6].

We fabricate OEECTs through a combination of solution and vapor deposition and etching processes, and use photolithography to pattern them, mainly to be able to access micron-scale dimensions that are of interest for interfacing with single neurons.

The PEDOT:PSS film is deposited from a commercial dispersion using spin coating to a thickness of around 100 nm. It can be patterned either by using an underlying sacrificial layer that forms a contact mask on the substrate, or by protecting parts of it with a photoresist and removing the rest using an oxygen plasma^[7]. Au source and drain electrodes are deposited by vacuum evaporation and patterned with photolithography and etching, and then covered with an insulator such as Parylene-C, deposited from vapor. The gate electrode can be held on top of the channel, as shown in Figure 5.1, or patterned on the side of the channel (planar configuration) using microfabrication. It is made of Ag/AgCl, PEDOT:PSS, or Pt – the choice of material is known to affect performance^[6]. The processes discussed above can be combined in a number of different ways to yield OEECTs on glass or plastic substrates. An example of a microfabricated OEECT channel is shown in Figure 5.2. It should be noted that OEECTs can also be fabricated using additive processes such as ink-jet printing^[8], and we expect this to be a major advantage for custom-made biosensing applications.

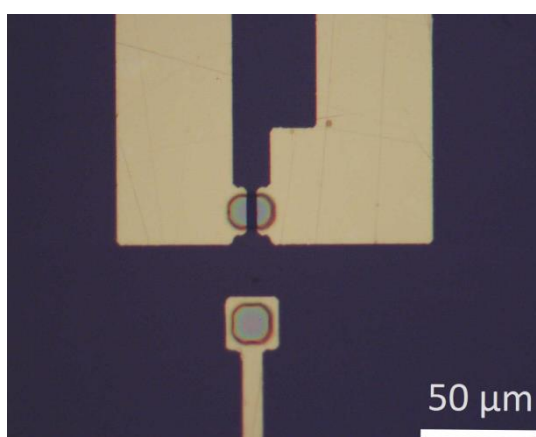


Figure 5.2: Micrograph of microfabricated PEDOT:PSS OEECT and electrode. A film of parylene coats the entire surface with the exception of the areas where PEDOT:PSS was deposited.

The transfer curve and resulting transconductance of an OEET like the one presented in Figure 5.2 are shown in Figure 5.3. The transfer curve is typical for depletion operation, where application of positive gate bias causes cations to enter the channel, which decreases hole density and reduces the drain current. The transconductance reaches its highest value around zero gate bias, meaning that the OEET can be used with the gate electrode directly connected with the source (it was designed so intentionally^[6]). The transconductance exceeds 4 mS, which is a very high value for a thin film transistor.

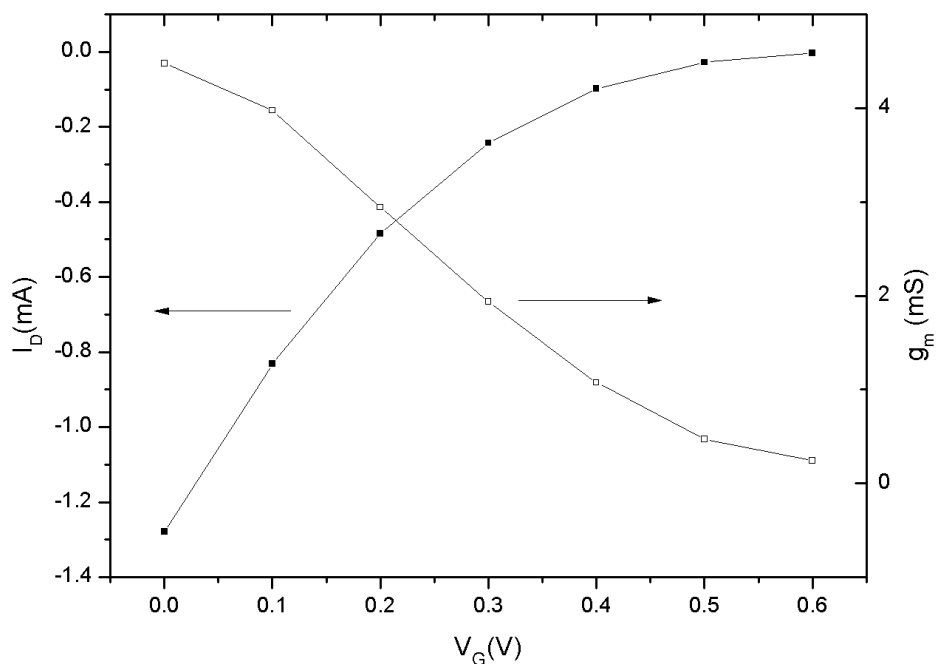


Figure 5.3: Transfer curve of an OEET (black symbols) and corresponding transconductance (white symbols). The device dimensions are $W=10\mu\text{m}^2$, $L=5\mu\text{m}^2$ and PEDOT:PSS thickness $t=100\text{nm}$.

These high values of transconductance, though, grace of the volumetric capacitance come with a penalty in the response time of the device. This can be understood if we consider a RC circuit with a response time τ of:

$$\tau = RC \quad (5.1)$$

This means that if a signal is faster than τ the capacitor will not have the time to be charged and as a consequence the OEET's channel will not be able to follow the induced changes. Luckily the biological signals are rather slow (the faster ones are the

action potentials of frequency ~ 1 kHz) and as result OEECTs can be engineered to have faster response time than the fastest bio signal.

5.2 Organic Electrochemical Transistors measuring system

As mentioned earlier, OEECTs present a great potential to be used in electrophysiological recordings due to their special architecture and the lack of insulation between gate and channel. They have already been successfully used for recording epileptiform activity *in vivo* and showed a greater signal to noise ratio compared to electrodes which are considered to be the gold standard for electrophysiology^[9].

Nevertheless, the true challenge OEECTs have to face is recording action potentials, the basic signaling unit of the nervous system. As presented in Chapter 1, an action potential is a fast event (typical duration ~ 1 ms) with a low amplitude (typically $\sim 100\mu\text{V}$ extracellularly). (Figure 5.4)

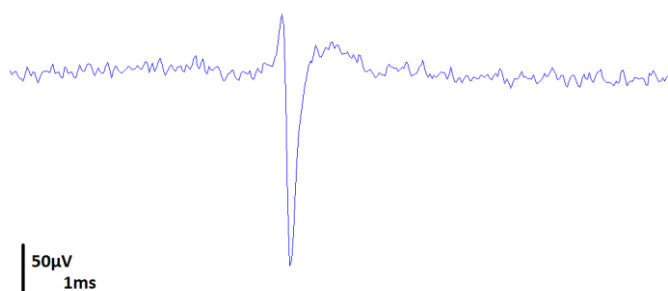


Figure 5.4: An action potential as recorded with a PEDOT:PSS covered electrode from a mouse brain slice.

The OEECTs engineered to record these signals are the ones with dimension $W=10\mu\text{m}$, $L=5\mu\text{m}$ and with channel thickness $t\sim 100\text{nm}$. Typical transconductance value for this geometry is about 2mS . As a consequence, any biological signal in the order of $\Delta V=100\mu\text{V}$ would result in a current modulation (ΔI) inside the OEECT channel of :

$$\Delta I = \Delta V \times g_m = 100\mu\text{V} \times 2\text{mS} = 200\text{nA} \quad (6.2)$$

The problem of recording a modulation of this size is that it rests on top of the bias current of the OEECT. For the above mentioned channel dimension this current is

in the mA range (typically ~ 1 mA). Thus, the real challenge is recording a 200 nA current fluctuation on top of a 1 mA bearing signal.

In addition, a second issue when it comes to recordings like these is the background noise. Noise could be either of biological origin or can be generated by the recording devices and the electronic systems themselves. In any case, this noise is unwanted and should be filtered out in order for the bio signal to be revealed.

The situation becomes even more complicated if we take into account the fact that the already established electrophysiological technology employs electrodes for performing measurements. Hence, the majority of the commercially available acquisition systems are built to measure difference in potential. The output of an OECT, though, is current and therefore not compatible with the classic electrophysiology chips.

The strategy for dealing with the above problems is to convert the signal from current to a voltage, to separate it from the bearing OECT steady state current and to clean it from the unwanted noise. Two different ways were used to realize this strategy. The Transimpedance Amplifier circuit and the Gyrator circuit.

Transimpedance Amplifier

A transimpedance amplifier (TA) is the standard way of converting current into voltage and was used in similar recordings before^{[10][11]}. The circuit is presented in Figure 5.5

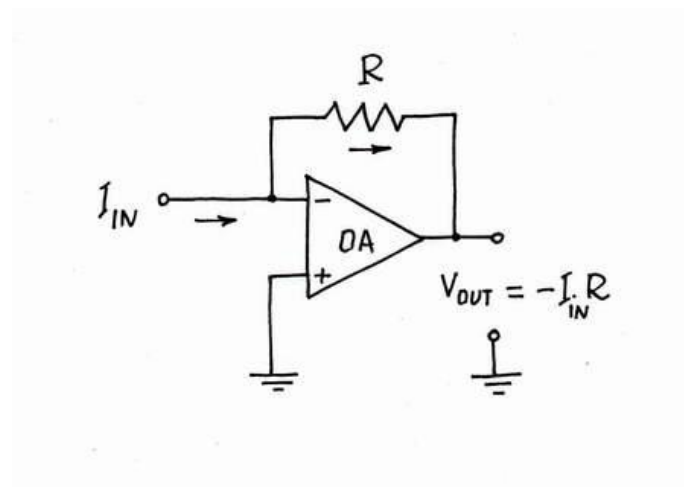


Figure 5.5: Schematics of a transimpedance amplifier.

It consists of an Operational Amplifier (OP-AMP) which converts the incoming current into voltage through a resistor R. The output is the negative product of the input current times the resistor value $V_{out} = -I_{IN}R$.

A system like this was realized on a Printed Board Circuit (PCB) and tested with the use of a “Phantom neuron”. The term refers to a pair of NiCr metal wires (50 μ m in diameter) twisted together, through which a voltage pulse is introduced inside the electrolyte chamber of the OECT (Figure 5.6).

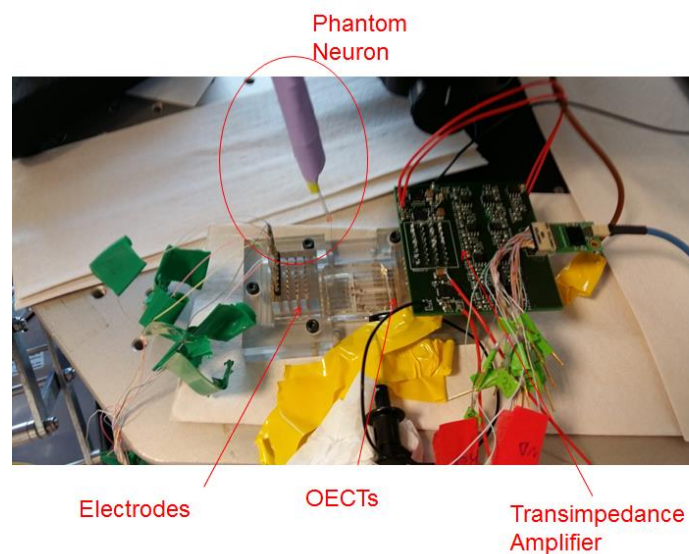


Figure 5.6: Experimental set up of testing the transimpedance amplifier

The device used for this testing was a hybrid device hosting both electrodes and OECTs

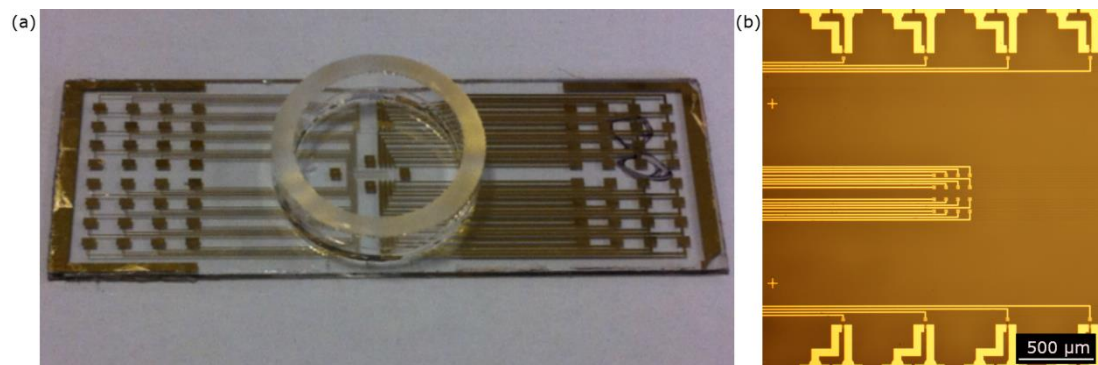


Figure 5.7: (a) A hybrid device which hosts two arrays of 16 OECTs and 16 electrodes (b) A close up in the device active area presenting two rows of 4 OECTs and their corresponding electrodes. In the

center of the picture, it is shown an extra MEA array of 16 electrodes. The channel of each OEET is $10 \times 5 \mu\text{m}^2$ exactly like the one presented in Figure 5.2 while the electrode dimensions are $12.25 \times 12.25 \mu\text{m}^2$.

The transistors channel was of dimensions of $10 \times 5 \mu\text{m}^2$ which made them fast enough to be able to record signals of 1ms in duration but with the ability to amplify them due to their increased transconductance. The used electrodes were PEDOT:PSS covered gold electrodes with dimension $12.25 \mu\text{m} \times 12.25 \mu\text{m}$. The OEETs output characteristics are presented in Figure 5.8.

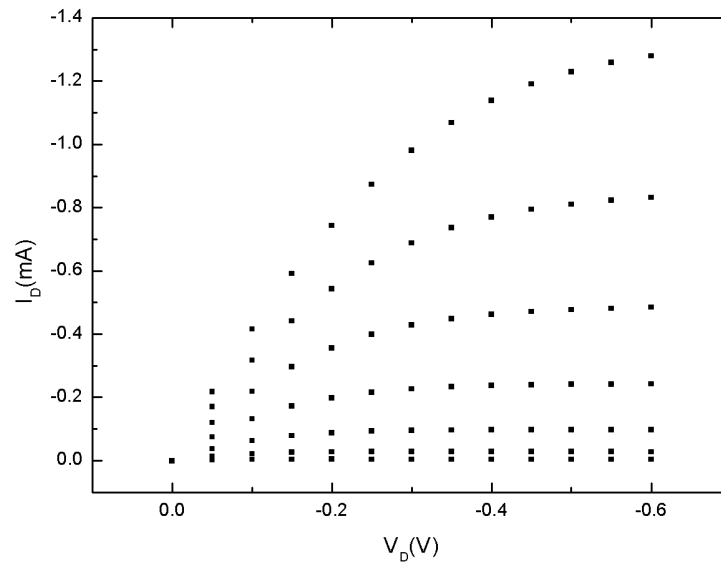


Figure 5.8: Output characteristics of an OEET with channel dimensions $W=10\mu\text{m}, L=5\mu\text{m}$ and PEDOT:PSS thickness $t=100\text{nm}$.

Theoretically, the introduced by the “phantom neuron” voltage pulses modulate the current of the channel. This current modulation is converted into voltage modulation on the transimpedance amplifier and can be recorded through a commercial available electrophysiological chip (INTAN amplifier chip, INTAN technologies).

Test Measurements

The minimum detectable signal with this board was a train of 10 pulses, each one of which had a frequency of 1kHz and a voltage amplitude of 100mV. The train was introduced by the “Phantom neuron” inside the electrolyte chamber. This signal was resolved by the system OEET-PCB-INTAN as a fluctuation in voltage in the range of

100 μ V which is about the magnitude of the fluctuation induced by a firing neuron. Nevertheless, the comparison of the signal-to-noise ratio (SNR) between OECTs and electrodes favors the latter due to the extra noise induced in the system from the board electronic components.

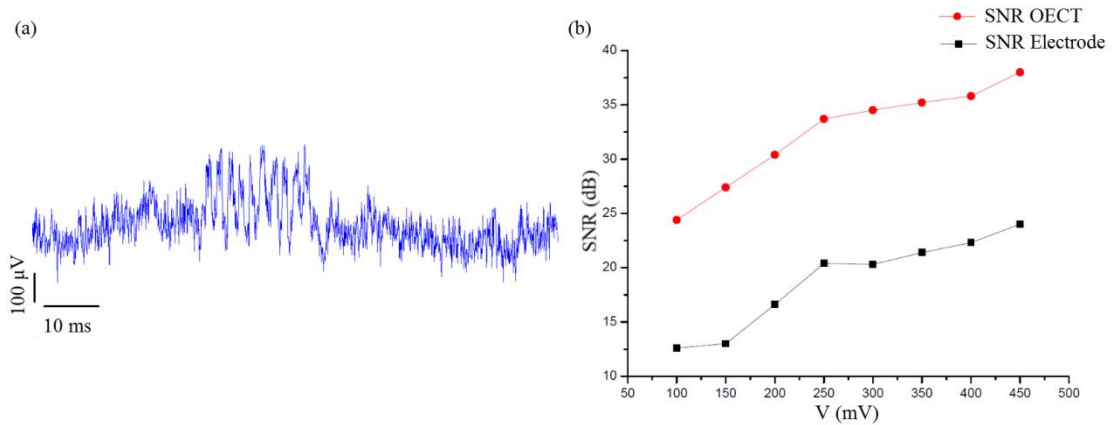


Figure 5.9: (a) Minimum detectable signal (b) Comparison of OECT vs Electrode SNR.

Gyrator

Having to face the problem of the minimum amplitude detection limit and the lower OECT SNR new approaches for the conversion system were explored. The new strategy was decided to have two key points. A new read out circuit and a better filtering part. The new recording system was based on a circuit known as Gyrator.

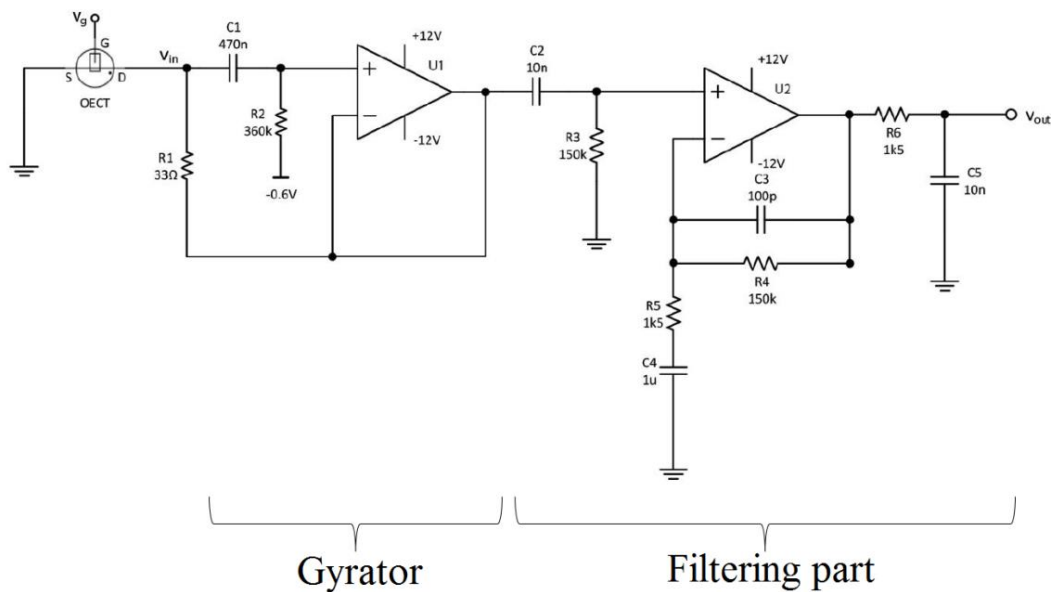


Figure 5.10: Read out system based on Gyrator.

Gyrator is an operational amplifier (OP-AMP) based circuit that simulates a grounded inductor. According to theory its inductance is given by:

$$L=C_1 R_1R_2 \quad (5.2)$$

where C_1 is the capacitance of the circuit's capacitor, R_1 and R_2 the resistances values of the circuit's resistors.

The current flowing through R_1 is given by:

$$I_{R1} = \frac{V_i - V_o}{R_1} \quad (5.3)$$

Due to the fact that an OP-AMP has an infinite input impedance the current passes through R_2 is equal to the current through the capacitor C

$$I_c = I_{R2} = \frac{V_{in}}{Z_c + R_2} \quad (5.4)$$

And since the OP-AMP is a follower the output voltage V_o is:

$$V_o = \frac{V_i}{Z_c + R_2} R_2 \quad (5.5)$$

What is important in equation (5.5) is that the impedance of the capacitor equals to

$$Z_c = \frac{1}{j\omega C} \quad (6.6)$$

In the case of a DC current ($\omega=0$), the capacitive reactance becomes infinite $Z_c = \infty$ and the output voltage V_o equals to zero. Consequently, the DC current is not found in the output of the circuit which is extremely convenient in our case as it means that we eliminate the unwanted steady state current of the OECT. The alternative signal ($f=1$ kHz) of the neuron, though, is not filtered out as it can be found in the circuit's output as the product of the current times the resistance R_2 .

$$V_o = i_{in}R_2 \quad (6.7)$$

Going back to the idea of the inductor simulation the equivalent circuit is presented in Figure 5.11.

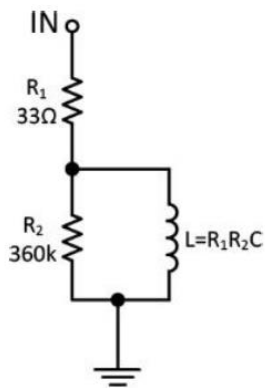


Figure 5.11: The Gyrator equivalent circuit. The inductor is a shortcut for the DC current that is led to ground. The drop of potential on R_2 converts the input voltage into an output current (with a small potential loss on R_1)

The inductor offers an easy pathway for DC to the ground, allowing for the alternative component of the signal to be converted into voltage on the resistance R_2

Filtering

Concerning the filtering part of the circuit, it was optimized in order to give a transfer curve which peaks at 1 kHz and attenuates fast for lower and higher frequencies. The overall filtering part consists of passive (a high pass and a low pass filter) and active components, resulting in an overall very steep drop of the transfer function.

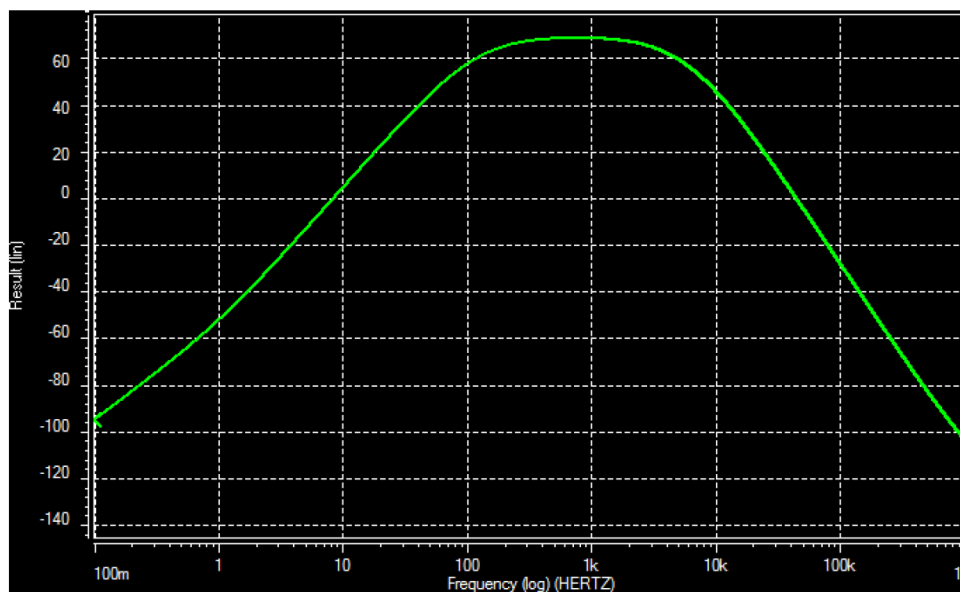


Figure 5.12: Frequency response of the measuring system (SPICE model)

The final result is a band pass filter with a bandwidth of 10 kHz and center frequency at 1 kHz. The gain at that frequency is 40 dB.

Test Measurements

A measuring system incorporating a Gyrator and a filtering part was realized and presented in Figure 5.13

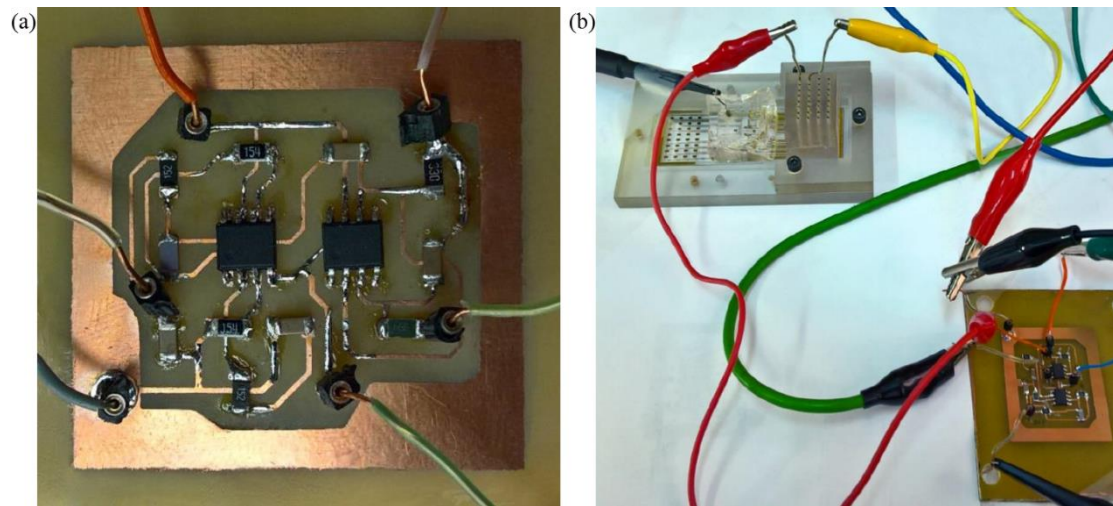


Figure 5.13: (a) A Gyrator read out circuit with the appropriate filtering system (b) Experimental set up for testing the readout system

Interestingly the Gyrator-filtering system was able to detect pulses of voltage as small as of $42 \mu\text{V}$ peak to peak in amplitude, 1ms in duration with a frequency of 1 kHz. These signals were applied in bursts of 3 spikes on the transistors gate and were used to simulate the action potential of neuronal cells. Figure 5.14 presents these measurements.

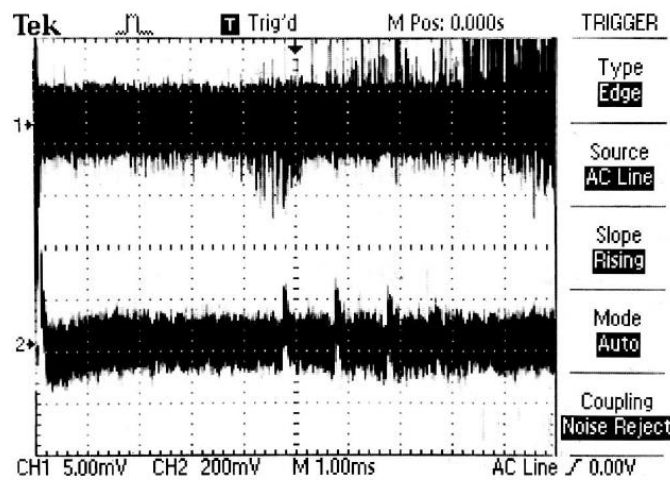


Figure 5.14: A picture of the oscilloscope screen used to monitor the input train of spikes and the recording of this train from the OECT/readout system.

Both the stimulating and the recorded signals were led to two separate channels of an oscilloscope. On the top half part of the oscilloscope (channel 1) it is represented the input pulse on the gate voltage. In the lower half (channel 2) we can see the output of the read out system. Interestingly, the $42\mu\text{V}$ input pulses are not visible in channel 1 as they are “buried” inside the noise background. Nevertheless, the output in channel 2 shows the spike train proving the potential of the circuit to record real neurophysiological signals similar to the simulated ones.

5.3 Conclusions

In conclusion, a complete read out system was theoretically designed, realized and tested in order to facilitate neural cell activity recordings with OECTs. The system consists of two main parts.

An I/V conversion part responsible for converting the output current of the OECT into a voltage through two different circuits. A Transimpedance Amplifier and a Gyrator. Both these circuits allow the transistor output current to pass through a resistor R and produce voltage according to Ohms law ($V=IR$). What is even more important is that, especially, the Gyrator removes the DC component from the signal leaving only the biological part behind by performing a first filtering step.

The second part of the circuit consists of a filtering element which employs passive and active filters tuned to filter out any unwanted noise except from the 1 kHz neural activity.

During the readout system design special care was taken for the optimal choice of the OP-AMPs and the passive circuit components (resistors/capacitors) so that the induced noise by the read out system to be kept to minimum. The values of the electronic components on the figures above were chosen in order to serve this cause.

The next step would be the manufacturing of a PCB board which can realize the studied circuits and facilitate biological measurements on neural networks.

References

- [1] G. P. Kittlesen, H. S. White, M. S. Wrighton, *Journal of the American Chemical Society* 1984, 106, 7389.
- [2] D. A. Bernards, G. G. Malliaras, *Advanced Functional Materials* 2007, 17, 3538.
- [3] D. Khodagholy, J. Rivnay, M. Sessolo, M. Gurfinkel, P. Leleux, L. H. Jimison, E. Stavrinidou, T. Herve, S. Sanaur, R. M. Owens, G. G. Malliaras, *Nature Communications* 2013, 4, 2133.
- [4] P. Lin, F. Yan, *Advanced Materials* 2012, 24, 34.
- [5] J. Rivnay, R. M. Owens, G. G. Malliaras, *Chemistry of Materials* 2014, 26, 679.
- [6] J. Rivnay, P. Leleux, M. Sessolo, D. Khodagholy, T. Hervé, M. Fiocchi, G. G. Malliaras, *Advanced Materials* 2013, 25, 7010.
- [7] J. A. DeFranco, B. S. Schmidt, M. Lipson, G. G. Malliaras, *Organic Electronics* 2006, 7, 22.
- [8] L. Basiricò, P. Cosseddu, A. Scidà, B. Fraboni, G. G. Malliaras, A. Bonfiglio, *Organic Electronics* 2012, 13, 244.
- [9] D. Khodagholy, T. Doublet, P. Quilichini, M. Gurfinkel, P. Leleux, A. Ghestem, E. Ismailova, T. Hervé, S. Sanaur, C. Bernard, G. G. Malliaras, *Nature Communications* 2013, 4, 1575.
- [10] C. Yao, Q. Li, J. Guo, F. Yan, I. M. Hsing, *Adv Healthc Mater* 2015, 4, 528.
- [11] A. Spanu, S. Lai, P. Cosseddu, M. Tedesco, S. Martinoia, A. Bonfiglio, *Sci Rep* 2015, 5, 8807.

Chapter 6 Organic Electrochemical Transistor for Astrocytes activity recordings

The work presented in this chapter is the result of the collaboration between BEL and CNR-ISMN in Bologna and was realized during my Olimpia Project secondment in Bologna Italy

Simone Bonetti: Device characterization and Biological measurements, Report writing.

Dimitrios A.Koutsouras: Device Fabrication and characterization, Biological measurements, Input in report writing.

Ana Borrachero: Biocompatibility studies and Biological measurements, Input in report writing

Valentina Benfenati, Michele Muccini and George G. Malliaras: Supervisors

6.1 Introduction

Astrocytes are one of the most abundant type of cells in brain and they play an important role in many processes^{[1] [2]}. Some of these include maintaining control of local ion and water homeostasis, clearing of the neuronal environment by removing neurotransmitter and metabolic molecules, supporting synapses transmission, regulating blood flow, etc.^{[1, 3] [4] [5] [6]}. They are not electrically active themselves but they express several types of ion channels and receptors in their plasma membrane, a fact that makes them able to change their membrane potential and increase cytosolic Ca^{2+} as a response to neuronal activity^{[6] [7]}. In any case, understanding their role in the physiology and pathophysiology of the central nervous system is one of the main goals in order to comprehend how brain works^{[8] [9]}. Despite of the extended study held during the past few decades, there is still much work that needs to be done on deciphering how astrocytes really function. Due to this fact, development of new, state of the art devices able to be used for this cause is mandatory. Organic electronics devices have emerged during the past years as ideal candidates for biological measurements. Organic Electrochemical Transistors (OECTs), in particular, have proven to be a powerful tool to record brain cells electrical activity both *in vivo*^[10] and *in vitro*^[11] due to their enhanced transistor proprieties. In this project we explore the potential of OECTs to be used in Astrocytes activity recordings.

6.2 Experiment- Results

6.2.1 Astrocytes biocompatibility on PEDOT: PSS

At the project's beginning, the first step to be taken was the biocompatibility assessment of the recording devices. In order to investigate the viability of astrocytes on PEDOT:PSS, cells were re-plated from confluent astrocytes preparations on PEDOT:PSS, PEDOT:PSS + PDL(Poly-D-lysine) and control glass + PDL substrates. As a result PDL was proven to successfully work as extracellular matrix material, promoting *in vitro* adhesion of primary cells.

Fluorescein diacetate (FDA) cell viability assays were performed for days 1 and 5 days *in vitro* (DIV) after re-plating (Figures 6.1 (a-f)). Imaging analysis showed viable astrocytes plated in both conditions. Histogram plot of cell counting at 1 and 5 DIV (Figure 6.1(g)) indicated that there is no statistical difference between the different conditions confirming the suitability of PEDOT:PSS as a biocompatible substrate for adhesion and growth of rat primary cortical astrocytes.

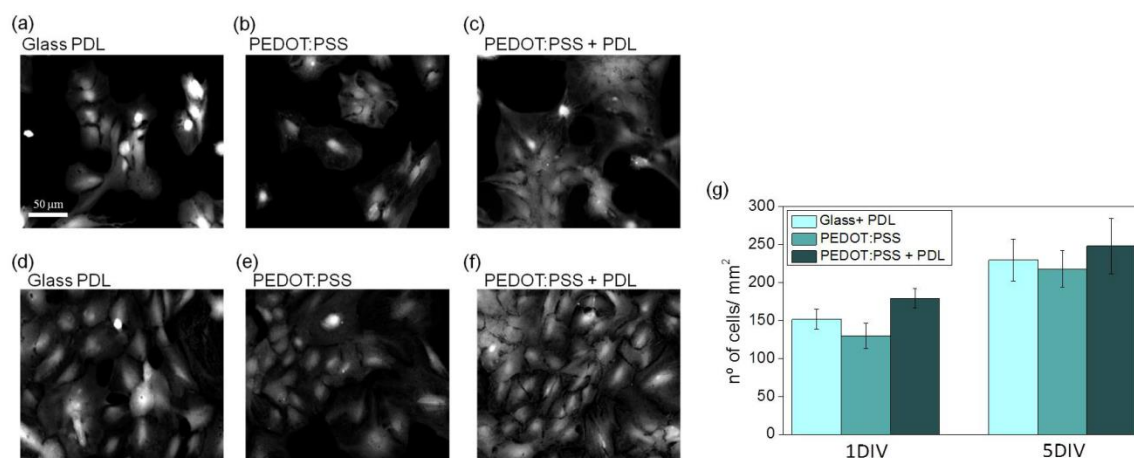


Figure 6.1: Biocompatibility test of astrocytes on PEDOT:PSS. (a-f) Micrographs representing astrocytes stained with Fluorescein Diacetate (FDA) grown on PEDOT:PSS (b and e) and on PEDOT:PSS + PDL (c and f) using as a control GLASS+PDL (a and d) at different time points: (a-c) 1 day *in vitro* (DIV) and (d-f) 5 DIV. (g) Histogram plot shows averaged FDA positive cells/areas plated on GLASS+PDL, PEDOT:PSS and PEDOT:PSS+PDL, after 1 and 5 DIV. Significant difference was not observed (** $p < 0.01$).

6.2.2 Device characterization in external standard solution

After the biocompatibility between cells and devices was ensured the later were electrically tested in extracellular standard solution. During the experimental

procedure, OECTs with width $W=30\mu\text{m}$, length $L=30\mu\text{m}$ and PEDOT:PSS film thickness of 500 nm were used.

Before the experiments, the OECT were tested in external standard solution, used to maintain the stable electrophysiological equilibrium. As shown in Figures 6.2(a) and 2(b) the transfer curve and output characteristics of the devices are typical of OECTs of those geometries. The dedoping of the channel caused by the ion penetration inside the channel after a positive gate bias results in a decrease in the hole concentration in the channel and a consequent reduction of the drain current^[12].

Plots in Figure 6.2(c) and 6.2(d) present the electrical characteristics of OECTs after 1 day of Astrocytes cultured on them. The OECT drain current decreases due to the cell device interaction. Nevertheless, similar device treatment with a biological protocol without cells, show less electrical differences after the same time period (Figure S 6.1).

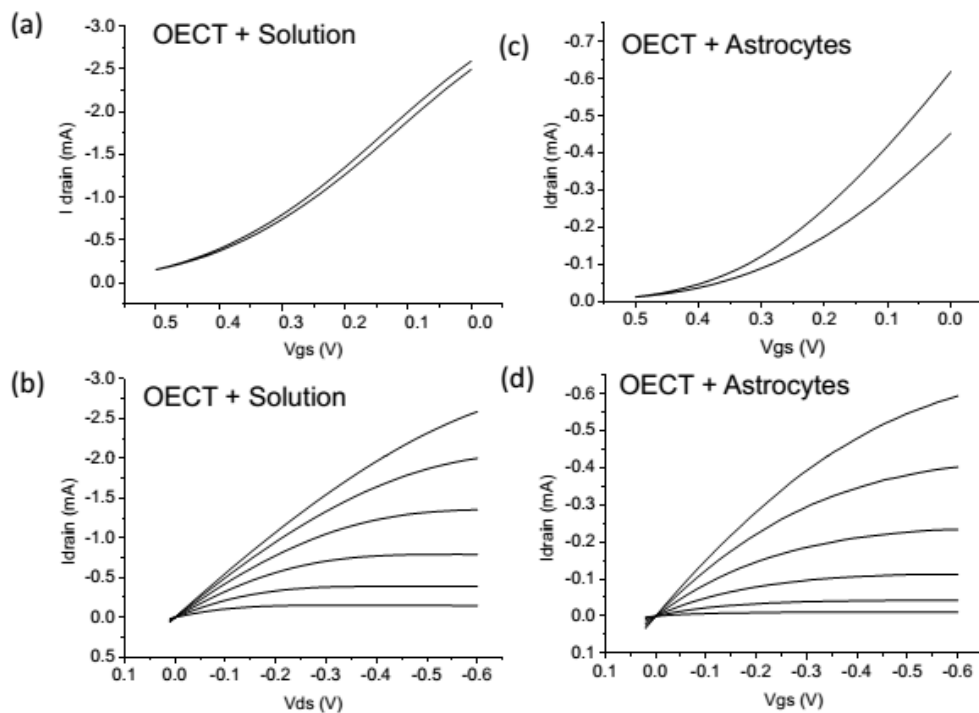


Figure 6.2: (a) Transistor Transfer characteristic for V_{gs} varying from 0 to 0.5 V (bottom curve) and maintaining a bias $V_{\text{ds}} = -0.6$ V in external solution. (b) Transistor Output characteristics for V_{G} varying from 0 (top curve) to 0.5 V (bottom curve) with a step of 0.1 V in external solution. (c) Transistor Transfer characteristics with astrocytes on the OECT. (d) Transistor Output characteristics with astrocytes on the OECT.

6.2.3 Recordings of astrocytes' activity using OECT

In order to test our ability to record astrocyte activity, we performed a current vs time measurement (I vs t) with the help of a B1500A Agilent semiconductor device parametric analyser. The OECT was biased at $V_{ds} = -0.6V$ while the gate potential was kept at zero $V_{gs} = 0$. The OECT current I_{DS} was monitored over extended time periods ($t = 1000$ s) with and without astrocytes plated on the device. In every case, we observed a capacitive drop at the beginning of the measurement caused by the re-arrangement of the ions at the channel-solution interface. Nevertheless, after that a stable working level was achieved with a slow decrease of the current during the measurement (drift phenomenon).

Measurements with astrocytes seeded on top of the device presented current modulation events (black line, Figure 6.3 A, B). These events are connected to the presence of astrocytes on the devices since removing the cells from the devices caused these fluctuations to disappear. The devices were thoroughly trypsinized and biased again resulting in a I_{DS} current without observable modulations over the same time period of 1000 seconds (red line, Figure 6.3 (a), (b)).

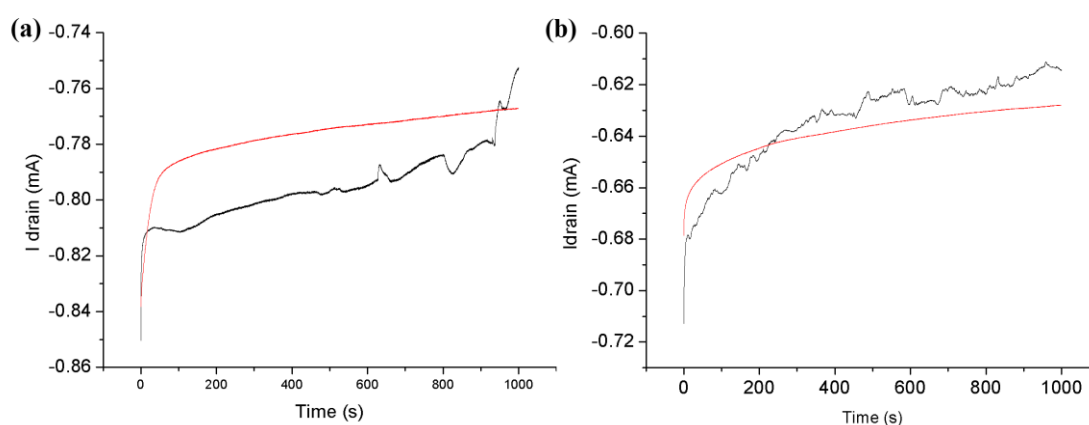


Figure 6.3: Astrocyte recordings on OECT. (a-b) OECT Drain current recorded with astrocytes plate on top of OECT (black line) and without astrocytes (red line) on the same devices applying $V_{ds} = -0.6$ V and $V_{gs} = 0$ for 1000s.

6.2.4 OECT astrocytes recordings using pharmacological inhibitor and ATP

In order to verify the biological origin of the recorded signals a new batch of experiments were planned. These experiments introduced the use of chemical agents that can modify the cell activity.

Hence, the same current vs time measurements were repeated but this time an external solution of 200 μM BaCl_2 was added in the culturing chamber. BaCl_2 acts as an activity inhibitor and is expected to suppress the electrophysiological activity. On the other hand, ATP acts as an activity enhancer as it provides energy to the cells. Therefore 10 μM of ATP should theoretical boost the activity of the under study cells. The used device was still the 30x30 μm^2 channel OECTs.

BaCl_2 is an inhibitor of the K^+ channels. Ba^{2+} ions can block K^+ channels by closing the transmembrane protein pore. Due to their similar size, Ba^{2+} can replace K^+ in its place in the potassium channel. Nevertheless, its higher charge allows it to stay there longer preventing the passage of $\text{K}^{+1,2}$ and as consequence eliminates its action.

Figure 6.4(a) presents the measurement of OECT covered with the astrocytes, before (red line) and after (black line) the inhibitor addition. The initial current modulations disappear after the BaCl_2 treatment validating, the thoughts for the biological origin of the recorded activity.

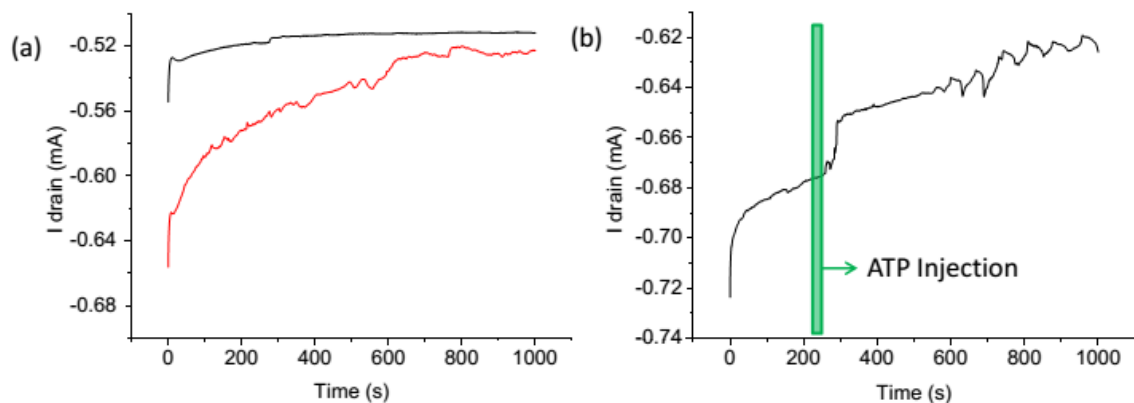


Figure 6.4: (a) Transistor Drain current recorded with astrocytes plate on top of the OECT pre (red line) and after BaCl_2 200 μM treatment (black line). (b) Transistor Drain current recorded with astrocytes plate on top of the OECT, adding at the solution ATP 10 μM at 250 seconds.

The second testing condition employed ATP as a way to increase the biological activity. The device used was initially covered with astrocytes but none

intense activity was recorded. Figure 6.4(b) presents the ATP addition and the induced current fluctuations at the last part of the measurement possibly related to the presence of cells. What is worth noticing is the current drop that takes place exactly after the ATP injection (green line), a phenomenon of interest regarding the interaction between OECTs electrical performance and the presence of chemical substances and biological tissue inside the electrolyte chamber.

6.2.5 OECT Astrocytes recordings during calcium microfluorimetry

The last recording test involved a new set of electrical measurements coupled this time with a calcium imaging technique. Calcium imaging has been extensively used to determine the status of calcium (Ca^{2+}) inside the cell and could be of extreme value in our effort to understand the connection, if any, between the calcium signaling of the cell and the recorded current modulations. Figure 6.5 presents the results of this set of experiments.

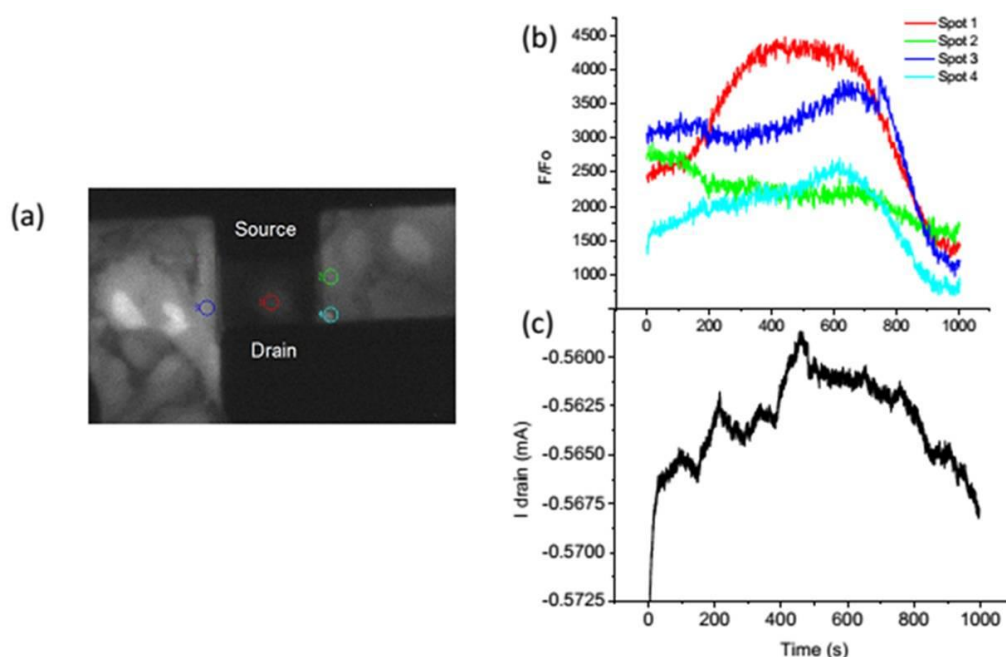


Figure 6.5: (a) Micrograph representing astrocytes grown on the OECT during the Calcium microfluorimetry. (b) Calcium microfluorimetry of the astrocytes plated on the OECT. The recorded traces show the behaviour of the spot highlighted in (a). (c) Transistor drain current recorded during Calcium microfluorimetry of astrocytes seeded on the device depicted in (a).

Figure 6.5(a) shows a micrograph of the OECT with the astrocytes plated on it, during a calcium microfluorimetry measurement. The colored circles on the center

and on the sides of the device active area correspond to the fluorescence data plotted as a function of time in Figure 6.5(b). Figure 6.5(c) on the other hand shows the simultaneous electrical recordings from the OECT during the calcium microfluorimetry. Interestingly enough, Figures 6.5(b) and 6.5(c) present similarities in the long time kinetics of the two measurements suggesting an implication of calcium signaling on the current measured on OECT devices.

The OECTs used during this experiment were of the same geometry as the ones used throughout the whole project ($W = 30 \mu\text{m}$, $L = 30 \mu\text{m}$, thickness $t = 500\text{nm}$). In addition the effect of single-wavelength fluorescent Ca^{2+} indicator Fluo4 device treatment was also tested. The transfer curve and the output characteristics were similar to the ones obtained without the treatment suggesting that Fluo4 does not affect the device performance (Figure S6.2).

6.3 Conclusions

PEDOT:PSS was proved to be suitable environment for astrocyte's growth and proliferation. This fact paves the way for the use of OECTs as the device of choice for studying the electrical properties of glia, an emerging scientific field of extreme interest. Nevertheless, due to lack of long term experiments chronic tests should also be performed in order for the effect of PEDOT:PSS (and Parylene-C) on astrocyte to be studied.

Moving to the actual electrical measurements, an intense current modulation observed on OECTs under the presence of astrocytes. In contrast, a steady state current, free of modulation, was recorded when the cells were removed from the devices.

In addition, the number of the recorded events decreased drastically with the use of BaCl_2 , a well-known inhibitor of the K^+ ions channels. At the same an increase was noted after ATP addition. The calcium microfluorimetry measurement performed simultaneously with the extracellular recordings revealed a similar shape trace for both these techniques.

Nevertheless, the origin of those fluctuations remains a mystery. The effect of the presences of astrocytes on top of the OECT channel is clear but studies will have to go on in order for the mechanism involved to become clear.

Therefore the next project steps should be::

- Long term testing of cells' biocompatibility with PEDOT:PSS and Parylene C
- GFAP (Glial fibrillary acidic protein) immunostaining.
- Extracellular recording using other pharmacological inhibitor of astrocytes biological activity and of astrocytes movement activity.

6.4 Experimental Section

6.4.1 Cell viability assay: Cell viability was investigated by Fluorescein diacetate (FDA) assay. FDA stock solution (5mg/ml) was prepared in acetone and stored a -20 C°. Astrocytes seeded on PEDOT:PSS, PEDOT:PSS coated with poly-D-lysine (PDL) and glass control substrates + PDL were incubated for 5 min with Fluorescein diacetate (Sigma Aldrich). After rinsing with physiological saline a sequence of images was taken using a Nikon Eclipse Ti-S optical microscope (20x). Alive cells were counted and the number of cells/mm² was calculated and compared at different time points. For each condition at least 6 coverslips were used.

6.4.2 Device Fabrication: Devices were fabricated in previously published way. The first photolithography step was performed by spin coating photoresists (S1813) on a glass slide substrate followed by a UV light exposure with the help of a chromium mask. After development in a suitable base solution, gold was evaporated creating the desired 100 nm pattern on the substrate with the help of a lift off procedure in a mixture of acetone/isopropanol. A 2 µm thick layer of Parylene C was used for the insulation of the device. This layer is attached on the glass slide with the help of 3-(trimethoxysilyl)propyl methacrylate(A-174 Silane) which acts as an adhesion promoter on the substrate. A 1% soap solution is spin coated on the Parylene C in order to act as an anti-adhesive layer and then a second 2µm Parylene C sacrificial

layer was deposit. A second photolithography step allowed us to define the area where the PEDOT:PSS would be spun after the opening of windows corresponding to the channel by plasma etching. The PEDOT:PSS layer is about 500nm thick . The sacrificial layer was peeled off after a short annealing at 110°C so that the final pattern is well defined. The final steps of the fabrication were the hard baking of PEDOT:PSS at 140°C for an hour and the soaking and rinsing of the devices in DI water in order for any low molecular weights residues to be removed.

Device testing :Electrical characterization of the OECTs was carried out using a SUSS probe station coupled to a B1500A Agilent semiconductor device parametric analyzer in air and using external cellular solution (NaCl 140 mM, MgCl₂ 2 mM, KCl 4 mM, CaCl₂ 2 mM, HEPES 10 mM, Glucose 5 mM, Mannitol 20mM, pH = 7.4) as gate solution. V_{gs} is the voltage difference applied between the gate solution and source electrodes, V_{ds} is the voltage difference applied between the drain and source electrodes. The source electrode is grounded. The output characterization is obtained by varying V_{DS} from 0 to -600 mV and keeping V_{GS} constant for six different voltages (0, 100, 200, 300, 400 and 500 mV).

6.4.3 Biological measurement: Biological measurements of astrocytes activity using OECT was carried out using a SUSS probe station coupled to a B1500A Agilent semiconductor device parametric analyzer in air and using extracellular standard solution and a sampling recording rate of 10 Hz. To the biological measurements V_{DS} was imposed at -600 mV and V_{GS} at 0 V.

6.4.4 Calcium microfluorometry: Variations in intracellular free Ca²⁺ concentration ([Ca²⁺]) were monitored by calcium microfluorometry using the single-wavelength fluorescent Ca²⁺ indicator Fluo-4 AM (life technologies). Before measurements, high-density astrocytes seeded on OECT devices prior coated with poly-D-lysine (PDL) were loaded with 10 μM Fluo-4 AM dissolved in standard bath solution, for 30 min plus 15 min at room temperature. Samples were rinsed with standard bath solution after incubation. Measurements of [Ca²⁺] were performed by using a fluorescence microscope (Nikon Eclipse Ti-S) equipped with long-distance dry objective (40x) and appropriate filters. The excitation wavelength was 470 nm with light pulse duration of 200 ms and a sampling rate of 1.5 Hz. Complete data acquisition was controlled by MetaFluor software (Molecular Devices).

References

- [1] H. K. Kimelberg, *The Neuroscientist : a review journal bringing neurobiology, neurology and psychiatry* 2010, 16, 79.
- [2] Y. Zhang, B. A. Barres, *Curr. Opin. Neurobiol.* 2010, 20, 588.
- [3] M. Nedergaard, B. Ransom, S. A. Goldman, *Trends in neurosciences* 2003, 26, 523.
- [4] E. A. Newman, *Trends in neurosciences* 2003, 26, 536.
- [5] V. Benfenati, S. Ferroni, *Neuroscience* 2010, 168, 926.
- [6] N. A. Oberheim, X. Wang, S. Goldman, M. Nedergaard, *Trends in neurosciences* 2006, 29, 547.
- [7] A. Volterra, N. Liaudet, I. Savtchouk, *Nature reviews. Neuroscience* 2014, 15, 327.
- [8] I. Markiewicz, B. Lukomska, *Acta neurobiologiae experimentalis* 2006, 66, 343.
- [9] M. T. Heneka, J. J. Rodriguez, A. Verkhratsky, *Brain research reviews* 2010, 63, 189.
- [10] D. Khodagholy, T. Doublet, P. Quilichini, M. Gurfinkel, P. Leleux, A. Ghestem, E. Ismailova, T. Herve, S. Sanaur, C. Bernard, G. G. Malliaras, *Nat Commun* 2013, 4, 1575.
- [11] C. Yao, Q. Li, J. Guo, F. Yan, I. M. Hsing, *Adv Healthc Mater* 2015, 4, 528.
- [12] D. Khodagholy, J. Rivnay, M. Sessolo, M. Gurfinkel, P. Leleux, L. H. Jimison, E. Stavrinidou, T. Herve, S. Sanaur, R. M. Owens, G. G. Malliaras, *Nature Communications* 2013, 4, 2133.

Supplementary Information

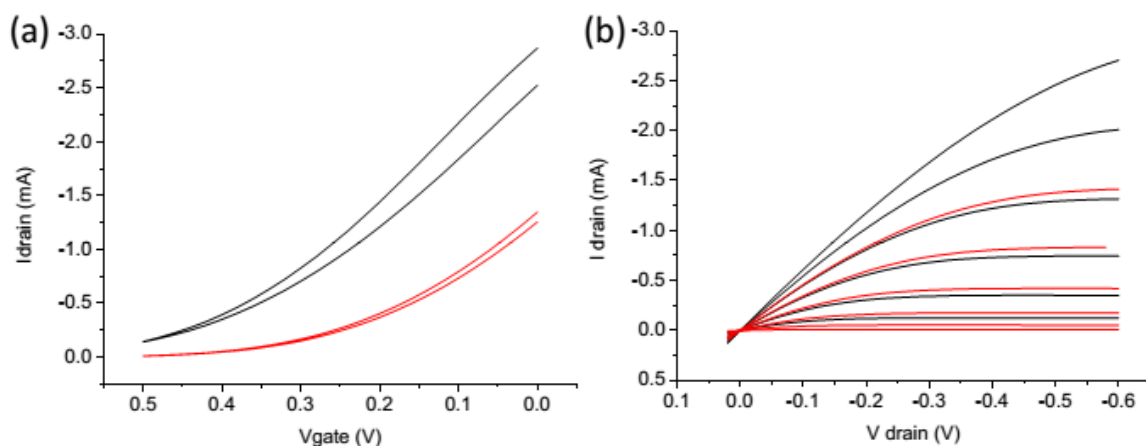


Figure S 6.1: (a) Transistor Transfer characteristic for V_{gs} varying from 0 to 0.5 V and a biasing voltage of $V_{\text{ds}} = 0.6$ V in external solution at time zero (black line) and after 1 day of biological treatment without cells (red line). (b) Transistor Output characteristics for V_G varying from 0 (top curve) to 0.5 V (bottom curve) with a step of 0.1 V in external solution at time zero (black line) and after 1 day of biological treatment without cells (red line).

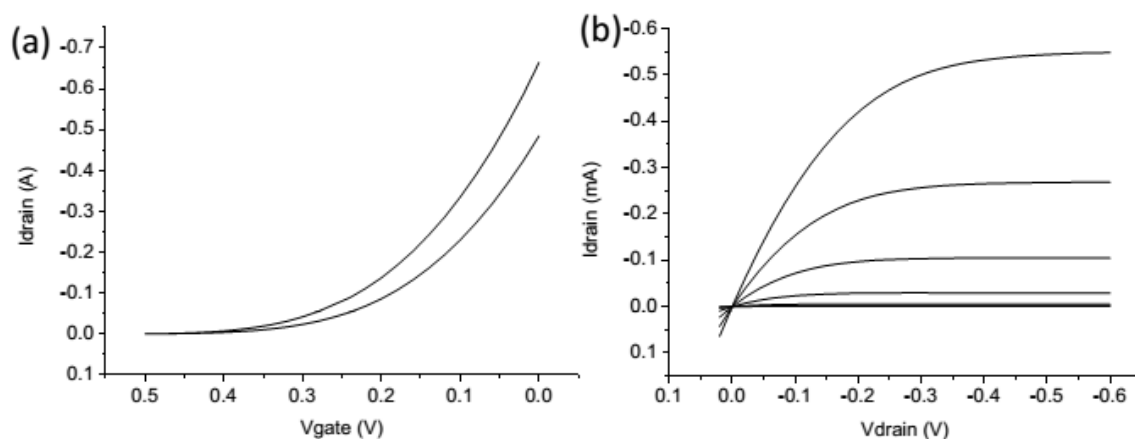


Figure S 6.2: (a) Transistor Transfer characteristics for V_{gs} varying from 0 to 0.5 V and a bias voltage $V_{\text{ds}} = -0.6$ V in external solution after treatment with Fluo4. (b) Transistor Output characteristics for V_G varying from 0 (top curve) to 0.5 V (bottom curve) with a step of 0.1 V in external solution after treatment with Fluo4.

Chapter 7: Conclusion – Outlook

In this Thesis we explore the potential of organic devices to revolutionize the world of bioelectronics. Especially, in the field of electrophysiology, conducting polymers pave new pathways for brain machine interactions mostly due to their unique set of properties. Their “soft” nature and their mixed ionic/electronic conductivity along with their oxide free interfaces in aqueous electrolytes and the freedom for chemical modification they provide make them ideal transducers between the worlds of electronics and biology.

Nevertheless, designing and realizing devices using organics is a challenging task due to the materials’ special nature. Chapter 1 presents some of the most popular fabrication approaches focusing on the problems device fabrication faces and the strategies to circumvent them. Having an introductory character, the chapter carries on and presents some concepts of neuroscience and electrophysiology as both these fields will be needed in the chapters to come.

Chapter 2 focuses on electrodes as the gold standard for electrophysiology. The basic theory behind electrode – neuronal cells interaction is presented along with the electrophysiological recording techniques and the issues the field has to face. Conducting polymers are introduced as a way to overcome these difficulties grace to their properties and to the benefits that come when used as coating films on metal electrodes. Going a step further, electrodes with variations on their area, shape and PEDOT:PSS thickness made it possible to examine the fundamental origins of their behavior. Electrochemical impedance spectroscopy (EIS) data were studied and modeled with a 2-element model involving a capacitor C (electrolyte-film interface) and a resistor R_s (electrolyte spreading resistance) in series. The systems’ characteristic frequency f_c was extracted, scaling laws were presented and f_c was used along with R_s to normalize plots to an impedance spectrum master curve ($\frac{Z}{R_s}$ vs $\frac{f}{f_c}$). The chapter closes with an introduction to electrodeposition, a popular method for covering metal electrodes with polymer coatings and its comparison with spin coating, a different coating technique, which is our lab’s method of choice.

Chapters 3 and 4 come as the implementation of Chapter’s 2 gained knowledge to real electrophysiological measurements.

Chapter 3 presents activity recordings of hippocampal neuronal cultures on a PEDOT:PSS covered Multi Electrode Array (MEA). Action potentials (APs) and local field potentials (LFPs) were recorded and analyzed while chemical stimulation was used to prove the potential of our conducting polymer based MEAs to perform high quality electrophysiology and drug screening.

Chapter 4 moves the project's interest to a slightly different direction as it deals with electrophysiological recordings on a different kind of cells than neurons. Pancreatic cell islets play a key role in preserving nutrition homeostasis in human body while disruption in their activity is linked with pathological conditions or type 2 diabetes. This is why their study is of great importance and this is why an *in vitro* PEDOT:PSS MEA recording platform, like the one presented in this Chapter, with the ability to offer improved electrophysiological recordings is of extreme value. Slow Potentials (SPs) and fast Action Potentials (APs) were successfully recorded and analyzed while the electrophysiological activity of pancreatic cells, and consequently their insulin secretion, in response to glucose, hormones, and multiple environmental factors was monitored in real time.

Chapter 5 introduces us a different organic device. The Organic Electrochemical Transistor (OECTs). Despite the fact that the device architecture is known from the mid 1980's, OECT has recently attracted interest in bioelectronics as signal transducers. As a consequence, its working principle is presented in this Chapter along with the advantages it offers in electrophysiological recordings. Nevertheless, the greatest obstacle for its use in unitary activity recordings is a complete read out system that will allow for the device to be used to its full potential. That is why an OECT measuring recording system was designed, fabricated and tested with artificial signals of the same characteristics of biological action potentials. The system was able to successfully resolve these signals so the next step can be the implementation of this technology in biological measurements.

Chapter 6 concludes this Thesis with a project concerning measurements on astrocytes. Despite the fact that astrocytes are not electrogenic cells their membrane possesses neurotransmitter receptors which could trigger electrical and biochemical events inside the cells. Taking advantage of the OECT's large transconductance we

tried to investigate if astrocyte cultures could be coupled to an electrical electrochemical transistor and modulate its current.

Appendix A: Noise characterization and modeling

As thoroughly discussed in Chapter 2, the greatest issue every electrophysiological measurement has to deal with is the unwanted noise which is superimposed with the neural activity and causes the degradation of the recording quality. In general, noise during a measurement, scales with the recording device impedance and consequently devices with lower impedance result in better signal to noise ratio (SNR). Nonetheless, many more sources contribute to the total noise and these sources are presented here.

Let us start by defining what noise is. Noise is any disturbance that interferes with the measurement of the desired signal^[1]. These disturbances may arise from:

- 1) Other neurons (biological noise)
- 2) The electrode-electrolyte interface
- 3) The recording electronic circuits

The overall noise exhibits a non-Gaussian profile and can be approximated as a $1/f^x$ noise^[2].

- 1) Neuron noise

During a measurement the recording electrode is picking up signals not only from the neuron(s) in its proximity but also from distant ones. These action potentials sum up and result in a background activity which can be mathematically described as^[2]:

$$V_{neu} = \sum_i \sum_k v_{i,neu}(t - t_{i,k}) \quad (\text{A.1})$$

where V_{neu} is the sum of the background signaling from distant neurons, i and $t_{i,k}$ is the i^{th} neuron and its activation time respectively and $v_{i,neu}$ is the voltage disturbance (spike) created by the i^{th} neuron during an action potential.

The power spectrum of V_{neu} is given by^[2]:

$$P\{V_{neu}\} = \sum_i \sum_k \frac{|X_i(f)|^2 f_i}{2} \langle e^{2\pi i f(t_{i,k_1+k} - t_{i,k_1})} \rangle \quad (\text{A.2})$$

where $\langle \rangle$ is the average over the ensemble and over k_1 , $P\{ \}$ is the spectrum operation, $X_i(f)$ is the Fourier transform of $v_{i,neu}$ and f_i is the frequency of spiking activity $v_{i,neu}$ (number of activations divided by a period of time).

Equation (A.2) contributes a $N_{neur} = 1/f\alpha$ term within the signal spectrum.

2) Electrode noise

Let us, first, imagine an electrode-electrolyte interface where non-charge transfer reactions occur (non faradaic process). The current flux of the i^{th} charged particle $J_i(x)$ at location x , assuming spatial concentration $n_i(x)$, is given by the Nerst equation^[2]:

$$J_i(x) = -D_i \nabla n_i(x) + n_i(x)v - \frac{z_i q}{kT} D_i n_i \nabla \Phi(x) \quad (A.3)$$

where D_i the diffusion coefficient, Φ the electrical potential, z_i the particle charge, q the electron charge, k the Boltzmann constant, T the temperature and v the convection coefficient.

In steady state, $J_i(x)$ is zero while the boundary condition dictates a voltage drop of 1V between metal and electrolyte. In this case, the electrode-electrolyte interface can be modeled with a lumped resistor R_{ee} in parallel with a lumped capacitor C_{ee} (double layer capacitance). Consequently, a low pass filter for the interface noise is formed and the induced noise from R_{ee} at the amplifier input is ^[2]:

$$N_{e,e} = \frac{4kT}{R_{ee}} (R_{ee} \parallel i\omega C_{ee} \parallel (R_b + i\omega C_i))^2 = \frac{4kT}{R_{ee}} \left| \frac{1}{\frac{1}{R_{ee}} + j\omega C_{ee} + \left(R_b + \frac{1}{i\omega C_i}\right)} \right|^2 \quad (A.4)$$

where C_i is the amplifier input capacitance. This capacitance should be negligible in order not to introduce waveform distortion. In that case, the integrated noise induced by the electrode-electrolyte interface is^[2, 3]:

$$\int_{f_{c1}}^{f_{c2}} N_{e,e} df \approx \int_{f_{c1}}^{f_{c2}} \frac{4kT}{R_{ee}} \left| \frac{1}{\frac{1}{R_{ee}} + j\omega C_{ee}} \right|^2 df = \frac{2kT}{\pi C_{ee}} \tan^{-1} 2\pi R_{ee} C_{ee} f \Big|_{f_{c1}}^{f_{c2}} < \frac{kT}{C_{ee}} \quad (\text{A.5})$$

What is important with equation (A.5) is that documents what it was stated in Chapter 2 regarding the connection between the electrodes impedance (capacitive-dominated impedance ($Z_{C_{ee}} = \frac{1}{i\omega C_{ee}}$) and the noise level during a measurement. In order for the noise level to be reduced the capacitance (C_{ee}) should be increased. Conducting polymer coated electrodes improve the measurement's SNR by reducing the electrode-electrolyte interface noise through a double layer capacitance (C_{ee}) increase.

Let us now consider regions of the electrolyte away from the electrode-electrolyte interface. In that case, spatial concentration gradient equals to zero ($\nabla n_i(x)=0$) and as a result we have a flat noise spectrum. In that case, noise is modeled with the help of a lumped bulk resistance R_b (usually referred to in literature as spreading resistance R_s ^{[4] [5]}) placed in series with the resistor R_{ee} that is itself in parallel to the capacitor C_{ee} . This approach results in ^[2, 3]:

$$N_{e,b} = 4kTR_b \quad (\text{A.6})$$

and since

$$R_b = 4kT\chi \frac{\rho}{\pi r_s} \quad (\text{A.7})$$

$$N_{e,b} = 4kT\chi \frac{\rho}{\pi r_s} \quad (\text{A.8})$$

where ρ the electrolyte resistivity, r_s the electrode radius and χ a constant that relates to the electrode geometry. For a plate electrode $\chi \approx 0.5$. The total electrode induced noise is the sum of $N_{e,e}$ and $N_{e,b}$.

3) Electronic noise

The third noise source is the recording electronic circuits themselves. Two main components can be identified in this category.

- i. Thermal noise of the transistors (also referred to as Johnson or Nyquist noise)
- ii. Flicker noise (also referred to as pink noise or $1/f$ noise)

Thermal noise $N_{c,thermal}$ is the result of random motion of thermally excited charge carriers in conductors and it happens regardless of any applied voltage. Its power spectra density (PSD) is white, i.e. it does not vary with frequency.

$$N_{c,thermal} = \gamma \frac{4kT}{g_m} \text{ (units: } V/\sqrt{Hz} \text{)} \quad (\text{A.9})$$

where g_m is the amplifiers transconductance ($\frac{\partial i_{out}}{\partial v_{in}}$), γ a circuit architecture dependent constant.

Flicker noise $N_{c,flicker}$ is present in all active devices and has various origins. It is always associated with DC current:

$$N_{c,flicker} = \frac{K}{C_{ox}WL} \frac{1}{f} \quad (\text{A.10})$$

where K a process-dependent constant on the order of $10^{-25}V^2F$, C_{ox} the transistor gate capacitance density and W and L the transistor width and length respectively.

Combining (A.9) and (A.10) we have

$$N_{electronic} = N_{c,thermal} + N_{c,flicker} = \gamma \frac{4kT}{g_m} + \frac{K}{C_{ox}WL} \frac{1}{f} \quad (\text{A.11})$$

For a given circuit design thermal noise can be reduced by increasing transconductance (g_m). Transconductance is to the first order linear to bias current and thus thermal noise is reduced when power consumption is reduced. Flicker noise on the other hand can be reduced through design techniques such as large size input transistors and chopper modulations^[2, 6]. In general, the contribution of electronic noise to the overall measurement noise can or it cannot be negligible depending of the strength of other noise sources^[3].

Combining equations (A.2) to (A.11) we get the equation for the total noise $N_{Total}(f)$ as a function of frequency:

$$N_{Total}(f) = N_{neur} + N_{e,e} + N_{e,b} + N_{c,thermal} + N_{c,flicker} \approx \frac{N_1}{f^x} + N_o \quad (\text{A.12})$$

where $\frac{N_1}{f^x}$ represents the frequency dependent while N_o for the frequency independent flat terms.

References

- [1] L. L. C. Molecular Devices, 2012.
- [2] Z. Yang, Q. Zhao, E. Keefer, W. Liu, in *Advances in Neural Information Processing Systems 22*, (Eds: Y. Bengio, D. Schuurmans, J. Lafferty, C. K. I. Williams, A. Culotta), 2009, 2160.
- [3] L. C. M, x00F, pez, M. Welkenhuysen, S. Musa, W. Eberle, C. Bartic, R. Puers, G. Gielen, "Towards a noise prediction model for in vivo neural recording", presented at *2012 Annual International Conference of the IEEE Engineering in Medicine and Biology Society*, Aug. 28 2012-Sept. 1 2012, 2012.
- [4] J. Newman, *Journal of The Electrochemical Society* 1966, 113, 501.
- [5] G. T. A. Kovacs, in *Enabling Technologies for Cultured Neural Networks*, (Eds: D. A. Stenger, T. M. McKenna), Academic Press, London 1994, 121.
- [6] T. Denison, K. Consoer, A. Kelly, A. Hachenburg, W. Santa, "A $2.2\mu\text{W}$, $94\text{nV}/\sqrt{\text{Hz}}$, Chopper-Stabilized Instrumentation Amplifier for EEG Detection in Chronic Implants", presented at *2007 IEEE International Solid-State Circuits Conference. Digest of Technical Papers*, 11-15 Feb. 2007, 2007.

Appendix B: Spreading resistance R_s

In Chapter 2 the biopotential electrode was modeled with the help of a resistor R_s in series with a resistor R that is itself in parallel to a capacitor C - (R_s -(R // C)).

R_s refers to the net resistance encounter by a current spreading out from an electrode into a conductive solution. In general this resistance is calculated by integrating the series resistance of shells of solution outward from the electrode^[1]:

$$R_s = \int_{x=0}^{x=\alpha} dR_s \quad (\text{B.1})$$

where x is the distance “nominal” to the surface.

Let us now consider a spherical source of current. In that case, the spreading resistance is:

$$R_s = \int_{r=r_s}^{r=\alpha} \frac{\rho}{4\pi r^2} dr = \frac{\rho}{4\pi r_s} \quad (\text{B.2})$$

where ρ is the conductivity of the solution in $\Omega \cdot cm$ and r_s is the radius of the sphere in centimeters.

For a planar electrode (one side exposed) things are getting bit more complicated. Newman calculated R_s in that case as follows^[2]:

In order to calculate the potential distribution from Laplace equation we use rotational elliptic coordinates ξ and η which are related to cylindrical by:

$$z = \alpha \xi \eta \quad (\text{B.3})$$

$$r = \alpha \sqrt{(1 + \xi^2)(1 - \eta^2)} \quad (\text{B.4})$$

where α is the disk radius, z is the normal distance from the disk and r the distance from the axon of symmetry. Laplace equation can now be written as:

$$\frac{\partial}{\partial} \left[(1 + \xi^2) \frac{\partial \Phi}{\partial \xi} \right] + \frac{\partial}{\partial} \left[(1 - \eta^2) \frac{\partial \Phi}{\partial \eta} \right] = 0 \quad (\text{B.5})$$

with boundary conditions :

$$\left\{ \begin{array}{l} \Phi = \Phi_0 \text{ at } \xi = 0 \text{ (on the disk electrode)} \\ \frac{\partial \Phi}{\partial \eta} = 0 \text{ at } \eta = 0 \text{ (on the insulating annulus)} \\ \Phi = 0 \text{ at } \xi = \infty \text{ (far from the disk)} \\ \Phi \text{ well behaved at } \eta = 1 \text{ (on the axis of the disk)} \end{array} \right.$$

Using the method of separation of variables we set

$$\Phi = P(\eta)Q(\xi) \quad (\text{B.6})$$

and now we have :

$$\frac{d}{d\eta} \left[(1 - \eta^2) \frac{dP}{d\eta} \right] + nP = 0, \quad \frac{d}{d\xi} \left[(1 + \xi^2) \frac{dQ}{d\xi} \right] - nQ = 0 \quad (\text{B.7})$$

where n is the separation constant. The solutions of these equations are Legendre functions. In order to have well behaved solutions:

$$n = l(l + 1) \text{ where } l = 0, 1, 2, \dots$$

and in order to satisfy the condition on the insulating surface, l must be even. The condition $\Phi = \Phi_0$ on the disk electrode can be satisfied simply for $n = 0$. Hence, integration yields:

$$\frac{\Phi}{\Phi_0} = 1 - \frac{2}{\pi} \tan^{-1} \xi \quad (\text{B.8})$$

The current density at the disk surface is:

$$i = - \frac{\partial \Phi}{\rho \partial z} \Big|_{z=0} = - \frac{1}{\alpha \eta \rho} \frac{\partial \Phi}{\partial \xi} \Big|_{\xi=0} = \frac{2}{\pi} \frac{\Phi_0}{\alpha \eta} = \frac{2\Phi_0}{\pi \sqrt{\alpha^2 - r^2}} \quad (\text{B.9})$$

where ρ is the resistivity of the solution in $\Omega \cdot cm$. The total current to the disk is

$$I = 2\pi \int_0^a ir dr = \frac{4a\Phi_o}{\rho} \quad (\text{B.10})$$

and the spreading R_s resistance is :

$$R_s = \frac{\Phi_o}{I} = \frac{\rho}{4a} \quad (\text{B.11})$$

In the case of a planar rectangular electrode (one side exposed) and by direct analogy to the thermodynamic shape factors used in heat-flow problems , R_s is given by the equation^[1]:

$$R_s = \frac{\rho \ln(4l/w)}{\pi l} \quad (\text{B.12})$$

where ρ is the resistivity of the solution in $\Omega \cdot cm$, l and w the length and the width of the rectangular respectively in centimeters.

Especially for a square planar electrode equation (B.12) becomes :

$$R_s = \frac{\rho \ln(4)}{\pi a} \quad (\text{B.13})$$

where a is the length of the side of the square.

Most importantly, equations (B.11), (B.12) and (B.13) show that for symmetrical shapes, R_s is proportional to the square root of the surface area

References

- [1] G. T. A. Kovacs, in *Enabling Technologies for Cultured Neural Networks*, (Eds: D. A. Stenger, T. M. McKenna), Academic Press, London 1994, 121.
- [2] J. Newman, *Journal of The Electrochemical Society* 1966, 113, 501.

Appendix C: List of Abbreviations

4-AP 4-aminopyridine	MEA microelectrode array
AFM atomic force microscopy	OEET organic electrochemical transistor
AP action potential	OFET organic field effect transistor
ATP adenosine triphosphate	OLED light emitting diode
CVD chemical vapor deposition	OP-AMP operational amplifier
DBSA 4-dodecylbenzenesulfonic acid	OPVs organic photovoltaics
DIC differential interference contrast	OTFTs organic thin film transistors
DIV days <i>in vitro</i>	PAB post-apply bake
DNQ diazonaphthoquinone	Pa-C parylene-C
DPP dry photolithography process	PCB printed circuit board
DUV deep ultraviolet	PDL poly-D-lysine
EDOT 3,4-ethylenedioxythiophene	PEDOT:PSS Poly(3,4-ethylenedioxythiophene):poly(styrenesulfonate)
EGTA ethylene glycol-bis(b-aminoethylether)-N,N,N', N-tetraacetic acid	PLL poly-L-lysine
EUV extreme ultraviolet	PMMA poly(methylmethacrylate)
FDA fluorescein diacetate	PVD physical vapor deposition
FDMA perfluorodecyl methacrylate	RIE reactive ion etching
FR firing rate	RMS root mean square
GABA gamma-aminobutyric acid	scCO ₂ supercritical carbon dioxide
GFAP glial fibrillary acidic protein	SEM scanning electron microscopy
GOPS 3-methacryloxypropyltrimethoxysilane	SNR signal-to-noise ratio
GSA geometric surface area	SP slow potentials
HEPES N-2-hydroxyethylpiperazine-N-2-ethanesulphonic acid	TA transimpedance amplifier
HFEs hydrofluoroethers	TBMA tert-butyl methacrylate
IPE ideally polarizable electrode	TMAH tetramethyl ammonium hydroxide
ITO indium tin oxide	TTX tetrodotoxine
KTFR Kodak thin film resists	UV ultraviolet light
LEP light emitting polymer	
LFP local field potential	

Appendix D: List of Publications

D.A. Koutsouras*, R. Perrier*, M. Raoux, A. Villaroel, A. Pirog, E. Pedraza, S. Renaud, G.G. Malliaras and J. Lang “PEDOT:PSS specifically increases detection of small action potentials from rodent and human pancreatic islets” (2016) **in preparation**

D.A. Koutsouras, P. Gkoupidenis, C. Stolz, V. Subramaninan, G.G. Malliaras, and D.C. Martin “Impedance Spectroscopy of Spun Cast and Electrochemically Deposited PEDOT:PSS on Electrodes of Various Areas” (2016) **in preparation**

D.A. Koutsouras, A. Hama, J. Pas, P. Gkoupidenis, B. Hivert, C. Faivre-Sarrailh, E. Di Pasquale, R.M. Owens, and G.G. Malliaras “*In vitro* PEDOT:PSS Microelectrode Arrays for hippocampal cell culture electrophysiological recordings” (2016) **in preparation**

P.Gkoupidenis, **D.A. Koutsouras** and G.G. Malliaras “Neuromorphic device architectures with global connectivity through electrolyte gating” (2016) **Nature Communication submitted**

P.Gkoupidenis, **D.A. Koutsouras**, T. Lonjaret, J.A. Fairfield, and G.G. Malliaras “Orientation selectivity in a multi - gated organic electrochemical transistor” (2016) **Scientific Reports 6, Article number: 27007 (2016)**

D.A. Koutsouras, E. Bihar, J.A. Fairfield, M. Saadaoui and G.G. Malliaras “Fabrication Approaches for Conducting Polymer Devices” (2016) **Book chapter in press**

J. Rivnay, P. Leleux, M. Ferro, M. Sessolo, A. Williamson, **D.A. Koutsouras**, D.Khodagholy, M. Ramuz, X. Strakosas, R.M. Owens, C. Benar, J.-M. Badiet, C. Bernard and G.G. Malliaras, “*High Performance Transistors for Bioelectronics Through Tuning of Channel Thickness*” (2015) **Sci. Adv.** 1, e1400251

D.A. Koutsouras, P. Leleux, M. Ramuz, J. Rivnay and G.G. Malliaras, “*Organic Electrochemical Transistors for BioMEMS Applications*” **Electron Devices Meeting (IEDM), 2014 IEEE International** p. 31.4.1 - 31.4.4 (2014)

NNT : 2016LYSEM017

Dimitrios A. Koutsouras

Conducting Polymer Devices for *in vitro* Electrophysiology

Speciality: Bioelectronics

Keywords: Conducting Polymers, Organic Bioelectronics, Electrophysiology, Neuroscience

Abstract:

Bioelectronics is an emerging field that is aiming to combine the worlds of biology and electronics. Among all the other materials, organics present a unique set of features that renders them ideal candidates for *this new field*. Their soft nature gives better mechanical stability, while the fact that they can conduct both electrically and ionically makes them ideal candidates to bridge the gap between electronic devices and living tissue. In addition they provide oxide free interfaces that could interact more efficiently with biology and allow chemical modification that increase biological functionality. These ideas, together with the organic devices fabrication approaches are presented in Chapter 1.

Electrodes are the main experimental tool for electrophysiology and this is why Chapter 2 presents the main physics principle behind them. Chapters 3 and 4 implement the knowledge obtained from the electrode modeling to real biological measurements. Chapter 3 presents activity recordings from Hippocampal cell cultures and Chapter 4 from pancreatic cells.

Chapter 5 introduces us to a different device as it presents the Organic electrochemical transistor (OECT) and presents a read out circuit board that could facilitate OECT electrophysiological recordings. Chapter 6 closes this thesis with an application of OECT on astrocyte recordings.

NNT : 2016LYSEM017

Dimitrios A. Koutsouras

Dispositifs à base de Polymères Conducteurs pour l'Électrophysiologie *in vitro*

Spécialité: Bioélectronique

Mots clefs : Polymères Conducteurs, Bioélectronique, Electrophysiologie, Neurosciences

Résume :

La bioélectronique est un domaine émergent qui vise à combiner les mondes de la biologie et de l'électronique. Les matériaux organiques présentent un ensemble de caractéristiques uniques qui les rendent candidats idéaux pour répondre aux contraintes spécifiques de ce domaine. Leur flexibilité leur donne une meilleure stabilité mécanique, tandis que leur nature de conducteurs ioniques et électroniques leur permet d'interférer parfaitement entre un tissu vivant et un dispositif électronique. En outre, ils présentent des interfaces non oxydées pour des interactions biologiques plus efficaces. Il est également possible de modifier chimiquement ces matériaux afin de les fonctionnaliser. Ces idées, ainsi que les différentes approches de fabrication des dispositifs organiques sont présentées au chapitre 1.

L'électrode est le principal outil expérimental pour l'électrophysiologie *in vitro*. Les principes physiques du fonctionnement de l'électrode sont donc tout d'abord présentés au chapitre 2. Dans les chapitres 3 et 4, les connaissances acquises à partir de la modélisation de l'électrode sont mises en applications sur des mesures biologiques réelles. Le chapitre 3 présente des enregistrements d'activité de cellules hippocampiques de culture et le chapitre 4 de cellules pancréatiques.

Le chapitre 5 introduit un autre dispositif, le transistor électrochimique organique (OECT) et présente une carte électronique de conversion qui pourrait faciliter l'usage d'OECT dans futures applications d'électrophysiologie. Le chapitre 6 clôture cette thèse en décrivant des mesures effectuées sur des astrocytes à l'aide d'OECT.